BIOSENSORS BASED ON BOVINE ODORANT BINDING PROTEIN (bOBP)

SASINEE BUNYARATAPHAN

A THESIS SUBMITTED IN PARTIAL FULFILLMENT OF THE REQUIREMENTS FOR THE DEGREE OF DOCTOR OF PHILOSOPHY AND DIPLOMA OF IMPERIAL COLLEGE

DEPARTMENT OF CHEMISTRY
FACULTY OF NATURAL SCIENCES
IMPERIAL COLLEGE LONDON

2013

BIOSENSORS BASED ON BOVINE ODORANT BINDING PROTEIN (bOBP)

Sasinee Bunyaratapha
PhD (Chemistry) of Imperial College
Supervisor: Professor Tony Cass, DPhil FRSC CChem MIET

ABSTRACT

Recombinant bovine odorant binding protein (bOBP) is a very promising platform for building protein-based biosensors. The protein possesses a broad binding specificity for hydrophobic molecules with affinities in the sub-micromolar range. Previous work has shown non-covalent binding of 1-aminoanthracene (1-AMA) in the internal cavities of bOBP that results in a large enhancement of fluorescence intensity. We have shown fluorescence titrations of recombinant bOBP with 1-AMA yielded a single type of binding site with a K_d of 0.16 ± 0.023 µM. Competitive displacement assays between 1-AMA and other ligands such as thymol were established and the results indicated their binding to bOBP. The strategy of competitive binding with 1-AMA was thus employed to quantify thymol concentration for the bOBP biosensors.

Ten different solid supports for the bOBP biosensors were examined for their biocompatibility with bOBP function using 1-AMA as a probe. The result was that nitrocellulose was chosen as the best membrane for immobilization, probably due to its 3-D micro-porous matrix (sponge structure) that provides a much larger surface area for protein binding compared with 2-D surfaces. It was found that the optimum operating concentrations of bOBP and 1-AMA and the method for the immobilization was incubation of nitrocellulose with the complex of 100µM bOBP and 100µM 1-AMA solution. The amounts of the total and functional protein binding to nitrocellulose were 7 ± 0.1 and 7 ± 0.4 nmol bOBP per cm^2 of membrane, respectively.

A fibre-optic biosensor based on bOBP has therefore been constructed. It has been an extrinsic sensor with bOBP immobilized on a nitrocellulose membrane placed at the tip of a probe of a bifurcated fibre-optic bundle that was in turn connected to the LLS-385 LED light source and the HR2000 spectrometer. The light emitted by fluorescent 1-AMA bound bOBP was detected by 2048-element CCD array of the spectrometer. The LODs for thymol in the liquid phase were found to be 14 ± 6 µM (calculated as S/N = 3), which is less than the guideline values considered to be toxic to humans. Moreover, this fibre-optic bOBP biosensor was also capable of sensing thymol vapour, and some potential uses of this sensor will be described.

ACKNOWLEDGEMENTS

First of all, I would like to thank Thai government, who sponsored me throughout four years and made my PhD study possible.

Most importantly, I wish to thank my supervisor; Prof. Tony Cass for his support, his invaluable advice, and his kindness. This thesis would not be achieved without him.

Many thanks go to everyone in the Tony Cass lab for their friendship and being supported. I have been happy for working with these peoples. Special thanks go to Chung-Pei, Melissa, and Steve who helped me a lot in my first-year study.

Finally, I would like to say thank you to my parents and my friends for their love, encouragement and support.

Sasinee Bunyarataphan

CONTENTS

		Page
ABSTRACT		2
ACKNOWLEDGEMENTS		3
CONTENTS		4
LIST OF FIGURES		10
LIST OF TABLES		15
LIST OF ABBREVIATIONS		16
CHAPTER 1	INTRODUCTION	18
1.1	Biosensors	18
1.2	Fluorescence	20
1.2.1	Basic principles of fluorescence	20
1.2.2	Principles of Förster resonance energy transfer (FRET)	23
1.3	Protein-Based Fluorescent Biosensors	26
1.4	Vertebrate Odorant Binding Protein (OBPs)	30
1.4.1	Bovine odorant binding protein (bOBP)	33
1.5	bOBP as a Potential Biosensing Element	38
1.6	Inventory of Devised Biosensors Based on bOBPs	39
1.7	Aim of the Project	40
1.8	The Application of Biosensors Based on bOBP to Thymol Determination	41
CHAPTER 2	MATERIALS AND METHODS	43
2.1	Materials	43
2.1.1	Bacterial Strains and Plasmid	43
2.1.2	Chemicals	44

2.1.2.1 General chemicals 44
2.1.2.2 Main chemicals 45
2.1.2.3 Ligands 46
2.1.2.4 Chromophores 46
2.1.3 Culture Media, Stock Solutions, and Buffers 47
2.1.4 Apparatus 48
2.2 Methods 49
2.2.1 Production of the Recombinant bOBPs 49
2.2.1.1 Expression of the recombinant bOBPs 49
2.2.1.1.1 Transformation of plasmid DNA 49
2.2.1.1.2 Extraction of plasmid DNA 49
2.2.1.1.3 Expression of protein 49
2.2.1.2 Purification of the recombinant bOBPs 50
2.2.1.2.1 Cell lysis 50
2.2.1.2.2 Chromatographic column preparation 50
2.2.1.2.3 Protein purification 51
2.2.1.2.4 Protein electrophoresis (SDS-PAGE) 51
2.2.1.2.5 Estimation of protein concentration 51
2.2.2 CD Spectroscopy of Thymol Binding to bOBP 52
2.2.2.1 Near-and far-UV CD measurements 52
2.2.2.2 Thermal denaturation 52
2.2.3 Characterization of the Recombinant bOBPs with DTNB and IANBD amide 53
2.2.3.1 Calculation of the SASA of cysteine residues in the recombinant bOBPs 53
2.2.3.2 Quantification of free thiol groups based on the reaction with Ellman’s reagent 55
2.2.3.3 Reaction of IANBD amide with thiol 55
2.2.3.4 Reaction of IANBD amide with bOBPwt 56
2.2.3.5 Determination of molar binding ratio of IANBD amide and bOBPwt 56

2.2.4 Fluorescence and Absorbance Spectroscopy of bOBP-Ligand Interactions 57
2.2.4.1 Fluorescence spectral analysis of 1-AMA 57
2.2.4.2 A binding assay based on 1-AMA 58
2.2.4.3 Competitive Binding Assays with 1-AMA 58
2.2.4.4 Dual Ligand Titration with 1-AMA 59
2.2.4.5 Titration of chromophore with bOBPwt 60
2.2.4.6 Competitive Binding Assays with chromophore 60
2.2.5 Immobilization of bOBP on Solid Surfaces 61
2.2.5.1 Screening of solid surfaces for immobilization of bOBP 61
2.2.5.2 Amount of bOBP immobilized on nitrocellulose 62
2.2.5.3 Titration of bOBP and 1-AMA on nitrocellulose 62
2.2.5.4 Amount of functional bOBP immobilized on nitrocellulose 63
2.2.5.5 Effect of immobilization method for bOBP and 1-AMA on nitrocellulose 63
2.2.6 Development of Fibre-Optic Sensor Based on bOBP 64
2.2.6.1 Construction of fibre-optic biosensor based on bOBP 64
2.2.6.2 Signal to background ratio of fibre-optic biosensor based on bOBP 65
2.2.6.3 Limit-of-Detection (LOD) of fibre-optic biosensor based on bOBP for thymol in liquid phase 65
2.2.6.4 Ability to sense thymol vapour of fibre-optic biosensor based on bOBP 66
2.2.6.5 Analysis of thymol vapour by fibre-optic biosensor based on bOBP 66

CHAPTER 3 PRODUCTION OF THE RECOMBINANT BOVINE ODORANT BINDING PROTEINS (bOBPs) 68
3.1 Expression of the Recombinant bOBPs 68
3.2 Purification of the Recombinant bOBPs 70

CHAPTER 4 CD SPECTROSCOPY OF THYMOL BINDING TO bOBP 74
4.1 Structural Information of Protein and Binding Interaction 75
4.1.1 Tertiary structure 75
4.1.2 Secondary structure 78
4.2 Thermodynamic Information of Protein Unfolding and Binding 82
4.2.1 Thermal stability 82
4.2.2 Enthalpy (ΔH), free energy (ΔG), entropy (ΔS) of unfolding and binding 87
4.2.3 Dissociation constants (K_d) of bOBP-thymol interaction 95

CHAPTER 5 CHARACTERIZATION OF THE RECOMBINANT bOBPs WITH DTNB AND IANBD AMIDE 97
5.1 Calculation of the Solvent Accessible Surface Areas (SASA) of Cysteine Residues in the Recombinant bOBPs 98
5.2 Quantification of Free Thiol Groups Based on the Reaction with Ellman's Reagent 103
5.3 Characterization of the Reaction of the Recombinant bOBPs with IANBD Amide 105
5.3.1 Reaction of IANBD amide with thiol 108
5.3.2 Molar binding ratio of IANBD amide and bOBPwt 110
5.3.3 Reaction of IANBD amide with bOBP 112

CHAPTER 6 FLUORESCENCE AND ABSORBANCE SPECTROSCOPY OF bOBP-LIGAND INTERACTIONS 114
6.1 Fluorescence-Binding Assay 114
6.1.1 A binding assay based on 1-AMA 116
6.1.2 Competitive binding assays with 1-AMA 120

6.1.3 Dual ligand titration with 1-AMA 123
6.2 Absorbance-Binding Assay 127

CHAPTER 7 IMMOBILIZATION OF bOBP ON SOLID SURFACES 132
7.1 Screening of Solid Surfaces for Immobilization of bOBP 136
7.2 Amount of bOBP Immobilized on Nitrocellulose 140
7.3 Titration of bOBP and 1-AMA on Nitrocellulose 142
7.4 Amount of Functional bOBP Immobilized on Nitrocellulose 143
7.5 Effect of Immobilization Method for bOBP and 1-AMA on Nitrocellulose 147

CHAPTER 8 DEVELOPMENT OF FIBRE-OPTIC SENSOR BASED ON bOBP 149
8.1 Construction of Fibre-Optic Biosensor Based on bOBP 155
8.2 Signal to Background Ratio of Fibre-Optic Biosensor Based on bOBP 157
8.3 Limit-of-Detection (LOD) of Fibre-Optic Biosensor Based on bOBP for Liquid-Phase Thymol 159
8.4 Ability to Sense Thymol Vapour of Fibre-Optic Biosensor Based on bOBP 162
8.5 Analysis of Thymol Vapour by Fibre-Optic Biosensor Based on bOBP 164

CHAPTER 9 CONCLUSIONS AND FUTURE WORK 168
9.1 Conclusions 168
9.2 Future Work 174
9.2.1 Optimization of the fibre-optic biosensor based on bOBP 174
9.2.2 Development of a more practical fibre-optic biosensor based on bOBP 175
9.2.3 Application of the fibre-optic biosensor based on bOBP 175

REFERENCES 178
APPENDIX A DNA AND AMINO ACID SEQUENCE OF bOBP-WT 194

APPENDIX B SUMMARY OF PERMISSION FOR THIRD PARTY COPYRIGHT WORKS 195
APPENDIX C PERMISSION INFORMATION FOR THIRD PARTY COPYRIGHT WORKS 198

LIST OF FIGURES

Page

Figure 1.1: Schematic design of a generic biosensor 19

Figure 1.2: Jablonski energy diagram showing the basic principles of fluorescence 21

Figure 1.3: Stoke's Shift demonstrating the difference between the maximum wavelengths of fluorescence excitation and emission spectra 22

Figure 1.4: FRET Jablonski diagram illustrating the coupled transitions (dashed lines) involved in resonance energy transfer (a violet arrow) 24

Figure 1.5: Spectral overlap region (a gray area) of absorption and emission spectra of cyan fluorescent protein (CFP, the donor) and red fluorescent protein (DsRFP, the acceptor) 25

Figure 1.6: Exponential relationship between energy transfer efficiency and the distance separating the donor and acceptor molecules 26

Figure 1.7: Representative scheme for construction of chemically assembled fluorescent biosensors 28

Figure 1.8: Schematic diagrams showing binding mechanism of a hybrid QD−antibody fragment FRET-based nanosensor for the detection of the explosive TNT 29

Figure 1.9: Three proposed models for the role of OBP 31

Figure 1.10: The olfactory neuroepithelium 32

Figure 1.11: A pathway of olfactory signal transduction 32

Figure 1.12: Secondary structures of the bOBP dimer 34

Figure 1.13: The internal ligand binding site of bOBP containing its natural ligand (1-octen-3-ol) 35

Figure 1.14: Binding of odorants to bOBP 36

Figure 1.15: Schematic representation of the proposed biosensors based on bOBP 41

Figure 2.1:	Plasmid map of the *bOBPwt* gene	44
Figure 2.2:	Structure of Ellman's Reagent	45
Figure 2.3:	Structure of IANBD amide	45
Figure 2.4:	Structure of 1-AMA	45
Figure 2.5:	Structures of ligands	46
Figure 3.1:	SDS-PAGE of bOBP expression	69
Figure 3.2:	SDS-PAGE of bOBP expression in soluble form after induction at 30^{o}C	70
Figure 3.3:	SDS-PAGE of the purification of bOBP	71
Figure 3.4:	SDS-PAGE of the purified bOBP	72
Figure 4.1:	Near UV CD spectra of bOBP in the absence (blue) and presence of thymol (red) demonstrated as ellipticity in millidegree unit	77
Figure 4.2:	Absorption spectrum of 200µM thymol in 0.01X PBS with 10µM EDTA supplement, pH 7.4 at 25°C	78
Figure 4.3:	Characteristic of far-UV CD spectra for an α-helix, a β-sheet and a random coil secondary structure of protein	79
Figure 4.4:	Far-UV CD spectra of bOBP in the absence (blue) and presence of thymol (red) demonstrated as ellipticity in millidegrees	81
Figure 4.5:	Far-UV CD spectra of 5µM bOBP at various temperatures of 20, 60, 70, 74, 80, 82 and 90^{o}C	83
Figure 4.6:	Far-UV CD spectra of 5µM bOBP in the presence of 100µM thymol at various temperatures of 20, 60, 70, 74, 80, 82 and 90^{o}C	83
Figure 4.7:	First derivatives of 5µM bOBP as a function of the temperature (the data in Figure 4.5 at 195nm)	84
Figure 4.8:	First derivatives of 5µM bOBP in the presence of 100µM thymol as a function of the temperature (the data in Figure 4.6 at 195nm)	84
Figure 4.9:	Unfolding transition curves of the ellipticity at 195nm for unfolding of bOBP in the absence (black squares) and presence of thymol (red circles) as a function of temperature	86
Figure 4.10:	Change in fraction folded (α); $\alpha = (\theta_{obs} - \theta_{unfold})/(\theta_{fold} - \theta_{unfold})$ of bOBP in the absence (blue diamond) and presence of thymol (red square) from the change in ellipticity as a function of temperature	90

Figure 4.11: Enthalpies of unfolding (ΔH_U) for bOBP in the absence (blue diamond) and presence of thymol (red square) from the change in ellipticity as a function of temperature 91
Figure 4.12: Free energies of unfolding (ΔG_U) for bOBP in the absence (blue diamond) and presence of thymol (red square) from the change in ellipticity as a function of temperature 92
Figure 4.13: Plot of linear dependence of ΔG of binding (ΔG_B) between bOBPwt and thymol as a function of temperature 92
Figure 4.14: Entropies of unfolding (ΔS_U) for bOBP in the absence (blue diamond) and presence of thymol (red square), and Entropy of binding (ΔS_B) between bOBPwt and thymol (green triangle) from the change in ellipticity as a function of temperature 95
Figure 5.1: Simplified model showing the overview of a reporting probe labelling and ligand binding to bOBP 98
Figure 5.2: Principle of the calculation of solvent accessible surface area 99
Figure 5.3: SASA of the specific residues in the recombinant bOBPs complexed with eight different ligands 102
Figure 5.4: Reaction of DTNB with a thiol (R-SH) 103
Figure 5.5: Types of detection of fluorescence signal for protein quantification 106
Figure 5.6: Reaction of IANBD amide with thiol group on protein molecule 108
Figure 5.7: Fluorescence of IANBD amide in the presence of thiol 109
Figure 5.8: Binding curve of non-covalently bound complex of bOBPwt and conjugated IANBD amide 113
Figure 6.1: Simplified model of competitive binding strategy 115
Figure 6.2: Three-dimensional structure of 1-AMA/bOBP complex 116
Figure 6.3: Fluorescence emission spectra of unbound 1-AMA (blue diamond) and 1-AMA complexed with bOBPwt (red square) 117
Figure 6.4: Fluorescence excitation spectra of unbound 1-AMA (blue diamond) and 1-AMA complexed with bOBPwt (red square) 117
Figure 6.5: Fluorescence binding curve of the recombinant bOBPwt with the ligand 1-AMA (blue point) 119

Figure 6.6: Corrected emission fluorescence intensity of the recombinant bOBPwt with 1-AMA 119
Figure 6.7: Competitive binding curves of various ligands with 1-AMA on bOBP 121
Figure 6.8: Dual ligand titration using 1-AMA and thymol 124
Figure 6.9: Plot of -log K_d of 1-AMA with the presence of various thymol concentrations against their corresponding thymol concentrations 125
Figure 6.10: Double-reciprocal plots showing competitive type of reversible ligand inhibitor 126
Figure 6.11: Titration absorption spectra of binding 2μM bromocresol green to various concentrations of bOBPwt ranging from 0-19.2 μM 128
Figure 6.12: Absorbance titration curve at 625nm of binding of bromocresol green to bOBPwt in PBS with 1mM EDTA supplement, pH 7.4 128
Figure 6.13: Competitive binding curve between 2μM bromocresol green and various thymol concentrations on 1.25μM bOBPwt 129
Figure 6.14: Bromocresol green displacement by 1-AMA (1μM bOBP + 1μM Bromocresol green + 100μM 1-AMA) 130
Figure 6.15: 1-AMA displacement by Bromocresol green (1μM bOBP + 1μM 1-AMA + 100μM Bromocresol green) 130
Figure 7.1: Schematic representation of an amino group coupling to epoxysilane coated slide 134
Figure 7.2: Signal to background ratio of the immobilization on ten different commercially available solid supports 138
Figure 7.3: Nitrocellulose surface demonstrating microporous 3-D matrix 139
Figure 7.4: Amount of bOBP (nmol) immobilized on nitrocellulose as a function of the total protein applied 141
Figure 7.5: Fluorescence titration curve of bOBP with 1-AMA on nitrocellulose membrane 143
Figure 7.6: Fluorescence calibration curve of the bOBP/1-AMA binding reaction in solution phase 144

Figure 7.7: Amount of functional bOBP (nmol) immobilized on nitrocellulose relative to the stoichiometric bOBP and 1-AMA concentrations that were applied to the nitrocellulose membrane 145
Figure 7.8: Amounts of bOBP (nmol) immobilized on nitrocellulose membrane relative to the total bOBP applied 146
Figure 7.9: S/B ratio showing the effect of the two different immobilization methods on nitrocellulose for three different backgrounds 148
Figure 8.1: Optical fibre. (A) Image of a bundle of optical fibres, (B) Components of an optical fibre 150
Figure 8.2: Illustration of total internal reflection in a single-core optical fibre, showing the trajectory for bound rays 150
Figure 8.3: Schematic representation of a fibre-optic biosensor 151
Figure 8.4: Two basic types of fibre-optic sensors. (A) Intrinsic devices sense directly on the fibre itself, whereas (B) Extrinsic devices relay on a transducer 152
Figure 8.5: Designs of intrinsic (A) and extrinsic (B) fibre-optic sensors 153
Figure 8.6: Fibre-optic biosensor setup 156
Figure 8.7: Comparison of S/B ratios obtained using three different bOBP biosensing formats for their three different backgrounds 158
Figure 8.8: Response curve and LOD of three different bOBP biosensing formats for liquid phase thymol 160
Figure 8.9: Response curve of fibre-optic biosensor based on bOBP for thymol vapour 163
Figure 8.10: %Fluorescence remaining of bOBP immobilized membrane that was monitored by using the fibre-optic system 165
Figure 8.11: %Fluorescence remaining of bOBP immobilized membrane that was monitored by using SPECTRAmax^{TM} GEMINI XS spectrofluorometer 166

LIST OF TABLES

Page

Table 2.1: Differences of DNA sequence between the native protein described in the papers and the sequences from the recombinant bOBPs used in work, excluding their N-terminal T7 promoter and C-terminal His_{10} tag 54

Table 3.1: Yields of bOBP wild-type and cysteine mutants 72

Table 5.1: Summary of the 3D structures used in the calculation of SASA of the specific cysteine residues in the recombinant bOBPs 101

Table 5.2: Molar extinction coefficients of Ellman's Reagent in various solvents 103

Table 5.3: Concentration of thiol in each 10 µM mutant bOBP by the Ellman's assay 105

Table 6.1: Apparent dissociation constants (K_d^{app}) and Equilibrium dissociation constants (K_d^{corr}) values of ligands for bOBPwt derived from competitive binding assays with 1-AMA 123

Table 7.1: Information of the ten different commercially available solid surfaces used to immobilize bOBP 137

Table 8.1: Range of S/B ratios obtained from three different bOBP biosensing formats regarding their three different backgrounds 158

Table 8.2: Mammalian toxicity data for thymol 162

LIST OF ABBREVIATIONS

1-AMA	1-aminoanthracene
3D	Three-dimensional
bOBP	Bovine odorant binding protein
CD	Circular dichroism
DMSO	Dimethyl sulfoxide
DTNB	5,5'-dithiobis-(2-nitrobenzoic acid)
EDTA	Ethylene diamine tetra acetic acid
g	Gravity force
IANBD	N-((2-(iodoacetoxy)ethyl)-N-methyl)amino-7-nitrobenz-2-oxa-1,3 diazole
IPTG	Isopropyl -D-1-thiogalactopyranoside
K_d	Dissociation constant
K_d^{app}	Apparent dissociation constant
K_d^{corr}	Corrected dissociation constant
Km	Kanamycin
l	Litre
LB	Luria or Lenox broth
mg	Milligram
min	Minute
ml	Millilitre
NBD	7-nitrobenz-2-oxa-1,3-diazol-4-yl
ng	Nanogram
nm	Nanometre
NTA	Nickel-chelated tri-acetate acid
^oC	Degree Celsius
PAGE	Polyacrylamide gel electrophoresis
PBS	Phosphate buffered saline
rpm	Rotation per minute

S/B	Signal to background ratio
SASA	Solvent-accessible surface area
SD	Standard deviation
SDS	Sodium dodecyl sulphate
T_m	Melting temperature
UV	Ultra violet
wt	Wild type
3OL	1-Octen-3-ol
BZQ	Benzophenone
DHM	2,6-Dimethyl-7-octen-2-ol
PRZ	2-Isobutyl-3-methoxypyrazine
SES	4-Butyl-5-propyl-1,3-selenazol-2-amine
UNA	Undecanal
UNX	Unknown atom or ion
ΔG	Free energy change
ΔH	Enthalpy change
ΔS	Entropy change

CHAPTER 1

INTRODUCTION

1.1 Biosensors

Biosensors are powerful analytical devices used for the detection of target molecules in a sample by converting a biological response into a processable and quantifiable signal. In a biosensor, a biological recognition element e.g. binding proteins, antibodies, antigens, enzymes, nucleic acids, tissues, microorganisms, interact preferably specifically with a given analyte that is based on molecular recognition of the target. Where the chemical structure of the target is unchanged, the sensor is an affinity sensor and where there is a transformation of the analyte, the sensor is a catalytic sensor. The biological component is combined with a transducing (detecting) device that transforms the interaction of the analyte with the biological recognition element into a signal that can be further processed and displayed (Figure 1.1) [1]. Common transducer technologies are optical, electrochemical, acoustic, or calorimetric.

Biosensors are employed in the identification, quantification and final screening of specific molecules, as presented in complex mixtures from moderate to very low concentrations, and thus they provide advantages in many research fields, such as analytical research, clinical diagnosis, food and pharmaceutical industry, and environmental control and process monitoring [2]. Biosensors have been developed as a result of the demand of fast, routine, and low cost analysis of samples with robustness, sensitivity and reproducibility [3]. In addition, biosensor properties include miniaturization, simple instrumentation, and automatic processing [2, 4].

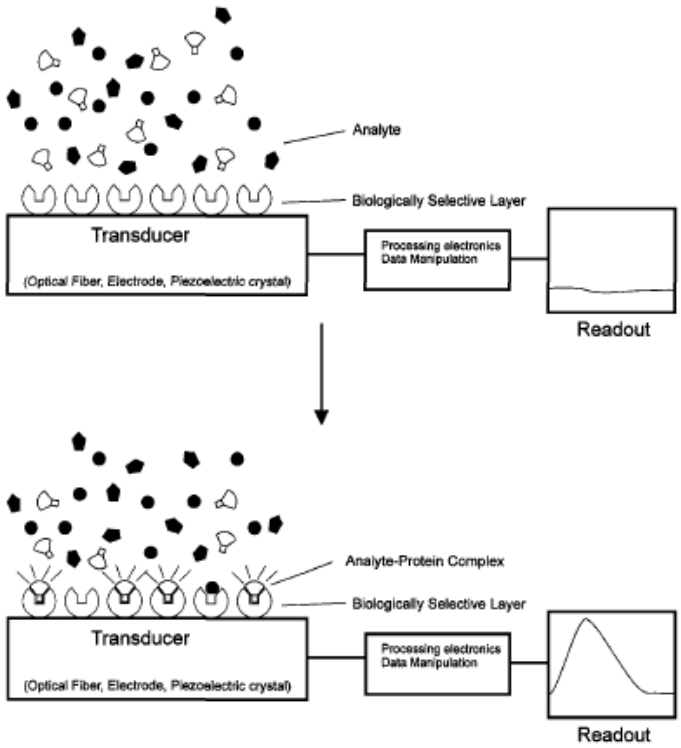

Figure 1.1: Schematic design of a generic biosensor. *The selective binding of the analyte to form an analyte-protein complex induces the generation of an analytical signal which is converted to a readout [5]. This image has been reproduced with the permission of the rights holder, Springer.*

Although current biosensors have been developed for the identification of an analyte that provides the desired specificity, each device is unique and requires considerable development time and optimization. To overcome this limitation, protein engineering techniques are being employed to adapt the signal-transduction properties of biological molecules to the detector instruments instead of adapting instruments to the unique requirements of each natural molecule. This can be accomplished by incorporating functional groups that provide simple signal-transduction mechanisms, such as optical or electrochemical changes into the proteins themselves. The ultimate goal is to obtain families of molecules that vary in their binding site, but keep a constant signal-transduction function, therefore generating generic biosensors that use the same detector instrumentation and measure a broad range of analytes [2, 6].

One of the most widely used detection instruments is based upon fluorescence.

1.2 Fluorescence

1.2.1 Basic principles of fluorescence

Fluorescence is process of light emission that occurs during molecular relaxation from an electronic excited state to the ground state by molecules that absorb light. The emitted light has a longer wavelength and therefore lower energy than the absorbed light [7-13].

The various energy levels involved in the absorption and emission of light by a fluorophore are classically presented by a Jablonski diagram (Figure 1.2). The fluorescence process is controlled by three important events, all of which occur on different timescales. When a fluorescent molecule absorbs light energy in the form of photons, this leads to excitation of photons at a stable ground state by a shift of electrons in the fluorescent molecule to a higher energy, unstable excited state; this happens in femtoseconds (10^{-15} seconds). Then, the molecule quickly relaxes to the lowest vibrational level of the excited electronic state. This vibrational relaxation process removes some of the energy in the fluorescent molecule gained from the photon absorption by converting it into heat. This process is known as internal conversion or vibrational relaxation; this generally occurs in picoseconds (10^{-12} seconds). The excited molecule then exists in this state for periods of nanoseconds (10^{-9} seconds), and defines as the fluorescence lifetime. Next, energy is released again by emitting a photon of light and the molecule returns to the ground state.

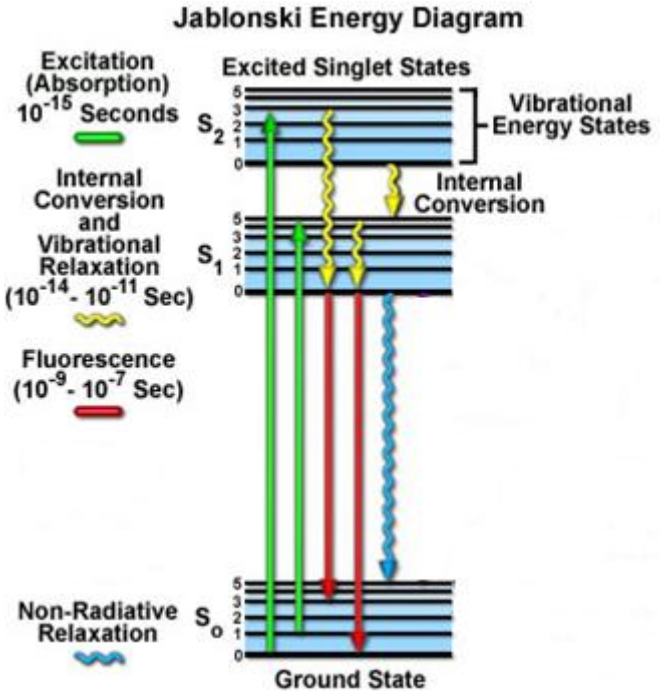

Figure 1.2: Jablonski energy diagram showing the basic principles of fluorescence. *Photon absorption and excitation to a vibrationally excited state is represented in green arrows. Vibrational relaxation and internal conversion are illustrated in yellow arrows. Fluorescence emission (or radiative decay) is depicted in red arrows, and non-radiation relaxation (or non-radiative decay) is shown in blue arrow. Radiative processes are shown in straight arrows, whereas non-radiative processes are shown using wavy arrows. Indicative timescales are shown, although are molecule dependant. For each electronic energy state (S_0, S_1 and S_2), vibrational energy levels are present as indicated by the closely packed horizontal lines – the higher energy states being at the top of the figure. This image has been reproduced from the reference [11] with the permission of the rights holder, Olympus America Inc.by Michael W. Davidson.*

The resulting emitted photon is less energetic and has a longer wavelength than original photon. This phenomenon called Stoke's Shift is the difference in wavelength or equivalently in the energy between the maxima of the excitation and the emission spectra (Figure 1.3) [7-13].

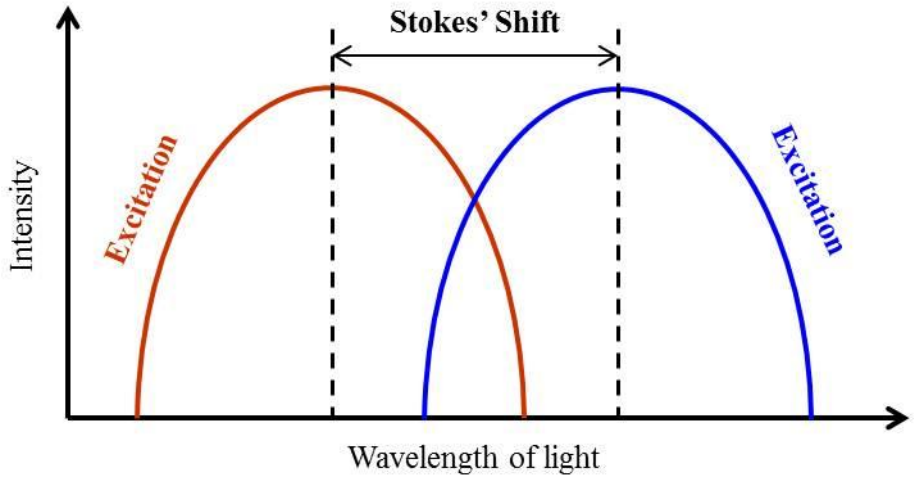

Figure 1.3: Stoke's Shift demonstrating the difference between the maximum wavelengths of fluorescence excitation and emission spectra.

In addition, molecules in the excited electronic states can also relax by non-radiative processes where excitation energy is not converted into photons but dissipated by thermal processes such as vibrational relaxation and collisional quenching [7-13]. Then, the total decay rate can be described by the sum over all rates: $k_d = k_r + k_{nr}$, where k_d is the total decay rate, k_r is the radiative decay rate and k_{nr} is the non-radiative decay rates [9]. In general k_{nr} is sensitive to environment e.g. protein binding.

Most fluorophores have a propensity of photobleaching, which is the excited state degrades either spontaneously or through reaction with other molecules presented. Despite this, the excitation and emission cycle can be repeated for many hundreds to thousands of times before the highly reactive excited state molecule is photobleached. For instance, the well-studied probe fluorescein isothiocyanate (FITC) can undergo excitation and relaxation for about 30,000 cycles before the molecule no longer responds to incident illumination [11].

Because of the extremely sensitive emission profiles, spatial resolution, and high specificity of fluorescence, this technique has become an important tool in genetics and cell biology, and in the context of this thesis; chemical sensors [11, 14, 15].

1.2.2 Principles of Förster resonance energy transfer (FRET)

FRET is a photophysical process that involves energy transfer between two chromophores. The excitation energy transfers from a donor molecule in its electronically excited state to an acceptor molecule via a non-radiative transmission [16, 17]. In other words, the donor molecule that initially absorbs the energy does not emit a photon, but transfers the energy to the acceptor molecule [17]. These coupled transitions involved in FRET are illustrated by the Jablonski diagram (Figure 1.4).

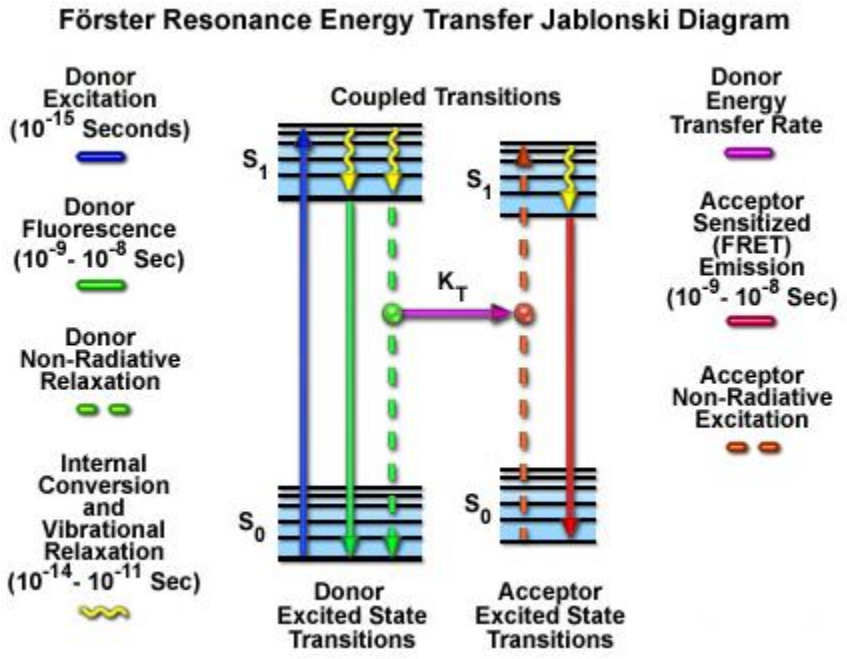

Figure 1.4: FRET Jablonski diagram illustrating the coupled transitions (dashed lines) involved in resonance energy transfer (a violet arrow). *The donor fluorophore can transfer excited state energy directly to the acceptor without emitting a photon. Absorption and emission transitions are indicated by straight vertical arrows (blue, green and red), while vibrational relaxation is represented by wavy yellow arrows. This image has been reproduced from the reference [18] with the permission of the rights holder, Michael W. Davidson.*

Several fundamental conditions are required for generating FRET. The donor and acceptor molecules must be in close proximity within a range of 1 to 10 nanometres of each other. The fluorescence emission spectrum of the donor molecule must overlap the absorption spectrum of the acceptor molecule (Figure 1.5). The relative orientations of the donor and acceptor transition dipole moments must be approximately parallel [19].

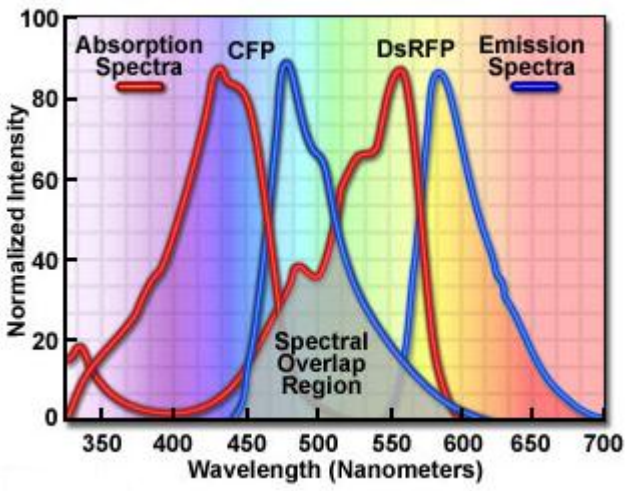

Figure 1.5: Spectral overlap region (the gray area) of absorption and emission spectra of cyan fluorescent protein (CFP, the donor) and red fluorescent protein (DsRFP, the acceptor). *Absorption spectra for both fluorescent proteins are presented as red curves, while the emission spectra are illustrated as blue curves. This image has been reproduced from the reference [20] with the permission of the rights holder, Olympus America Inc.by Michael W. Davidson.*

The efficiency of this energy transfer depends basically on the distance between the donor and acceptor fluorophore, which is proportional to the inverse sixth power of the distance between donor and acceptor molecules [17, 21]. The distance relationship between energy transfer efficiency and the separation of the donor and acceptor molecules is illustrated in Figure 1.6.

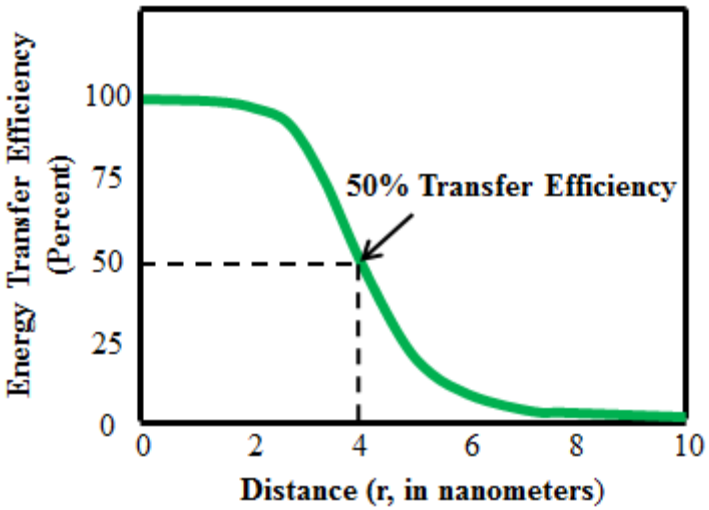

Figure 1.6: Relationship between energy transfer efficiency and the distance separating the donor and acceptor molecules. *The ability of the donor fluorophore to transfer its excitation energy to the acceptor by non-radiative interaction decreases as the sixth power of the distance separating the two molecules. Subsequently, the energy transfer efficiency between donor and acceptor molecules decreases dramatically with increasing distance between the molecules.*

Due to its extreme sensitivity to small distances, FRET is thus a valuable technique for studying interactions between molecules, such as protein-protein interactions, protein-DNA interactions, and protein conformational changes [22, 23].

1.3 Protein-Based Fluorescent Biosensors

Based on the construction method, the protein-based fluorescent biosensors can be classified into two types: the genetically encoded fluorescent biosensors and the chemically constructed biosensors. Firstly, a genetically encoded fluorescent biosensor makes use of fluorescent proteins (FP) such as green fluorescent protein (GFP) or its variants as signal transducer(s), which change in their fluorescence intensity or excitation/emission wavelengths [24]. FP-based biosensors can be endogenously expressed in cells or tissues simply by transfection with the plasmid DNA encoding it

and with the possibility of controlling the localization of the biosensors to sites of interest within the cell. This can be achieved by introducing organelle-specific targeting signals. Many kinds of FP-based biosensors have been developed by fusion of FP with appropriate protein scaffolds that act as the recognition platform [25, 26], and which are useful for imaging and sensing important molecules and key events in living cells [27, 28]. This type of biosensor has been a powerful tool for *in vivo* applications [25, 26].

An example of a fluorescent protein biosensor is a green fluorescent protein-based bacterial biosensor for benzene, toluene, ethylbenzene, and related compounds in aqueous solutions that was constructed and characterized. The biosensor was produced from *Pseudomonas fluorescens* strain A506 carrying the toluene-benzene utilization (*tbu*) pathway transcriptional activator. Its promoter *PtbuA1* was fused with a promoterless *gfp* gene on a broad-host-range promoter probe vector. TbuT was constitutively expressed by being fused to the neomycin phosphotransferase (*nptII*) promoter. After induction periods of 3 h, fluorescence emission from the cells correlated well with toluene, benzene, ethylbenzene, and trichloroethylene concentrations. Each inducer had a unique minimum concentration for induction (K_{app} values that ranged from 3.3 ± 1.8 μM for toluene to 35.6 ± 16.6 μM for trichloroethylene), and maximal fluorescence response [29].

The second class of fluorescent protein biosensor is chemically constructed and consists of a protein used as the molecular-recognition platform, conjugated with a synthetic fluorescent molecule to provide the signal transducer function. In order to control the modification sites and numbers, the site-specific incorporation of fluorophore is regularly required. Typical approaches that have been employed to yield fluorescent biosensors are shown in Figure 1.7. Usually, reactive residues like cysteine are introduced into the desired location by site-directed mutagenesis, or chemistry-based protein labeling techniques, and then followed by selective modification with functional fluorophore [24].

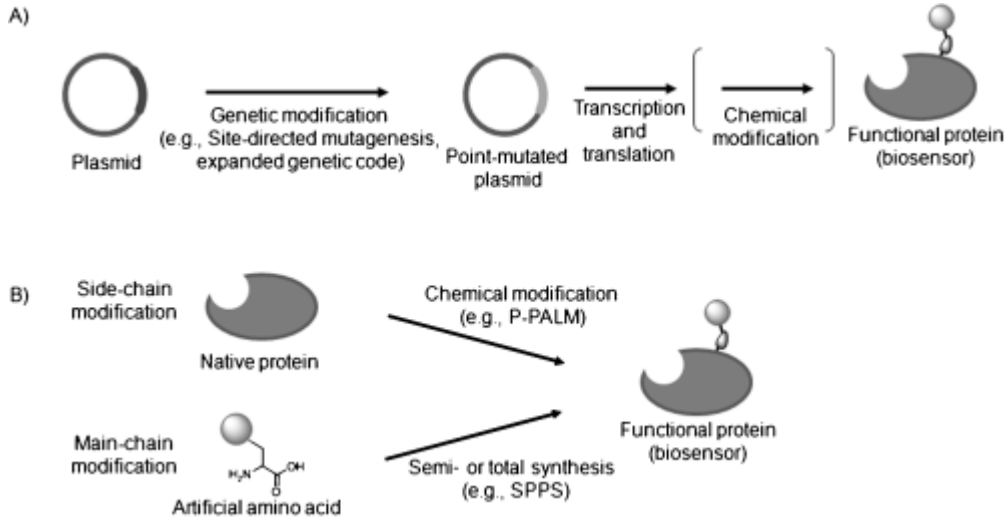

Figure 1.7: Representative scheme for construction of chemically assembled fluorescent biosensors. *(A) Genetic modification is performed to construct mutated protein that is subsequently incorporated with an artificial fluorophore. In many cases, this strategy requires advanced skills for gene manipulation. (B) Chemical modification can directly combine artificial fluorescent molecule on the protein [24]. This image has been reproduced with the permission of the rights holder, John Wiley and Sons.*

An example of the construction of a chemically modified fluorescent protein-based biosensor involves the applications of nanomaterials, such as quantum dots (QDs), semiconductor nanoparticles (NPs), or nanofibres conjugated with proteins. In these systems, competitive binding assays have been largely used for the signal read-out. In general, a fluorescently labeled protein is bound to the ligand linked with another fluorophore. The reaction occurs after an analyte is added to this complex. If the analyte has a stronger affinity for the protein, the bound ligand is displaced, leading to a change in the intermolecular fluorescence resonance energy transfer (FRET) signal, which is related to the affinity and concentration of the analyte [24].

A model of this type of sensors is demonstrated in Figure 1.8. A solution-phase hybrid nanosensor based on FRET has been created for the specific detection of the explosive 2,4,6-trinitrotoluene (TNT), a security threat and contaminant, in aqueous environments. The hybrid nanosensor consists of luminescent QDs conjugated to antibody fragments (anti-TNT) at which the pre-binding of a dye-labeled TNT analogue in the antibody binding site quenches the QD photoluminescence via proximity-induced FRET. Addition of soluble TNT displaces the quencher-labeled TNT analogue, abolishing FRET and resulting in a concentration-dependent recovery of QD photoluminescence [30].

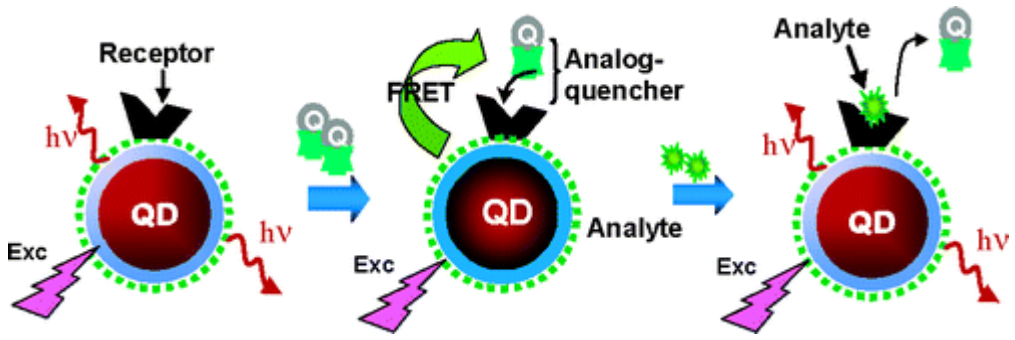

Figure 1.8: Schematic diagrams showing binding mechanism of a hybrid QD−antibody fragment FRET-based nanosensor for the detection of the explosive TNT. *The solution-phase hybrid nanosensor has been built by self-assembling anti-TNT specific antibody fragments onto a hydrophilic QD via metal-affinity coordination. This conjugate generates a substantial rate of FRET when pre-assembled with a dye-labeled TNT analogue. Exposure to soluble TNT displaces the analogue quencher away from the QD−anti-TNT conjugate, resulting in a systematic and concentration-dependent QD photoluminescent recovery [30].This image has been reproduced with the permission of the rights holder, American Chemical Society.*

FRET-based competition assays can also be used in a fibre-optic format. For example, glucose biosensors have been based on FRET competitive reactions for a fluorescent glucose-receptor protein (concanavalin A labeled with rhodamine; Rh-ConA) between glucose and a fluorescent glucose analog (dextran labeled with FITC; FITC-dextran). Addition of Rh-ConA to a solution of the FITC-dextran shows quenching of the FITC fluorescence and sensitization of the rhodamine fluorescence, whereas when glucose is added to this solution, the FITC fluorescence intensity increases as FITC-dextran is released from the Rh-ConA and is replaced by glucose. Therefore, glucose concentrations can be determined directly from the level of FITC quenching/rhodamine emission. The fibre-optic glucose biosensors has a working range up to 2.00 mg/ml of glucose [31].

1.4 Vertebrate Odorant Binding Protein (OBPs)

Vertebrate odorant-binding proteins (OBPs) are low-molecular-weight soluble extracellular proteins belonging to the lipocalin family [32-37], which are highly concentrated in the nasal mucus [38-40]. Although this class of proteins has a very low sequence homology, it is characterized by two conserved domains composed of an eight-stranded antiparallel β barrel that form the ligand binding site, and a carboxy terminal α helix [41-43]. OBPs generally bind small, hydrophobic molecules [36], and are able to bind a large number of volatile odorous compounds, belonging to different chemical classes [44]. Perhaps due to their broad ligand specificity, OBPs have been believed to play a fundamental role in odour perception by transporting, selecting, and/or deactivating odorant molecules toward specific olfactory receptors on sensory neurons across the aqueous compartment of the nasal mucus [45-48]. Figure 1.9 shows schematically three models that have been proposed the physiological functions of OBPs in olfaction. These are buffer, carrier, and transducer. Buffer: OBPs would work more efficiently by trapping high concentrations of odorants and diminishing binding with neuron receptors. Carrier: OBPs could bind and carry odorant molecules to the membrane receptors of the olfactory neurons; alternatively, OBP could remove the odorant molecules from the receptors. Transducer: OBPs could specifically and

selectively bind odorants and carry the relative information (but not the odorants) to the membrane-bound receptors [36].

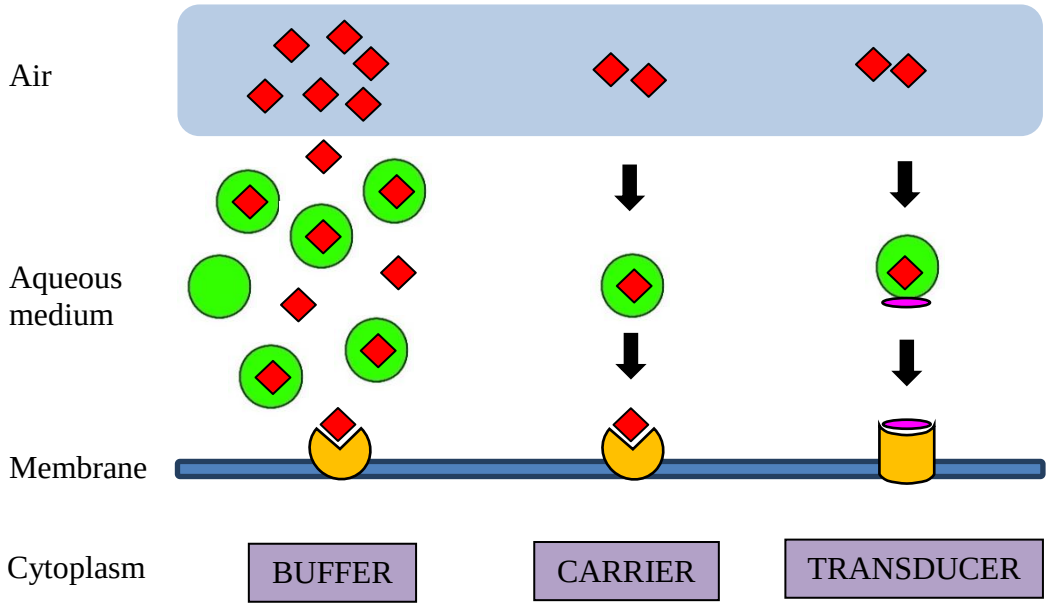

Figure 1.9: Three proposed models for the role of OBP [36]. *The red square are represented as odorants. The green circles are depicted as OBP. The yellow objects are shown as receptor neurons.*

The initial events in odour detection exist in a specialized olfactory neuroepithelium (Figure 1.10) located in the nasal cavity [49]. Odours are supposed to bind with specific receptors on the cilia of olfactory sensory neurons, generating the signals propagated by olfactory neuron axons to the olfactory bulb [50, 51]. Although, the mechanisms of OBPs in signal transduction are still not fully understood [38, 52], a pathway of olfactory signal transduction (Figure 1.11) has been suggested. In this model, the binding of an odorant molecule to an odour-specific transmembrane receptor activates specific G proteins, leading to the release of the GTP-coupled α subunit of the G protein, which then stimulates adenylyl cyclase to produce elevated levels of cAMP. The increased cAMP opens cyclic nucleotide-gated cation channels,

thus generating membrane potential changes that is propagated along the olfactory sensory axon to the brain [50, 51].

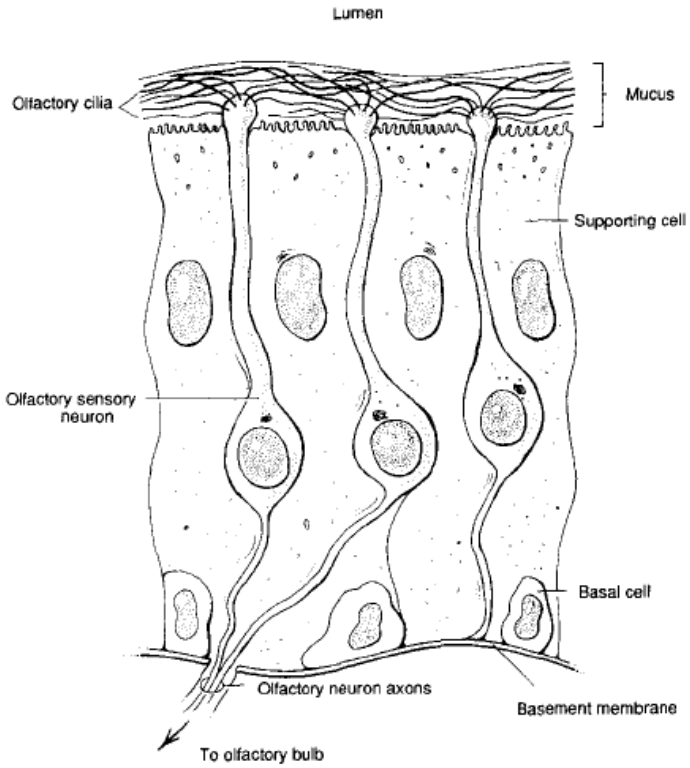

Figure 1.10: The olfactory neuroepithelium [50]. *This image has been reproduced with the permission of the rights holder, Elsevier.*

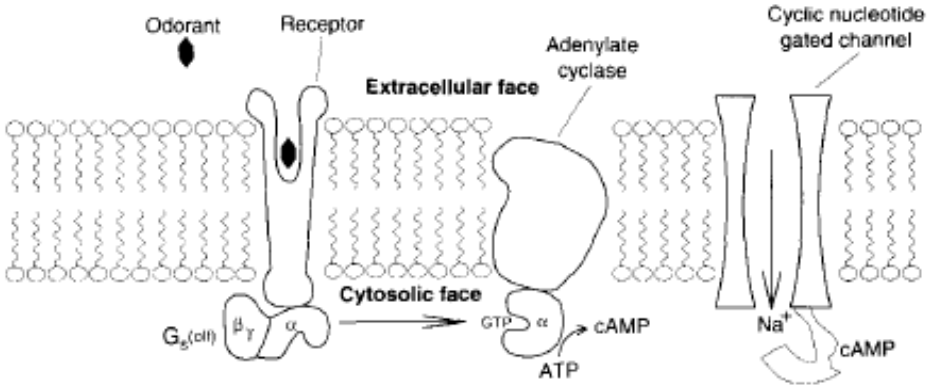

Figure 1.11: A pathway of olfactory signal transduction [50]. *This image has been reproduced with the permission of the rights holder, Elsevier.*

1.4.1 Bovine odorant binding protein (bOBP)

In contrast to other OBPs that are normally monomeric, the structure of bOBP revealed a striking feature of a homodimer in which each monomer has 159 residues, a molecular weight of 19 kDa, and consists of an eight-stranded antiparallel β barrel flanked by an α helix at the C-terminal end of the polypeptide chain [43]. A bOBP dimer is formed by domain swapping whereby two monomers exchange the domain of a C-terminal α helix over the β barrel domain of the other, resulting in a protein with an elongated shape conformation (40 × 40 × 70 $Å^3$) [53] (Figure 1.12). Inside the β barrel of each monomer of bOBP, a large buried cavity of about 407 $Å^3$ are mostly composed of hydrophobic residues, which are the general binding site for different types of small hydrophobic molecules including odorants [52-54]. Whereas the native porcine OBP (pOBP) as isolated is devoid of ligand, the binding site of purified bOBP has been shown to harbour a naturally occuring ligand; 1-octen-3-ol, a typical volatile component of bovine breath and an extremely potent olfactory attractant for many insect species [54] (Figure 1.13).

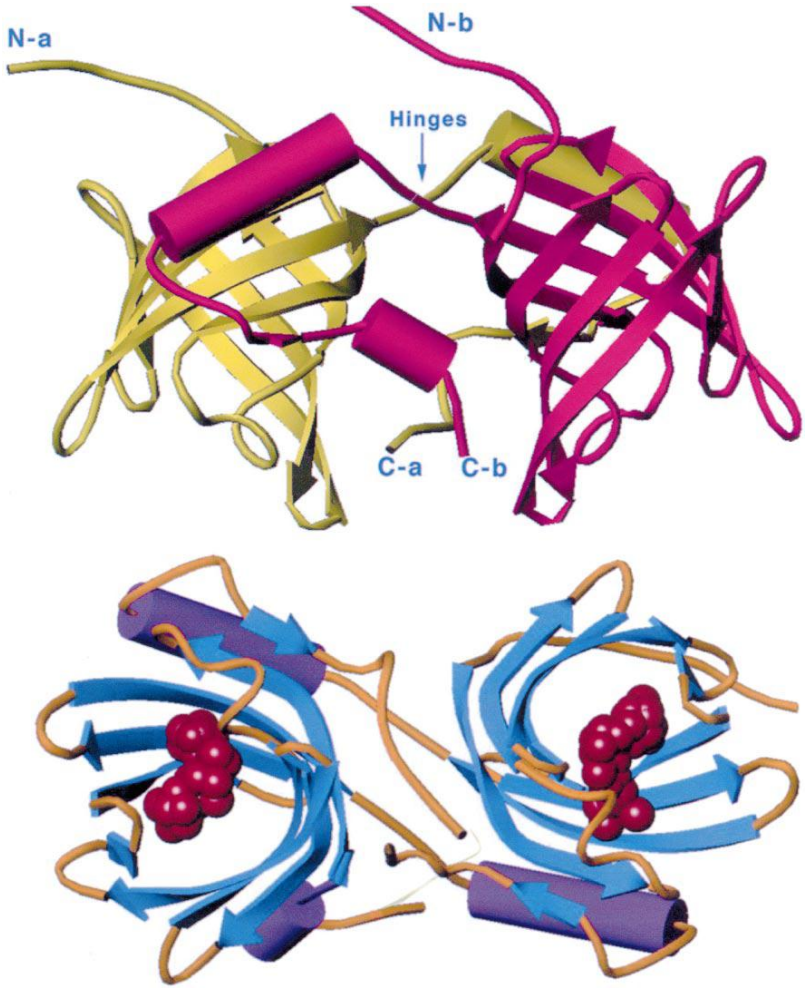

Figure 1.12: Secondary structures of the bOBP dimer. *They are depicted by cylinders (α-helices), and arrows (β-strands). Top: colour coding shows the domain swapping phenomenon; monomer A is yellow, B is pink. Bottom: colour coding is corresponding to the secondary structure; α-helices, violet; β-strands, blue; other motifs, brown. Pseudo-atoms presented in the two buried cavities are red [48]. It is note that this crystal structure (PDB ID. 1OBP) has been determined at a resolution of 2.00 Å by X-ray diffraction. This image has been reproduced with the permission of the rights holder, Elsevier.*

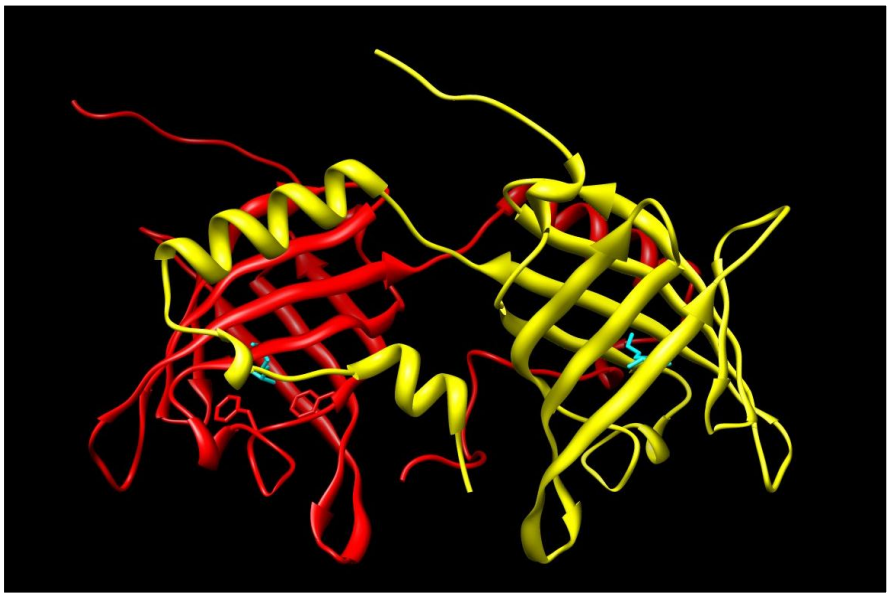

Figure 1.13: The internal ligand binding site of bOBP containing its natural ligand (1-octen-3-ol). *Crystal structure of bOBP displayed the two buried cavities complexed with its natural ligand (1-octen-3-ol). It is note that this crystal structure was created with Swiss PDB Viewer from PDB ID. 1G85, which was determined at a resolution of 1.80 Å by X-ray diffraction.*

With regard to its ligand binding property, bOBP has one unique characteristic of having broad specificity with modest to low affinity in the micromolar range [52, 55] that can bind not only to the odorants but also to other chemical substances having no odour [56]. Some odorants are not recognized by the protein while others are bound with various degrees of strength, indicating a certain capability of discrimination by bOBP [34]. Some examples of strong ligands and non-ligands for bOBP are represented in Figure 1.14. The strong ligands usually bind with dissociation constants between 0.1 and 1 µM, while non-ligands have been classified as compounds that do not bind considerably at concentrations around 100 µM [36]. It is observed that more-or-less planar compounds, such as thymol, pyrazines, and thiazoles, are among the best ligands. The compounds that have been reported to bind tightly to bOBP include green-smelling compounds in a series of thiazoles, and floral and green odorants, all belonging to the classes of 2-tetrahydropyranyl ethers or 2-tetrahydrofuranyl ethers

[57]. In addition, other molecules of different structures, such as retinol, benzyl benzoate, and tricyclic musky-smelling compounds were found to be good ligands for bOBP [36].

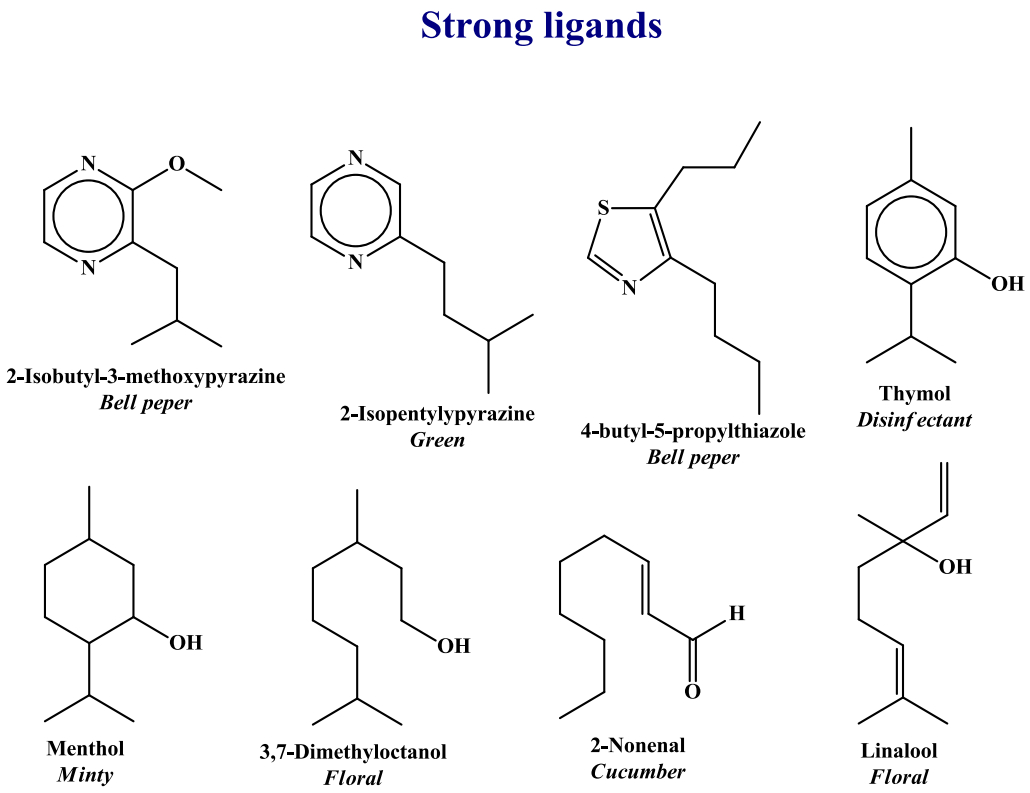

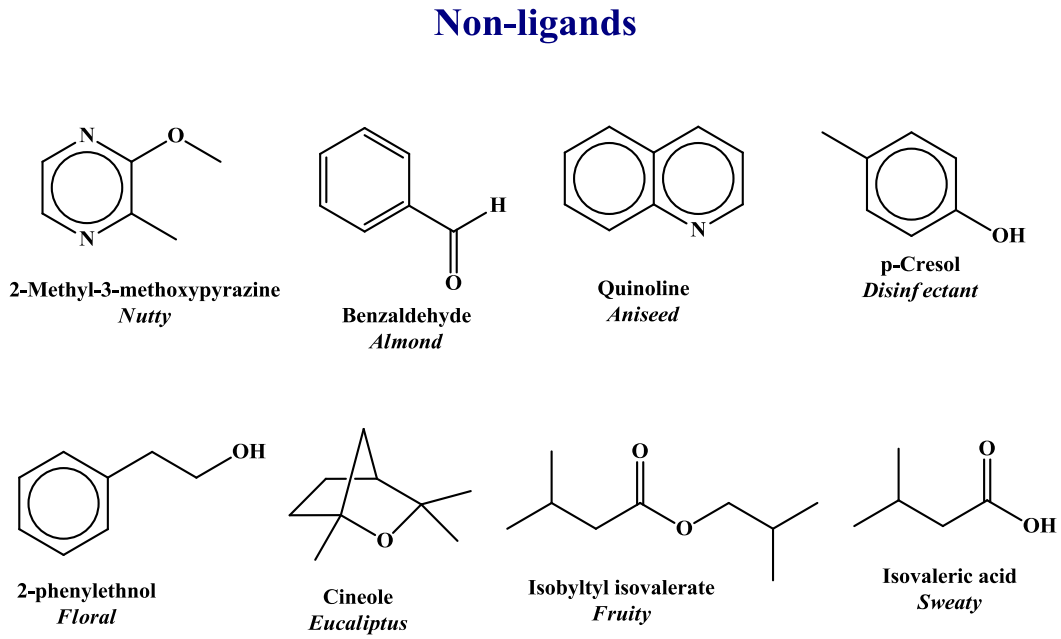

Figure 1.14: Binding of odorants to bOBP. *The strong ligands have dissociation constants between 0.1 and 1 µM. The non-ligands do not show significant binding at the concentration of 100 µM [47, 58].*

Pelosi *et al.* have summarized that the characteristics of good ligands for bOBP are medium-sized molecules with one polar group, such as hydroxy, carbonyl, or the heteroatom of an heterocycle and an extended hydrophobic area capable of assuming a planar or rather flat conformation [36]. Later, the characterization of the binding properties of pOBP [59] as well as bOBP [38] in solution and in the crystal has revealed common binding behaviours. X-ray structural analysis of binding interaction showed that odorant molecules interacted with a common set of residues forming the cavity wall, which do not exhibit specific interactions. Moreover, there are no significant conformational changes involving protein loops or backbone upon interaction with all odorants [38]. They have established that the main requirement for a ligand to match the β-barrel cavities is a high degree of hydrophobicity with a molecular mass between 160 and 200 daltons, regardless of its odorous properties, chemical class and molecular structure, particularly there is no special characteristic attributing to the good binders [38, 59].

1.5 bOBP as a Potential Biosensing Element

bOBP has been chosen in this project, because its scaffold can be considered as a potential platform for building robust, reliable, and inexpensive biosensors. The other useful characteristics of bOBP are as follows. This particular protein is well-characterized in its three-dimensional structures either alone [48, 52, 53] or in complexes with odorant molecules [38]. It can bind many structurally unrelated ligands, which means that a biosensor generally detects many different classes of compounds, and provides unique pattern recognition for each individual ligand compound [38]. This protein can also be expressed and purified in high yields from *Escherichia coli* [46] as well as eukaryotic systems [60, 61], therefore making its production easy and economical. In addition, the amino acid sequence of bOBP does not contain cysteine residues, which facilitates designing and engineering cysteine at any desired position through site-directed mutagenesis in order to conjugate with a fluorophore and/or to immobilize on a modified solid surface. This protein also tolerates point mutations even when they involve residues positioning in protein structure stabilization [46, 62]. Next, bOBP and its mutants are highly thermostable, since they can withstand temperatures up to 70-80^{o}C for mt-bOBP, and 75-85^{o}C for wt-bOBP [63]. Moreover, it is very stable to environmental conditions that might degrade or denature the proteins. Its compact fold consisting of a β-barrel makes it very durable to proteolytic degradation. Finally, the presence of the ligands in their interior cavity enhances protein stability [64]. These advantageous characteristics of bOBP will allow the possibility of using this protein as a sensing element for the creation of protein-based biosensors for the detection of chemical substances.

1.6 Inventory of Devised Biosensors Based on bOBPs

Biosensors using binding proteins instead of enzymes have rarely been reported (other than antibodies). Despite the fact that this type of biosensors could be beneficial in a more extensive range of applications due to no requirement for any reaction to occur on the analyte, but only a reversible interaction with the binding protein. Nevertheless, the main difficulty in their design is in the strategy to adopt for transducing all the necessary information about the analyte into output electrical signal that could be easily processed, leading to a direct result in monitoring and interpretation [65].

Until now there have been only a few reports on the invention of biosensors based on bOBP. M. Ikematsu has had two published patents on devising two chemical sensors for detection of a chemical substance contained in a sample. Firstly in 2002, the bOBP sensor was in a multi-well microplate by introduction of air containing odorants into the reaction solutions containing bOBP, the bonding of bOBP with the odorants has been detected by the internal fluorescence when irradiating bOBP with light [56].

In the second one in 2003, the bOBP sensor was in a cartridge layered with an immobilizer. A solution containing a sample and bOBP was fed into the micropassage of the cartridge and immobilized to the immobilizer. The chemical substance contained in the sample was detected on the basis of the quantity of immobilization of bOBP binding to the sample was compared with the reference value that is bOBP alone [66].

Then in 2008, Ramoni *et al.* presented nano-biosensors based on a mutant form of bOBP immobilized onto carbon nanotubes. The colour on/colour off bOBP-based biosensor is the application of the resonance energy transfer (RET) process for monitoring the addition of an odorant molecule to the bOBP–AMA complex, which displays the displacement of AMA from the binding site by which the carbon nanotubes become colourless [67].

Finally in 2010, a surface acoustic wave (SAW) biosensor system based on a recombinant bOBP for detection of the natural ligand (1-octen-3-ol) has been designed, fabricated and tested. bOBP was deposited on gold/aluminum multilayered interdigital transducers (IDTs) on ST-cut quartz. The differential frequency shift, due to the SAW velocity changes as consequence of odorant concentration, was measured by a Network Analyzer and showed a resolution of 44 ppb and a sensitivity of 314 Hz/ppm [68].

1.7 Aim of the Project

The aim of this project is to develop biosensors that have applications in broad detection of diverse chemical substances by using the recombinant bOBP as the biorecognition element.

The proposed bOBP-based biosensors will be generic biosensors that are hybrid devices comprising bOBP, a biological component acting as the analyte-binding site (receptor), and a signal transducer that converted the binding interaction with the analyte into a measurable signal which correlated to the concentration of the analyte target (Figure 1.15). Thus, the association of the optical transducer with bOBP is crucial for the biosensors in capable of inducing the optical signal in response to the detection of target. In this work, a fibre-optic is used as a transmitter.

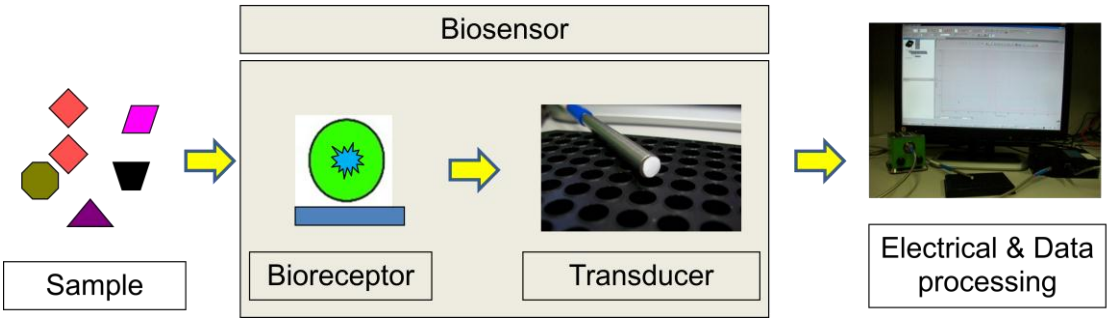

Figure 1.15: Schematic representation of the proposed biosensors based on bOBP. *bOBP (●), label (✸), solid surface (▬).*

The proposed approach will involve expression and purification of both wild type bOBP and cysteine mutants. Two alternative strategies were used; in the first, mutant bOBPs previously engineered via site-directed mutagenesis were used for site specific labelling with a probe. The proteins were characterized in their binding interaction with a number of ligands in order to select a labelling probe. A second approach used competitive displacement of 1-AMA (fluorescence when bound) by other ligands. bOBP was then be immobilized on a solid surface and characterized before being developed into a fibre-optic format. Finally, the fibre-optic bOBP biosensor was characterized.

1.8 The Application of Biosensors Based on bOBP to Thymol Determination

As a model analyte, thymol was chosen to demonstrate the application of the biosensors based on bOBP. Thymol is natural plant chemical that is largely extracted from *Thymus vulgaris* (thyme plant; a member of the mint family) and various other kinds of plants. It has a pleasant aromatic odor and strong flavor of thyme with antiseptic properties because of its phenolic structure [69, 70]. Thymol has been used as a pesticide agent [71], and as an antiseptic in mouthwash. It is an active ingredient

in Listerine® that is presented at the concentration of 0.64 mg/ml (4.3 mM) [72]. It is also the active antiseptic ingredient in some toothpaste e.g. Euthymol [73]. Thymol is also used as a preservative in an inhalational anaesthetic such as halothane (trademarked as Fluothane) [74]. Thus, detection of thymol by this biosensor could be performed as quality control tests of these items. Another application may be useful for increasing crop production by monitoring plant stresses. Aziz *et al*. presented that *Thymus vulgaris* plant which is under stress conditions releases the higher relative percentage of thymol [75].

CHAPTER 2

MATERIALS AND METHODS

2.1 Materials

2.1.1 Bacterial strains and plasmid

Bacterial strains

***E.coli* BL21(DE3)** [F^-*ompThsdS*$_B$($r_B^-M_B^-$)*gal dcm(DE3)*] from Novagen (*Nottingham, UK*) was used as a host cell containing the T7 RNA polymerase gene that is essential for expression of recombinant proteins encoded by the pET series of plasmids.

***E. coli* DH5α** [F^- Φ80d *lacZ* ΔM15 Δ(*lac*ZYA$^-$*arg*F) U169 *end*A1 *rec*A1 *hsd*R17(r_K^- m_K^+) *deo*R *thi*-1 *sup*E44 λ^- *gyr*A96 *rel*A1] was obtained from Invitrogen (*Paisley, UK*) and used as a general cloning host.

Plasmid

pET24(a)+ vector from Novagen (*Nottingham, UK*) carrying the *bobp* genes used in this project were provided by Dr. Chung-Pei Ou. Wild type and mutant sequences were confirmed by DNA sequencing prior to protein expression. pET24(a)+ contains a N-terminal T7 promoter and a C-terminal His_{10} tag sequence for purification of the recombinant protein of an IMAC (Immobilized Metal Affinity Chromatography). This vector also carries a kanamycin resistance gene, a *lac*UV5 promoter, and *lacI* promoter. The *lac*UV5 promoter controls expression of the T7 RNA polymerase in *E. coli* strain BL21(DE3), and *lacI* promoter further regulates expression of the recombinant protein from both promoters is induced by addition of IPTG. A plasmid map of the *bOBPwt* gene is shown in Figure 2.1.

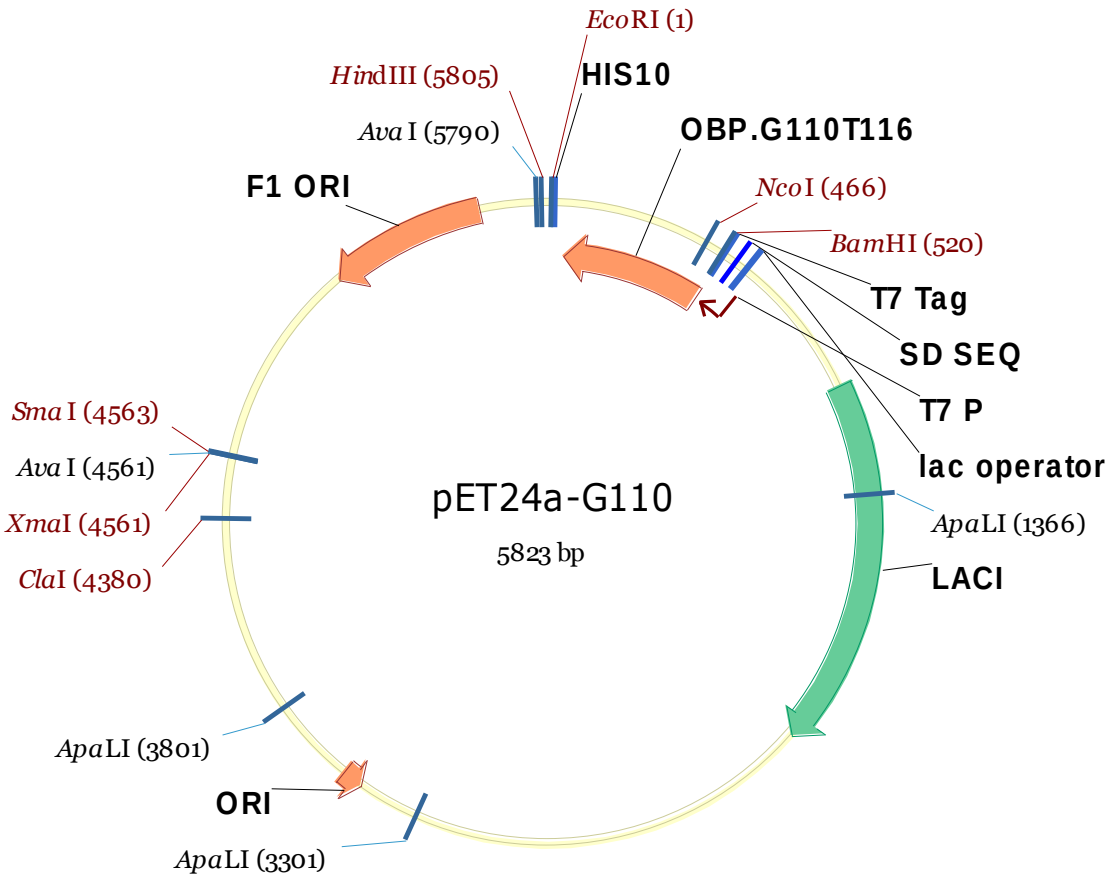

Figure 2.1: Plasmid map of the *bOBPwt* gene

2.1.2 Chemicals

2.1.2.1 General Chemicals

Yeast extract, peptone from casein (tryptone), bacterial agar, antibiotics, isopropyl-β-D-thiogalactoside (IPTG), sodium chloride, nickel sulfate, ethylenediaminetetraacetic acid (EDTA), dithiothreitol (DTT), imidazole, urea, DMSO and absolute ethanol were obtained from Sigma (Dorset, UK). PBS was from Fisher Scientific UK (Loughborough, UK). InstantBlue™ Coomassie staining was from Expedeon (Cambridgeshire, UK). Guanidine hydrochloride, potassium dihydrogen phosphate, glycerol were from VWR (Leicestershire, UK).

2.1.2.2 Main Chemicals

Ellman's reagent or DTNB (5,5'-dithiobis-(2-nitrobenzoic acid)) was purchased from Sigma-Aldrich (Dorset, UK). Its structure is shown in Figure 2.2.

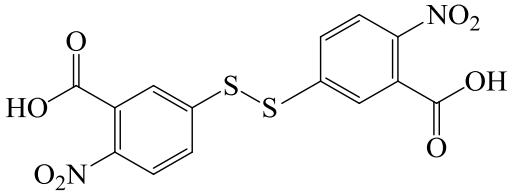

Figure 2.2: Structure of Ellman's Reagent

IANBD amide (N,N'-dimethyl-N-(iodoacetyl)-N'-(7-nitrobenz-2-oxa-1,3-diazol-4-yl)ethylenediamine) was purchased from Invitrogen (Paisley, UK). Its structure is shown in Figure 2.3.

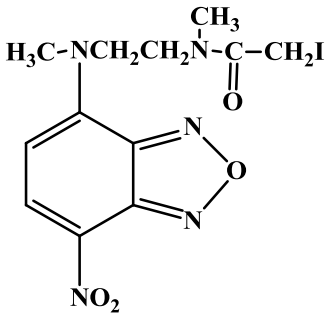

Figure 2.3: Structure of IANBD amide

1-Aminoanthracene (1-AMA) was purchased from Sigma (Dorset, UK). Its structure is shown in Figure 2.4.

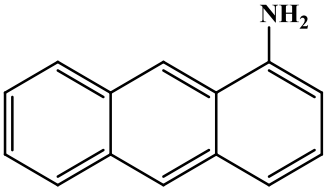

Figure 2.4: Structure of 1-AMA

2.1.2.3 Ligands

Thymol, bromocresol green, malachite green, and methyl salicylate, were purchased from Sigma (Dorset, UK). Stock solutions of these chemicals were prepared either in DMSO (bromocresol green and malachite green) or in absolute ethanol (thymol and methyl salicylate), and then further diluted in PBS with 1mM EDTA supplement, pH 7.4. Their structures are shown in Figure 2.5 A-D.

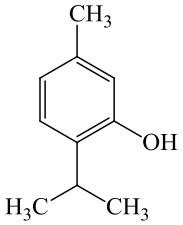

(A) Thymol

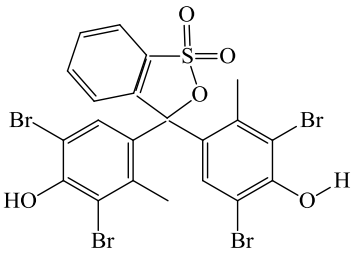

(B) Bromocresol green

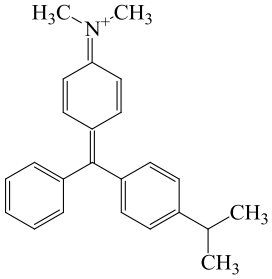

(C) Malachite green

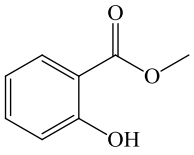

(D) Methyl salicylate

Figure 2.5: Structures of ligands. *(A) Thymol, (B) Bromocresol green, (C) Malachite green, and (D) Methyl salicylate.*

2.1.2.4 Chromophores

DTNB, bromocresol green, cibacron blue, thionin, benzohydroxamic acid, nickel(II) chloride, p-nitroaniline, potassium permanganate, 1,2-phenylenediamine dihydrochloride, potassium chromate, 3,4-dinitrotoluene, copper(II) nitrate, iodine, 4-nitrophenol, and 1-aminoanthracene were obtained from Sigma (Dorset, UK).

2.1.3 Culture media, stock solutions, and buffers

All solutions were prepared in water purified by reverse osmosis ion exchange and carbon filtration in a MilliQ water purification system.

LB medium

1% bacto-tryptone, 1% NaCl, 0.5% yeast extract, autoclaved.

LB agar

LB medium with 1.5% agar, autoclaved.

SOC

0.5% Yeast Extract, 2% Tryptone, 10 mM NaCl, 2.5 mM KCl, 10 mM MgCl2, 10 mM MgSO4, 20 mM Glucose

Kanamycin solution (Km)

25 mg/ml in water, sterilized by filtration through 0.2 µM membrane

Isopropyl-β-D-thiogalactopyranoside (IPTG)

1 M in water, sterilized by filtration through 0.2 µM membrane

Binding buffer

20 mM imidazole, 500 mM sodium chloride, 100 mM phosphate buffer pH 7.2

Washing buffer

50 mM imidazole, 500 mM sodium chloride, 100 mM phosphate buffer pH 7.2

Elution buffer

600 mM imidazole, 500 mM sodium chloride, 100 mM phosphate buffer pH7.2

Stripping buffer

6 M guanidine HCl, 0.2 M acetic acid

Recharging buffer

100 mM Nickel sulphate

Phosphate buffer saline (PBS)

PBS with 1 mM EDTA supplement, pH 7.4

4×SDS-PAGE loading buffer

0.2 M Tris-Cl pH 6.8, 0.4 M 2-mercaptoethanol, 0.4% (w/v) bromophenol blue, 8% (w/v) SDS, 40% (w/v) glycerol.

Denaturing buffer

8 M urea in PBS, pH 7.4, containing 1 mM EDTA

Ellman's reagent solution

10 mM (4.0 mg/mL) DTNB in absolute ethanol

2.1.4 Apparatus

A HisPrep™ FF 16/10 column that was prepacked with pre-charged Ni Sepharose™ 6 Fast Flow and used for preparative purification of histidine-tagged recombinant bOBPs was from GE Healthcare. PhastGel Gradient 8-25 and Strips SDS were obtained from Amersham (Buckinghamshire, UK). Microplate Microfluor 1, 96 well flat bottom polystyrene solid black well plates were from Thermo Scientific. The Lambda 25 UV/Vis spectrometer was from Perkin-Elmer (Massachusetts, USA). The SpectraMax^{TM} Gemini XS microplate spectrofluorometer was from Molecular Devices (Sunnyvale, USA). Data was analysed using Softmax Pro Version 3.1.1 software.

The instruments for engineering the fibre-optic biosensor based on bOBP are shown in Figure 8.6. The instrumental configuration consisted of an bOBP immobilized membrane, an excitation light-emitting diode (LED) light source (LLS-385, Ocean Optics; 3.86mW at 385nm), a tight bundle of 7 pure silica optical fibres in a stainless steel ferrule (6 illumination fibres around 1 read fibre) (Ocean Optics; 2m long, 400µm diameter), a 2048-element CCD array detector system (Sony, product no. ILX511) of a high-resolution spectrometer (HR2000, Ocean Optics; 200-643nm grating, a 50µm entrance slit, an L2 detector collection lens), the reflection probe (Ocean Optics; 76.2 mm long for probe ferrule), and a laptop (HP 6360b) with the SpectraSuite software.

2.2 Methods

2.2.1 Production of the recombinant bOBPs

2.2.1.1 Expression of the Recombinant bOBPs

2.2.1.1.1 Transformation of plasmid DNA

50 µl of competent cells were mixed with 1-2 ng of plasmid DNA, incubated on ice for 30 minutes, and heat shocked at 42˚C for 45 seconds in a water bath. They were then placed on ice for 1 min, after that they were added to 200 µL of SOC medium and incubated at 37˚C with shaking at 200 rpm for 1 hour. The cells were transferred on LB agar plates with 10 µg/ml kanamycin and spread with sterilised plastic rods. The plates were then incubated at 37˚C overnight (approximately 16 hours) for growth.

2.2.1.1.2 Extraction of plasmid DNA

The plasmid extraction and purification were performed using QIAprep Spin Miniprep Kit (QIAGEN, *West Sussex, UK*) according to the manufacturer's instructions.

2.2.1.1.3 Expression of protein

3 ml scale expression

Small-scale protein expression was carried out to examine the protein expression by inoculating a single colony of *E. coli* BL21(DE3) encoding the recombinant *bobpwt* gene into 3 ml of LB^{Km} medium. It was grown overnight at 37°C with shaking at 200 rpm. Expression of proteins was induced by addition of IPTG to a final concentration of 1 mM. 100 µl aliquots of induced and non-induced cells were collected at 2 hour intervals after induction and centrifuged at 12,000 rpm to collect the cell pellet. The packed cells were then lysed in 30 µl of SDS gel-loading buffer, and heated at 100°C for 3 min. The protein expression was assessed by SDS-PAGE.

7 l scale expression

A colony showing good protein expression was selected and inoculated into 70 ml LB^{Km} medium and grown overnight. The cells were then used to inoculate 7 litres of LB^{Km} medium, and incubated at 37^{o}C with shaking at 200 rpm. When the OD_{600} of cell culture reached 0.6, IPTG was added to a final concentration of 1 mM. The induced cells were incubated at room temperature for overnight before harvesting the cells by centrifugation at 5,000 rpm for 30 minutes. The supernatant was discarded, and the packed cells were stored at -80^{o}C until use.

2.2.1.2 Purification of the Recombinant bOBPs

2.2.1.2.1 Cell lysis

The cell pellet was resuspended in 40 ml binding buffer before being lysed by using a French Press operated at a pressure of around 11,000 psi. The procedure was repeated for 2-3 rounds for obtaining the clear and slightly viscous solution. The lysed solution was then centrifuged at 18,000 g for 30 min to separate the soluble and insoluble fraction of the recombinant protein. Cell debris and inclusion bodies remained in the pellet. The supernatant was further filtered by passing through a 0.2 µm disk filter in order to prevent blocking the purification column.

2.2.1.2.2 Chromatographic column preparation

The purification of bOBP involves using an Amersham Pharmacia XK16/20 column and a nickel-chelated nitrotriacetate (NTA) resin as a chromatographic medium. The column was attached to a P1 pump that controlled the flow rate. The column was filled with NTA resin to a final volume of 30 ml. Before purification, fresh Ni-NTA resin was packed in the column, washed with 3 volumes of filtered purified water, and equilibrated with 3 volumes of binding buffer before use. After purification the used resin was regenerated with 2 volumes of stripping buffer, and washed with 5 volumes of water before and after being washed with 2 volumes of recharging buffer.

2.2.1.2.3 Protein purification

The filtered solution was applied to the resin, and allowed to circulate in the column overnight in which the outlet of the XK16/20 column was connected with the inlet of the P1 pump with a flow rate of 20 ml/min. After that five column volumes of binding buffer were flowed through the resin. Another five volumes of washing buffer was then applied to elute low-affinity binding molecules. The protein was eluted by applying elution buffer. The collection of the protein was monitored with an online UV detection at 280 nm and then SDS-PAGE. The eluted protein solution was then concentrated and desalted using a Vivaspin 20 column from Sartorius Stedim Biotech. The purified protein was divided into small aliquots (50 µl) and kept at -80^{o}C.

2.2.1.2.4 Protein electrophoresis (SDS-PAGE)

Protein samples were analysed by SDS-PAGE using the PhastSystem (*GE Healthcare, Amersham, UK*). The samples were resuspended in 1×SDS-PAGE loading buffer, heated at 100°C for 3 minutes before loading into pre-cast gradient gels with an acrylamide concentration either 10-15% or 8-25%. Denaturing SDS buffer strips and Sigma low molecular weight marker (97k, 66k, 45k, 30k, 20k, and 14.4k) were used. The gel was stained using the Coomassie based protein stain InstantBlue (*Expedeon, Cambridgeshire, UK*).

2.2.1.2.5 Estimation of protein concentration

Concentrations of the protein samples were determined by means of their absorbance spectra obtained with a NanoDrop® ND-1000 UV-Vis Spectrophotometer and using the extinction coefficient of the wt bOBP (ε_{280} = 47,000 M^{-1} cm^{-1}) as derived from the aromatic residue content [76].

2.2.2 CD spectroscopy of thymol binding to bOBP

2.2.2.1 Near-and Far-UV CD Measurements

The circular dichroism (CD) spectra were recorded on a Jasco J-715 spectropolarimeter, equipped with a Peltier cell holder thermostatted at 20°C, using 1mm pathlength quartz cells. Each spectrum was an average of at least three accumulated scans with subtraction of the baseline recorded for 0.01X PBS solution [10mM potassium phosphate and 10µM EDTA (pH 7.4)] that was solvent of the protein and ligand solutions.

The near-UV CD spectra were scanned from 240−340nm. The concentration of the protein and ligand used was 200µM bOBP for the reaction of free bOBP, and 200µM bOBP and 200µM thymol for the reaction of thymol-bound bOBP complexes in 300µl total volume. In case of the far-UV CD, the spectra of reactions were scanned from 185−260nm. The concentration of the protein and ligand used was 5µM bOBP for the reaction of free bOBP, and 5µM bOBP mixed with 100µM thymol for the reaction of thymol-bound bOBP complexes in 300µl total volume.

2.2.2.2 Thermal Denaturation

Thermal unfolding of bOBP in the presence and absence of thymol was studied by recording the CD signal at 195nm as a function of temperature every 2°C from 20°C up to 98°C with the heating rate of 45°C/hr. Simultaneously, far-UV CD spectra between 185 and 260nm were also collected. The protein concentration was 5µM bOBPwt and the ligand concentration was 100µM thymol, by that they were dissolved in 0.01X PBS with 10µM EDTA supplement, pH 7.4. The quartz cuvette was 1mm pathlength. The thermal unfolding curves were analysed by either direct fitting the data to the Boltzmann sigmoidal function (Equation 5.1) or from the first derivative of the data using either SciDAVis or OriginPro8.5 or Prism5.0. It is noted that mean values of thermodynamic parameters in this study were obtained from three independent CD measurements.

2.2.3 Characterization of the recombinant bOBPs with DTNB and IANBD amide

2.2.3.1 Calculation of the Solvent Accessible Surface Areas (SASA) of Cysteine Residues in the Recombinant bOBPs

The three-dimensional (3D) models of bOBP-WT, bOBP-I22C, bOBP-S24C, bOBP-F54C, and bOBP-F91C were constructed on the basis of the crystallographic structures of complexes with each of eight different ligand complexes. The eight different files available in PDB were as following: 1). 1-octen-3-ol (PDB ID. 1G85), 2). Benzophenone (PDB ID. 1GT5), 3). a selenium containing odorant (PDB ID. 1PBO), 4). Undecanal (PDB ID. 1GT4), 5). Unknown atom or ion (PDB ID. 1OBP), 6). 1-Octen-3-ol and 1-Aminoanthracene (PDB ID. 1HN2), 7). 1-Octen-3-ol and 2,6-Dimethyl-7-octen-2-ol (PDB ID. 1GT3), 8). 1-Octen-3-ol, 1-Aminoanthracene, and 2-Isobutyl-3-methoxypyrazine (PDB ID. 1GT1). It should be noted that the DNA derived sequence of the recombinant bOBPs used in this thesis showed differences from the sequences of the native protein described in the papers. These are in addition to the cysteine mutations, a N-terminal T7 promoter and a C-terminal His_{10} tag. These differences are shown in Table 2.1. For each X-ray structure file, the ‘Mutate’ tool in DeepView was used to change all the residues to match the recombinant bOBP-WTsequence by introducing the relevant cysteine mutation. Finally, the SASA of each cysteine residue was calculated using the UCSF Chimera program.

Table 2.1: Differences of DNA sequence between the native protein described in the papers and the sequences from the recombinant bOBPs used in work, excluding their N-terminal T7 promoter and C-terminal His_{10} tag.

Position	Amino acid in native bOBP derived from x-ray structure								Amino acid in recombinant bOBP derived from DNA sequencing				
	PDB ID (reference)												
	1G85 [54]	1GT5 [38]	1PBO [77]	1GT4 [38]	1OBP [53]	1HN2 [54]	1GT3 [38]	1GT1 [38]	bOBP-WT	bOBP-F54C	bOBP-I91C	bOBP-I22C	bOBP-S24C
22	Ile	Ile	Ile	Ile	Ile	Ile	Ile	Ile	Ile	Ile	Ile	**Cys**	Ile
24	Ser	Ser	Ser	Ser	Ser	Ser	Ser	Ser	Ser	Ser	Ser	Ser	**Cys**
54	Phe	Phe	Phe	Phe	Phe	Phe	Phe	Phe	Phe	**Cys**	Phe	Phe	Phe
91	Ile	Ile	Ile	Ile	Ile	Ile	Ile	Ile	Ile	Ile	**Cys**	Ile	Ile
110	Gly	Gly	Gly	Gly	Gly	Gly	Gly	Gly	Gly	Gly	Gly	**Ser**	**Ser**
112	**Thr**	**Thr**	Lys	**Thr**	**Thr**	**Thr**	**Thr**	**Thr**	Lys	Lys	Lys	Lys	Lys
116	Thr	Thr	Thr	Thr	Thr	Thr	Thr	Thr	Thr	Thr	Thr	**Ala**	**Ala**
117	Gly	**Glu**	Gly	**Glu**	Gly	**Glu**	**Glu**	**Glu**	Gly	Gly	Gly	Gly	Gly
154	Asn	Asn	**Asp**	Asn	**Asp**	Asn	Asn	Asn	Asn	Asn	Asn	Asn	Asn

2.2.3.2 Quantification of Free Thiol Groups Based on the Reaction with Ellman's Reagent

To test that no additional cysteine residue had been accidently introduced during the PCR amplification steps, the protein was reacted with Ellman's reagent. It is necessary to expose the thiol group, which is buried in the interior of the protein. 5,000µM of the five recombinant bOBPs were therefore dissolved in denaturing buffer (8M urea in PBS, pH 7.4, containing 1mM EDTA). Each of the five bOBP sample reactions contained 99µl of 10µM bOBPs in denaturing buffer and 1µl of 10mM DTNB solution (4.0mg in 1ml absolute ethanol). The reference reaction consisted of 99µl of denaturing buffer and 1µl of 10mM DTNB solution. Therefore, the final concentration of resulting reactions was composed of 10µM bOBPs, 8M urea buffer, 100µM DTNB, and had 1% ethanol. The reactions were then mixed, recorded their absorbance at 412nm at room temperature and monitored the measurement every 1min for 15min or until there was no further change. Absorbance measurements were carried out with a Perkin Elmer's Lambda 25 UV/Vis spectrometer. The concentration of sulfhydryls in the samples was calculated from the molar extinction coefficient of TNB at 412nm ($14{,}290 M^{-1}cm^{-1}$) for 8M urea buffer solvent.

2.2.3.3 Reaction of IANBD Amide with Thiol

2-mercaptoethanol as a thiol was used to react with IANBD amide. The experiments were carried out in black 96-well microtitre plates with 100µl total volume containing 90µl of 10-fold molar excess 2-mercaptoethanol diluted in PBS with 10mM EDTA supplement, pH 7.4, and 10µl of various IANBD amide concentrations ranging from 0–307.2µM (final concentration). Each reaction contained 1% DMSO final concentration and was added in triplicate in the plate. The reactions were incubated at room temperature for 1 hour with shaking at 50 rpm in the dark before being measured their fluorescence using the Gemini XPS microplate spectrofluorometer with the excitation at 480nm and emission at 550nm.

2.2.3.4 Reaction of IANBD Amide with bOBPwt

The experiments were carried out in black 96-well microtitre plates with 100µl total volume containing 98µl of 20µM 2-mercaptoethanol diluted in PBS with 10mM EDTA supplement, pH 7.4, and 1µl of 2µM (final concentration) IANBD amide. Each reaction contained 1% DMSO final concentration and was added in triplicate in the plate. The reactions were incubated at room temperature for 1 hour with shaking at 50rpm in the dark before adding 1µl of various bOBPwt concentrations ranging from 0 – 40.96µM (final concentration). The reactions were then continued incubating at room temperature for another 1 hour with shaking at 50rpm in the dark before being measured their fluorescence using the Gemini XPS microplate spectrofluorometer with the excitation at 480nm and emission at 550nm. Titration curve was analyzed by fitting the data to an equation derived from simple binding equation (Equation 5.3) to yield the equilibrium dissociation constants (K_d). Analyses were carried out by using either SciDAVis or Origin 8.5 software.

2.2.3.5 Determination of Molar Binding Ratio of IANBD Amide and bOBPwt

100µM bOBPwt was incubated with a 10-fold molar excess of IANBD amide in PBS with 10mM EDTA supplement, pH 7.4 with 1% DMSO final concentration. The labeling reaction was carried out at room temperature for 1 hr in the dark, and terminated by addition of 2-mercaptoethanol to a final concentration of 1mM. The excess label in the labeling reaction was removed using a Vivaspin 500 centrifugal filter. The Vivaspin 500 column was first filled up with filtered deionised water to maximum volume (500µl) and spun at 12,000 x g for 2 minutes in a pre-rinsing step suggested by the manufacturer's manual to remove trace amounts of glycerine and sodium azide on the membrane. The rinsed column was then equilibrated with 500µl of PBS by centrifugation at 12,000 x g for 2 minutes and residues (< 5µl) were removed before being loaded with the labeling solution, and centrifuged at 12,000 x g for 5 minutes to remove the unbound label. The columns were washed with 500µl PBS

for three times to remove the excess label and concentrate the labeled protein solution at the same time. The labeled protein was then subjected to absorbance measurement immediately at 280nm for the bOBP protein and at 480nm for the fluorophore IANBD amide by NanoDrop® ND-1000 UV-Vis Spectrophotometer. A molar ratio of the reaction between the protein and the fluorophore was calculated using the Beer-Lambert's Law with the absorbance values measured, and the extinction coefficients of the bOBPwt; 47,000 M^{-1} cm^{-1} at 280nm [54] and IANBD amide; 25,000 M^{-1} cm^{-1} at 480nm [78].

2.2.4 Fluorescence and absorbance spectroscopy of bOBP-ligand interactions

2.2.4.1 Fluorescence Spectral Analysis of 1-AMA

In order to determine the maximum emission wavelength of the bOBP/1-AMA complex, the excitation wavelength was fixed, and the emission wavelength was fixed when the maximum excitation wavelength was determined. Measurements were performed on a Gemini XS microplate spectrofluorometer. The fluorescence excitation and emission spectra of the bOBP/1-AMA complex were scanned by having recorded at 10nm intervals. Emission spectra were recorded from 400nm to 600nm. Excitation spectra were recorded from 320nm to 460nm. The reaction of the bOBP/1-AMA complex consisted of 100µM bOBP and 100µM 1-AMA (1:1) in PBS with 1mM EDTA supplement, pH 7.4. Free 1-AMA was used as a background. The DMSO concentration in the final solution was equal to 0.1% (v/v). Each reaction was added in triplicate with at least three repetitive separate experiments.

2.2.4.2 A Binding Assay Based on 1-AMA

The fluorescence binding assay of 1-AMA to bOBPwt was carried out according to the method published by [54] with minor modifications. The stock solutions of 1-AMA in DMSO were freshly prepared in the dark. The experiments were carried out in black 96-well microtitre plates with 100µl total volume containing 99µl solution of various 1-AMA concentrations ranging from 0 to 12.8µM in PBS with 1mM EDTA supplement, pH 7.4, with 0.1% DMSO, and 1µl of 50µM bOBPwt (final bOBP monomer concentration was 0.5µM) by which the 1-AMA solution without bOBPwt addition was used as a background for comparison. Each reaction was added in triplicate and incubated at room temperature for 1 hour in the dark to have a stable signal, before being measured their fluorescence using a Gemini XS microplate spectrofluorometer with the excitation wavelength at 390nm (9 nm-bandwidth). The formation of the bOBP/1-AMA complex was detected by the increase of the fluorescence emission intensity at 490nm (9 nm-bandwidth). All trials were run with at least three repetitive separate experiments. Intensities from bOBP/1-AMA complex were corrected for contributions from unbound 1-AMA. Based on the assumption that one molecule of 1-AMA per monomer of bOBP, the dissociation constant (K_d) value of the AMA-bOBPwt complex was determined by fitting the binding curve to a single-site specific binding model; $Y = B_{max} * X / (K_d + X)$ (Equation 6.1). Data and error analysis were carried out by using either SciDAVis or OriginPro8.5 or Prism5.0.

2.2.4.3 Competitive Binding Assays with 1-AMA

The K_d values of complexes between the bOBPwt and the different ligands, particularly thymol, bromocresol green, malachite green, and methyl salicylate, were determined by competitive binding tests with the fluorescent ligand 1-AMA as previously described for other ligands [38, 46, 54, 59]. In the competitive binding assays, 1µM bOBPwt were incubated at room temperature for 1 hour with a fixed amount of 1µM AMA in the presence of increasing concentrations of each ligand (0–100µM). The reaction was in PBS with 1mM EDTA supplement, pH 7.4 with the final

concentration of 0.1% (V/V) DMSO solvent and 0.1% (V/V) absolute ethanol. The binding of the competitors to bOBPwt was followed as a decrease of the fluorescence emission of the 1-AMA/OBP complex at 490nm upon excitation at 390nm. In order to obtain the apparent dissociation constants (K_d^{app}) for the binding complexes, the competition curve for each ligand was analysed with the single-site specific binding model (Equation 6.1). The corrected K_d values were then calculated from apparent K_d using the formula [54] shown in Equation 6.3. Data and error analysis were carried out by using either SciDAVis or OriginPro8.5 or Prism5.0. The data reported were the average of triplicate from at least three determinations.

2.2.4.4 Dual Ligand Titration with 1-AMA

The analysis of the effect of two ligands, 1-AMA and thymol in competitive binding assay was carried out in order to estimate the equilibrium K_d values of thymol. The experimental set up involved with titration of a fixed amount of 0.5µM bOBPwt with varying 1-AMA and thymol concentrations. A set of the standard ligand titration of 0.5µM bOBPwt with 1-AMA ranging from 0–12.8µM, was added with a concentration of thymol. The concentrations of thymol used in each set of experiments were 0, 0.1, 10, 25, 50, and 100µM. The reaction was in PBS with 1mM EDTA supplement, pH 7.4 with the final concentration of 0.1% (v/v) DMSO and 0.1% (v/v) ethanol. Each reaction was added in triplicate and incubated at room temperature for 1 hour in the dark to have a stable signal, before being measured their fluorescence using a Gemini XS microplate spectrofluorometer with the excitation wavelength at 390nm. The K_d value of the thymol - bOBPwt complex was followed as the formation of the bOBP·1-AMA complex in the presence of each thymol concentration, which detected by the increase of the fluorescence emission intensity at 490nm. The titration curves plotted between fluorescence intensities of the bOBP·1-AMA complex at each thymol concentration against 1-AMA concentrations were used to determine for the K_d values of the 1-AMA/bOBPwt complexes by fitting to a single-site specific binding model (Equation 6.1). Then, the curve plotted between -log K_d of the 1-AMA/bOBPwt complexes at each thymol concentration against their corresponding thymol

concentrations were calculated for the equilibrium K_d values of the thymol/bOBPwt complexes based on global nonlinear regression method of Lew and Angus; - log K_d^{AMA} = - log ([L] + $10^{\log (Kd)}$) + C (Equation 6.4) [79]. Data and error analysis were carried out by using either SciDAVis or OriginPro8.5 or Prism5.0. All trials were run for at least three repetitive separate experiments.

2.2.4.5 Titration of Chromophore with bOBPwt

The titration absorption spectra studies were performed by keeping constant the concentration of chromophore at 2µM while varying the protein concentration at room temperature. Initially, the blank buffer solution of PBS with 1mM EDTA supplement, pH 7.4 used as a reference was placed in the micro UV cuvette (8.5mm centre height of the light path), and then the first spectrum was recorded in the range 200-1,000 nm on a Perkin Elmer Lambda 20 UV/VIS spectrophotometer. During titration, 99µl of buffered bOBPwt solution at the concentration ranging from 0-19.2µM was added with 1µl of 0.2mM chromophore (giving 1% DMSO to the reaction). The solutions were mixed; the UV-vis absorption spectra and/or the absorbance at maximum wavelength were then recorded.

2.2.4.6 Competitive Binding Assays with Chromophore

The competitive binding studies with chromophore were performed by keeping constant the concentration of bOBP and chromophore while varying the thymol concentration at room temperature. The blank buffer solution of PBS with 1mM EDTA supplement, pH 7.4 used as a reference was placed in the micro UV cuvette (8.5mm centre height of the light path), and then the absorbance at maximum wavelength was recorded on a Perkin Elmer Lambda 20 UV/VIS spectrophotometer. In the competitive binding assays, 98µl of buffered 1.25µM bOBPwt solution was added with 1µl of 0.2mM chromophore in the presence of increasing concentration of thymol (0, 0.0001, 0.001,…100µM). The final concentration contained 1% (V/V)

DMSO solvent and 0.1% (V/V) absolute ethanol. The solutions were mixed, incubated at room temperature for 1 hour. The binding of the thymol competitor to bOBPwt was followed as a decrease of the absorbance of the chromophore/OBP complex at their maximum wavelength.

2.2.5 Immobilization of bOBP on solid surfaces

2.2.5.1 Screening of Solid Surfaces for Immobilization of bOBP

Ten different commercially available solid surfaces were immobilized with wild type bOBP in order to examine their biocompatibility with bOBP function using 1-AMA as a probe. The details of the supports comprising their trade names, wettability, pore sizes, and particularly binding mechanisms are shown in Table 7.1. The immobilization on epoxysilane coated slide and 96-well nickel coated microtitreplate were performed according to the Nexterion® Slide E protocols for protein application, and HIS-Select® High Capacity (HC) technical bulletin, respectively. For coupling membranes, disks of 5mm in diameter were punched out of the membrane with the hole punch. 25µl of 100µM bOBP solution was supplied to the membrane placed in 96-well microtitre plate for 5min. Adsorption occurs spontaneously at room temperature. After coupling, the membranes were washed in 25µl of PBS solution containing 1mM EDTA, pH 7.4. The membranes were then placed in 25µl of 100µM 1-AMA for 5 min before being rinsed with 25µl of PBS solution containing 1mM EDTA, pH 7.4. It is noted that the final concentration of DMSO was 0.1%. Fluorescence measurements were performed with a SPECTRAmax GEMINI XS spectrofluorometer. Excitation was 390nm, and the fluorescence was measured at the emission maximum of 490nm.

2.2.5.2 Amount of bOBP Immobilized on Nitrocellulose

The extent of total bOBP immobilized on nitrocellulose was estimated by the Protran^{TM} nitrocellulose membrane with 0.5-cm diameter was placed in 25µl of bOBP solution with each concentration of 0, 1, 10, 40, 70 and 100µM, and allowed binding for 5min. The volume and OD_{280} of the bOBP solution before and after immobilization were then measured.

2.2.5.3 Titration of bOBP and 1-AMA on Nitrocellulose

Optimum concentrations of bOBP and 1-AMA for immobilization on nitrocellulose were determined by titration of bOBP and 1-AMA. The Protran^{TM} nitrocellulose membrane (0.5-cm diameter) was placed in 25µl of a concentration of bOBP solution (0, 1, 10, 40, 70, 100µM) for 5min and then washed with 25µl of PBS solution containing 1mM EDTA, pH 7.4 in order to remove the unbound protein. Next, each concentration of the immobilized bOBP was incubated with 25µl of a concentration of 1-AMA solution (0, 1, 10, 40, 70, 100µM) for 5min. After that the membranes were washed with 25µl of PBS solution containing 1mM EDTA, pH 7.4. The final concentration of DMSO was 0.1%. Finally, the fluorescence of each immobilized membrane was measured by using a SPECTRAmax GEMINI XS spectrofluorometer with excitation at 390nm and emission at 490nm. The fluorescence intensities of bOBP/1-AMA complex on nitrocellulose were thus plotted against respective concentration of bOBP as well as that of 1-AMA.

2.2.5.4 Amount of Functional bOBP Immobilized on Nitrocellulose

The quantity of functional bOBP immobilized on nitrocellulose was determined by the Protran^{TM} nitrocellulose membrane (0.5-cm diameter) was immersed into 25µl of a concentration of bOBP solution (0, 1, 10, 40, 70 and 100µM) for 5min, and washed with 25µl of PBS solution containing 1mM EDTA, pH 7.4. The 25µl of the stoichiometric 1-AMA was then added to the membranes for 5min, and washed again with 25µl of PBS solution containing 1mM EDTA, pH 7.4. After that the membranes were measured the emission intensity at 490nm with a SPECTRAmax GEMINI XS spectrofluorometer at a fixed excitation wavelength of 390nm. It is noted that the final concentration of DMSO was 0.1%.

The fluorescence calibration curve of the binding interaction between bOBP and 1-AMA was performed in the solution phase by 99µl of 1-AMA was added with 1 µl of bOBP with the stoichiometric final concentration of 0, 1, 10, 40, 70, and 100µM. The final concentration of DMSO was 0.1%. The binding reactions were incubated for 5min at room temperature. The fluorescence emission intensity at 490nm was recorded at a fixed excitation wavelength of 390nm using a SPECTRAmax GEMINI XS spectrofluorometer. Lastly, the corrected fluorescence intensities of the bOBP·AMA complex formation were derived by subtracting the fluorescence intensities of the backgrounds of individual bOBP and 1-AMA at their corresponding concentrations.

2.2.5.5 Effect of Immobilization Method for bOBP and 1-AMA on Nitrocellulose

Two different immobilization methods of bOBP and 1-AMA on nitrocellulose were performed in order to obtain the optimum immobilization method for the bOBP biosensor. The first method was individual immobilization of bOBP and 1-AMA step by step as the same as previously treated in section 7.1 – 7.4. The Protran^{TM} nitrocellulose membrane (0.5-cm diameter) was immersed in 25µl of 100µM bOBP solution for 5min and washed with 25µl of PBS solution containing 1mM EDTA, pH 7.4. The immobilized bOBP was then immersed in 25µl of 100µM 1-AMA solution

for 5min and washed again with 25µl of PBS solution containing 1mM EDTA, pH 7.4. The second method was the immobilization of bOBP/1-AMA complex by which the solution of the mixture consisting of 25µl of 100µM bOBP and 25µl of 100µM 1-AMA was added to the Protran^{TM} nitrocellulose membrane (0.5-cm diameter) for 5min. Then, the membrane was washed with 25µl of PBS solution containing 1mM EDTA, pH 7.4. The influence of this factor was evaluated by measuring S/B ratio. There were three different backgrounds, including PBS (containing 1mM EDTA, pH 7.4), 100µM 1-AMA, and 100µM bOBP backgrounds. The emission fluorescence intensity at 490nm was measured by a SPECTRAmax^{TM} GEMINI XS spectrofluorometer with excitation at 390nm.

2.2.6 Development of fibre-optic sensor based on bOBP

2.2.6.1 Construction of Fibre-Optic Biosensor Based on bOBP

The fibre-optic biosensor based on bOBP was constructed as shown in Figure 8.6. This is an extrinsic sensor with bOBP immobilized on a nitrocellulose membrane disk and mounted to the front surface of the probe at the end of a bifurcated bundle of optical fibres that were in turn connected to the light source and the spectrometer. Light from the LLS-385 light-emitting diode (LED) light source (at 385nm) was directed through one leg of a bifurcated bundle of optical fibres to the probe tip where the bOBP immobilized membrane disk is located. The light intensity emitted by the bOBP immobilized membrane was monitored by transmission through the second leg of silica fibre and impinging onto the 2048-element CCD array detector system of a HR2000 high-resolution spectrometer covering a wavelength range of 200nm to 643nm, with a 50µm entrance slit and an L2 detector collection lens. The HR2000 spectrometer was connected to a laptop with the supplied SpectraSuite software. The fluorescence emission signal was collected at 490nm. The integration time was set at 1 second. All experiments were carried out in the dark in order to avoid ambient light interference. For the reduction of possible photobleaching of 1-AMA, the light source was switched on only when readings were being taken.

2.2.6.2 Signal to Background Ratio of Fibre-Optic Biosensor Based on bOBP

The fibre-optic bOBP biosensor initially had its S/B ratio determined for based on three different backgrounds, which were PBS containing 1mM EDTA (pH 7.4), 1-AMA, and bOBP. The fibre-optic bOBP biosensor was compared to both the solution measurements and the membrane bound protein in a microplate reader. Solution-phase protein format consisted of 100µ1 of 1µM bOBP/1µM 1-AMA mixture solution and the signal was then measured by using the SPECTRAmax^{TM} GEMINI XS microplate spectrofluorometer. The signal of bOBP immobilized membrane format was obtained from 25µ1 of 100µM bOBP/25µ1 of 100µM 1-AMA mixture solution was immobilized on 0.5cm nitrocellulose disk and fluorescence intensity was detected by using the SPECTRAmax™ GEMINI XS microplate spectrofluorometer. The signal of fibre-optic bOBP biosensor format was obtained using 25µ1 of 100µM bOBP/25µ1 of 100µM 1-AMA mixture solution to immobilize on 0.5cm nitrocellulose disk and fluorescence intensity was detected by using the fibre-optic system shown in Figure 8.6.

2.2.6.3 Limit-of-Detection (LOD) of Fibre-Optic Biosensor Based on bOBP for Thymol in Liquid Phase

The limit-of-detection (LOD) for thymol in the liquid phase was determined to provide a quantitative comparison of the utility of the fibre-optic bOBP biosensor with other two bOBP biosensing formats. The competitive binding assays with thymol in the liquid phase have been accomplished on the solution-phase and the immobilized protein. Different concentrations of thymol solution ranging from 0-100µM were added to each biosensing formats in triplicate and then incubated for 1 hour at room temperature. The amounts of thymol-bound bOBP were determined by measuring 1-AMA fluorescence at 490nm. bOBP solution phase format that composed of 100µ1 of 1µM bOBP, 1µM 1-AMA, and thymol was monitored the fluorescence signal by SPECTRAmax™ GEMINI XS microplate spectrofluorometer. bOBP immobilized

membrane format was analyzed by incubating the immobilized membrane containing 25µ1 of 100µM bOBP/25µ1 of 100µM 1-AMA mixture with 25µl of thymol, and detected by using SPECTRAmax™ GEMINI XS microplate spectrofluorometer. For the fibre-optic bOBP biosensor, the immobilized membrane containing 25µ1 of 100µM bOBP/25µ1 of 100µM 1-AMA mixture was incubated with 25µl of thymol, and measured by using the fibre-optic system shown in Figure 8.6.

2.2.6.4 Ability to Sense Thymol Vapour of Fibre-Optic Biosensor Based on bOBP

The ability to sense thymol vapour of the fibre-optic biosensor based on bOBP was then investigated. A simple preliminary experiment was set up by 0.5-cm bOBP immobilized nitrocellulose membrane disk containing 25µ1 of 100µM bOBP/25µ1 of 100µM 1-AMA mixture that was stuck at the lid of a 0.5-ml tube was incubated in triplicate for 1 hr at room temperature with thymol vapour produced from different concentrations of 50µl thymol solution ranging from 0-25mM at the bottom of the tube. Thymol solution was dissolved in PBS containing 1mM EDTA (pH 7.4) that had 0.1% ethanol final concentration. Blank comprised of five separate measurements of the bOBP immobilized membrane at the top of the tube incubating with 50µl of PBS containing 1mM EDTA (pH 7.4) and 0.1% ethanol at the bottom of the tube. The bOBP immobilized membrane was then attached to the edge of the fibre bundle, and the emission fluorescence intensity was measured at 490nm.

2.2.6.5 Analysis of Thymol Vapour by Fibre-Optic Biosensor Based on bOBP

The photostability of the bOBP immobilized membrane was investigated by monitoring % fluorescence remaining of the bOBP immobilized membrane containing 25µ1 of 100µM bOBP/25µ1 of 100µM 1-AMA mixture was mounted to the reflection probe at the end of the fibre bundle, and flashed using the fibre-optic system (Figure

8.6). The experiment was carried out in a dark room in order to avoid ambient light interferences. The LLS-385 LED light source (Ocean Optics; 3.86mW at 385nm) excited the membrane at 385nm, and was switched on only when readings were being taken. The emission fluorescence signal was collected at 490nm. The integration time was set at 1 second.

CHAPTER 3

PRODUCTION OF THE RECOMBINANT BOVINE ODORANT BINDING PROTEINS (bOBPs)

3.1 Expression of the Recombinant bOBPs

E.coli BL21(DE3) transformed by pET24a containing the *bobpwt* gene (its plasmid map shown in Figure 2.1) was revived from -80^{o}C storage by streaking on LB^{Km} agar plate. Then, the *bobpwt* gene was verified by DNA sequencing (Appendix). The verified clone was examined for its protein expression on a small-scale by inducing with 1 mM IPTG and growing at 37^{o}C in comparison with the non-induced cells by using non-transformed and pET24a-transformed bacteria as controls. The result of the SDS-PAGE analysis are shown in Figure 3.1 and revealed an intense band from the recombinant clone at the expected size of the bOBP subunit, indicating that bOBP was over-expressed. The molecular weight of the bOBP band was around 20 kDa which was a little larger than the one reported as 19 kDa (159 residues) [80] because of extra amino acid residues of a T7 tag (11 amino acids) and some carry-over sequence from pET24a (4 amino acids) attached to the N-terminus, and a 10-his tag at the C-terminus, which produced the total of 184 residues of this recombinant bOBP.

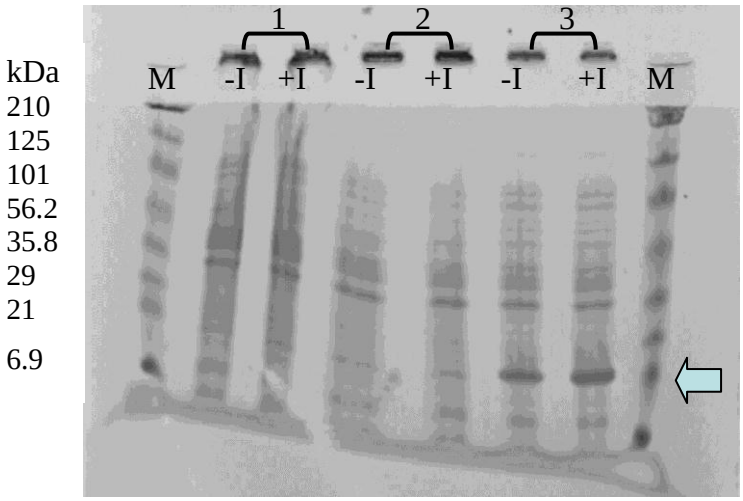

Figure 3.1: SDS-PAGE of bOBP expression. *M is prestained SDS-PAGE standards marker. 1 is E. coli BL21(DE3) lysate; 2 is E. coli BL21(DE3) transformed with pET24a lysate; 3 is E. coli BL21(DE3) transformed with pET24a carrying the bobpwt gene; -I is before induction; and +I is after induction.*

It was observed that both induced and non-induced cells over-expressed bOBPwt at 37^{o}C. Subsequently the expression of bOBPwt was then investigated at room temperature to determine whether the protein was expressed in the soluble form or as inclusion bodies by culturing the induced cells at room temperature overnight (or at 33^{o}C for 6 hr). The induced cells were then harvested, broken with French Press operated at the pressure of around 11,000 psi. The lysed solution was centrifuged to separate the soluble and insoluble fractions of the recombinant protein. It was found that bOBPwt expressed almost completely in the soluble form as shown in Figure 3.2.

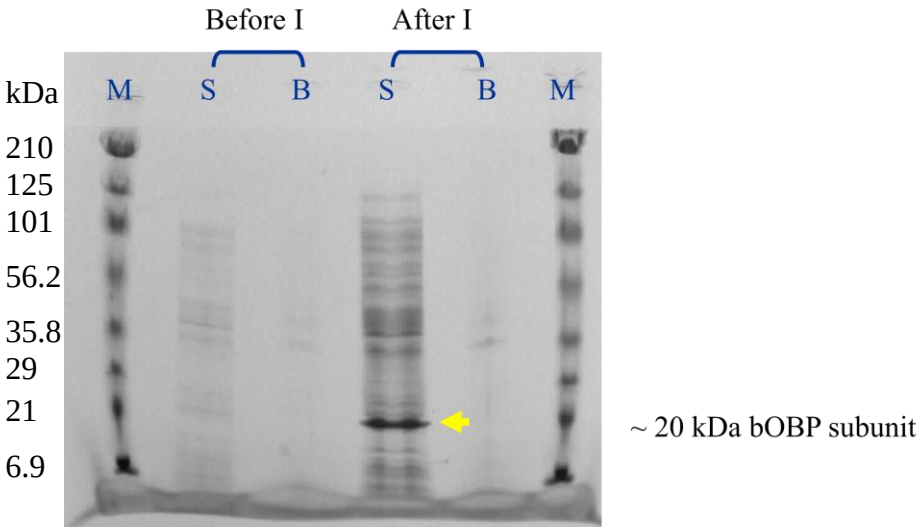

Figure 3.2: SDS-PAGE of bOBP expression in soluble form after induction at 30°C. *M is prestained SDS-PAGE standards marker. S is soluble form; B is inclusion bodies; and I is induction.*

3.2 Purification of the Recombinant bOBPs

The large-scale recombinant bOBP expression and purification was then performed by expressing 7 litres of the bOBPwt cell culture. The cells were lysed and the lysate was applied into the Ni-NTA sepharose affinity chromatographic column, then recirculated the column overnight at the flow rate of 20ml/min, and eluted using linear gradient to 100% elution buffer (600mM imidazole, 500mM sodium chloride, 100mM phosphate buffer, pH 7.2). The fractions eluting from the column were analysed by SDS-PAGE shown in Figure 3.3, demonstrating that no or insignificant traces of the target protein band were obtained from the flowthrough and washing fractions, indicating that bOBP in the lysate was tightly bound to the Ni-NTA resin. This is because bOBP fused with histidine tag, which binds to the nickel whereas non-specific proteins were eluted from the column with washing buffer containing low imidazole concentration (50mM imidazole). The histidine-tagged bOBP protein was eluted with buffer containing 600mM imidazole.

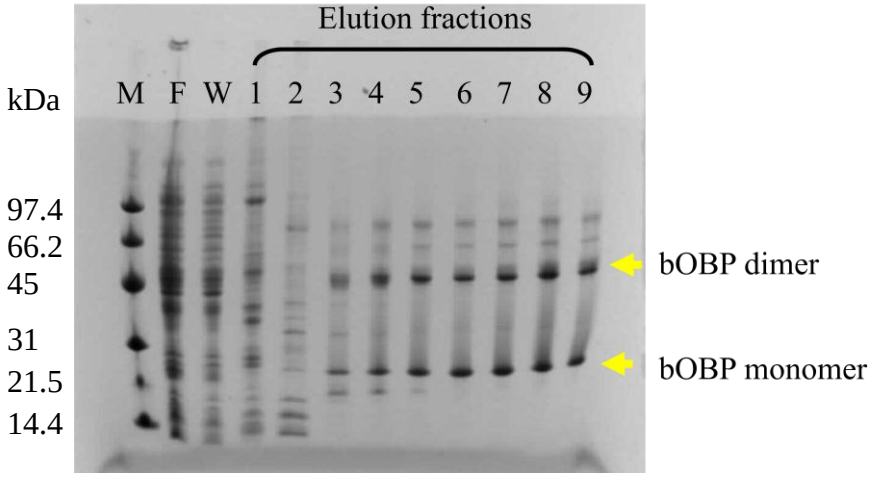

Figure 3.3: SDS-PAGE of the purification of bOBP. *M is SDS-PAGE standards marker. F is flowthrough fraction; W is washing fraction; and 1 - 9 are number of elution fractions.*

From Figure 3.3, it was observed that the concentrated bOBP solution showed more than one band in SDS-PAGE. This may have due to residual salts and/or imidazole. Therefore, fractions of the eluted proteins (E6 – E9**)** were pooled further desalted and concentrated using a Vivaspin20 centrifugal concentrator with 10-kDa MWCO membrane. The protein concentrations were estimated using a Nanodrop spectrophotometer. The purified protein was diluted to around 0.3 – 1.0 mg/ml for loading into the SDS-PAGE gel in order to get a sharp protein band without smears as shown in Figure 3.4. SDS-PAGE showed a single band at the expected size, indicating that the purified bOBP was obtained.

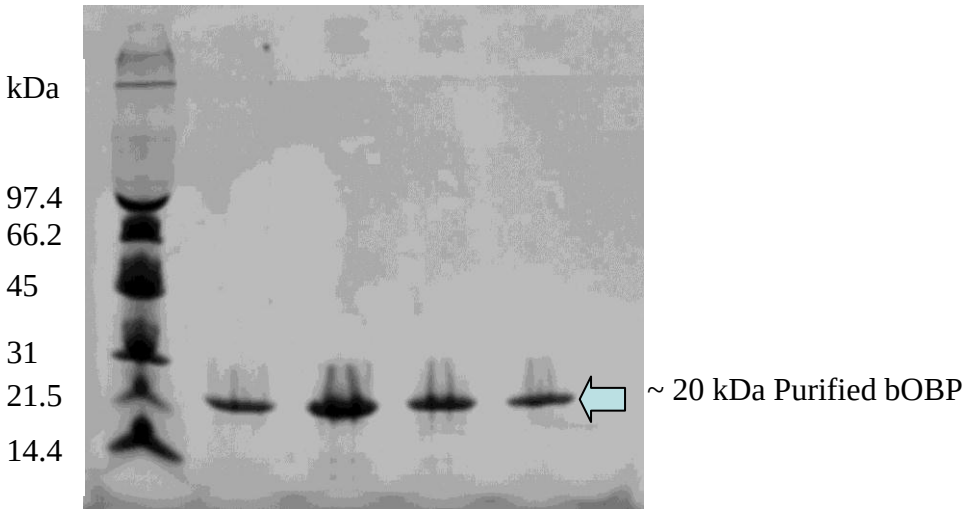

Figure 3.4: SDS-PAGE of the purified bOBP.

Mutant bOBPs that were also produced by Dr Chung-Pei Ou and Dr. Melanie Fennah were expressed and purified by using the same procedures as those described above for bOBPwt. These mutant bOBP clones all have the C-terminal decahistidine tags and site mutations in the ligand binding cavity at different locations introducing a unique cysteine residue in the bOBP sequence, which could allow later site specific binding of the environmental sensitive thiol reactive probe, and therefore report the protein-ligand binding events. The five cysteine bOBP mutants were as following: I22C, S24C, F36C, F54C, and F91C. The efficiencies of the bOBP expression and purification are shown in Table 3.1.

Table 3.1: Yields of bOBP wild-type and cysteine mutants

bOBP	Total yield (mg)
WT	368
I22C	444
S24C	691
F36C	77
F54C	13
F91C	351

Sequence confirmed wild-type and five cysteine mutants of bOBP were expressed and purified to homogeneity. Yields were 13-691 mg (7-L cultures) and in the following chapter, the CD spectroscopic studies of bOBP in binding to thymol are described.

CHAPTER 4

CD SPECTROSCOPY OF THYMOL BINDING TO bOBP

In the previous chapter, the expression and purification of recombinant bOBPs were described. In this chapter, the interaction of wild type bOBP with thymol as a ligand was characterized by means of CD spectroscopy.

Circular dichroism (CD) is the difference in the absorption of left-handed circularly polarized (LCP) light and right-handed circularly polarized (RCP) light which arises due to structural chirality. An ordered structure results in a spectrum which can contain both positive and negative signals, while the absence of regular structure results in zero CD intensity [81]. CD is dependent on the wavelength at which absorption occurs and therefore CD spectroscopy measures the differential absorbance as a function of wavelength. This technique is employed widely to study asymmetric molecules of all types and sizes, and it has found particular application in the study of large biological molecules [82]. Whilst experimentally the CD spectrum measures the differential absorption (ΔA), this is often converted to ellipticity (θ). The relation between these two quantities can be derived as following:

By applying Beer's law

$$\mathbf{A_L} = \boldsymbol{\varepsilon_L \cdot C \cdot l}$$

$$\mathbf{A_R} = \boldsymbol{\varepsilon_R \cdot C \cdot l}$$

So, $$\Delta\mathbf{A_{L\text{-}R}} = \Delta\boldsymbol{\varepsilon_{L\text{-}R} \cdot C \cdot l}$$

Where $\boldsymbol{\varepsilon_L}$ and $\boldsymbol{\varepsilon_R}$ are the molar extinction coefficients for LCP and RCP light, $\boldsymbol{C}$ is the molar concentration, $\boldsymbol{l}$ is the path length in centimeters (cm), and $\Delta\boldsymbol{\varepsilon}$ is the molar circular dichroism that is a function of wavelength.

Molar circular dichroism and molar ellipticity [θ] are readily interconnected by the equation

$$[\theta] = 3298 \cdot \Delta\varepsilon = \frac{3298 \cdot \Delta A}{C \cdot l}$$

The linear dependence of solute concentration and pathlength is removed by defining ellipticity as

$$\theta = 3298 \cdot \Delta A$$

CD is typically used to study macromolecules in solution, and thus it complements methods that study the solid state [83]. Its primary use is in analyzing the conformation (secondary, tertiary structure) or stability changes of macromolecules, particularly proteins with environmental conditions such as under stress or denaturants (temperature, chemicals (usually urea and guanidinium chloride) and extremes of pH (usually acidic)), or on protein-protein or protein-ligand interactions. In addition to structural information, thermodynamic and kinetics parameters of macromolecules can be acquired from CD spectroscopy as well.

Characterization of bOBP by using CD spectroscopy in this project presents structural and thermodynamics information of the protein.

4.1 Structural Information of Protein and Binding Interaction

4.1.1 Tertiary structure

The near-UV CD spectrum (250-300nm) of proteins provides information on the presence of tertiary structure. The signals obtained in this spectral region arise from the absorption, dipole orientation and the nature of the surrounding environment of the aromatic amino acids; tryptophan, tyrosine, phenylalanine, and cysteine (or S-S disulfide bonds) as following:

- Tryptophan: 280-300nm
- Tyrosine: 270-290nm
- Phenylalanine: 250-270nm
- Disulfide bonds: broad weak signals throughout 250-300nm

Generally, tryptophan will give the biggest signal, followed by tyrosine and then phenylalanine. The number of each type of aromatic amino acid present and the nature of their environment (H-bonding, polar groups) will determine the actual shape and magnitude of the near-UV CD spectrum of a protein [84]. The presence of significant near-UV signals is a good indication that the protein is folded into a well-defined structure.

In order to investigate the binding of a ligand molecule with bOBP in solution phase, CD spectroscopy has been exploited to obtain information about the protein structure upon the binding to thymol; a ligand for bOBP [34, 36]. The tertiary structure of bOBP in the presence of thymol (200µM bOBP and 200µM thymol) has been analyzed in comparison with unbound bOBP (200µM bOBP) by measuring near-UV CD spectra at 240 − 340nm. The result in Figure 4.1 showed the near-UV CD spectra with a negative band at about 280nm of tryptophan residue of bOBP in the absence and presence of thymol were nearly superimposed spectral profiles. Some small changes in the intensity were observed, but the number and positions of the spectral bands remained unchanged, pointing to the absence of any significant change of the tertiary structure of bOBP likely due to no perturbations of thymol binding to the environment of the aromatic region in the folded structure of bOBP.

Alternatively, the UV spectrum of thymol is shown in Figure 4.2, it has absorption in the same region as tryptophan (280nm) and tyrosine (270 - 290nm) residues in bOBP. It is possible that the bound thymol would show a CD spectrum in this region. It is probably overwhelmed by the strong signals of the four tryptophan and the five tyrosine aromatic residues in the protein itself.

However, it is interesting that this result found in bOBP in this study was also in a agreement with near-UV CD measurement of porcine OBP spectra in the presence of ligand (3,7-dimethyl-octan-1-ol; DMO). DMO, a molecule able to bind bOBP strongly, has the dissociation constant (K_d) value of 0.20 µM to pOBP. It revealed that state of its aromatic residues does not show significant changes in the presence of DMO ligand. In this case, this probe does not interfere the intrinsic protein CD spectra, since it does not absorb in the near UV region [85].

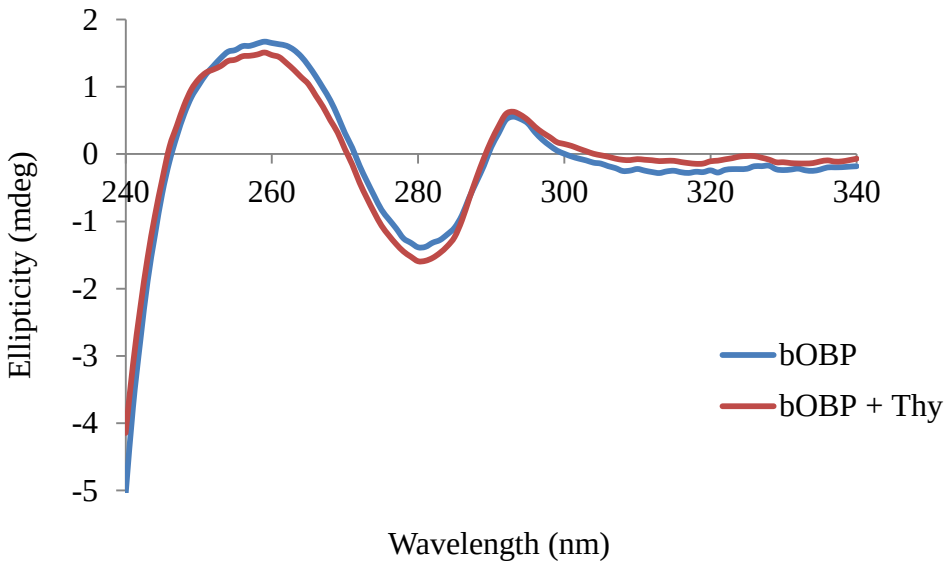

Figure 4.1: Near UV CD spectra of bOBP in the absence (blue) and presence of thymol (red) demonstrated as ellipticity in millidegree unit. *The protein concentration was 200µM bOBPwt and the ligand concentration was 200µM thymol, by which they were dissolved in 0.01X PBS with 10µM EDTA supplement, pH7.4. Data were collected in cell with 1mm pathlength, T = 20°C.*

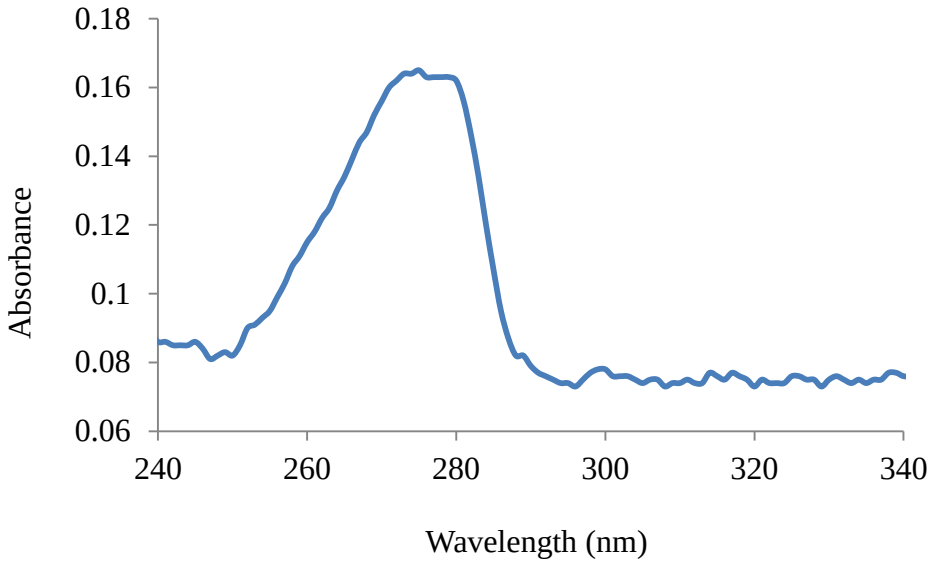

Figure 4.2: Absorption spectrum of 200µM thymol in 0.01X PBS with 10µM EDTA supplement, pH 7.4 at 25°C.

4.1.2 Secondary structure

Secondary structure can be estimated by CD spectroscopy in the far-UV range. Signals in the region from 180-250nm are attributable to the peptide bond and originate when it is located in a regular, folded environment. A characteristic shape and magnitude of the CD spectrum can be determined by alpha-helix, beta-sheet, or some other (e.g. random coil) structures. Figure 4.3 illustrates spectra of the three common different conformations.

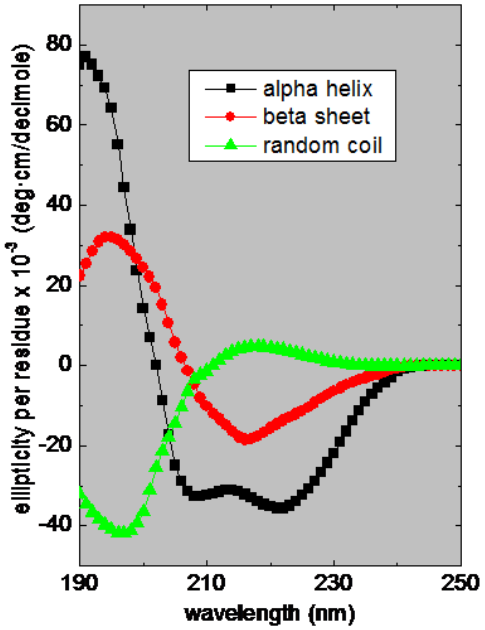

Figure 4.3: Characteristic of far-UV CD spectra for an α-helix, a β-sheet and a random coil secondary structure of protein [86]. *In general, the spectrum for an alpha-helix protein has two negative bands of similar magnitude at 222 and 208nm, and a positive band at ~190nm. The spectrum for a beta-sheet protein has mainly a negative band between 210 - 220nm and a positive band between 195 - 200nm. The spectrum for a disorderly (random) protein has a negative band of at around 200nm. This image has been reproduced with the permission of the rights holder, Alliance Protein Laboratories by Dr. John Philo.*

The far-UV CD spectroscopy (260–185nm) was also used to monitor changes in the secondary structure of bOBP in the presence of thymol. It was found that the spectrum of bOBP in the presence of thymol was similar to that of unbound bOBP (Figures 4.4), which showed the typical shape of a protein with characteristic of β structures that havve one maximum at 195nm and one minimum at 217nm, indicative of the comparable amount of secondary structure content.

Therefore, conclusions could be drawn that the protein-ligand binding interaction between bOBP and thymol was studied by using the near- and far-UV CD spectroscopy at the temperature of 20^{o}C, and the structural information upon the binding was obtained. It has been shown that the secondary and tertiary structures of bOBP are largely maintained on binding to thymol, suggesting the presence of thymol in the interior cavity of bOBP did not perturb the protein structure.

This finding was also in good agreement with several previous studies that reported on bOBP and pOBP; which are structurally similar. Mazzini and co-workers have shown that at acidic pH (2.5), bOBP loses its swapped dimeric conformation, but keeps its tertiary and secondary structure largely unaltered. This conclusion was based on size exclusion chromatography, 1-aminoanthracene (AMA) binding studies, CD spectroscopy, and molecular dynamics simulations [87]. Additionally, an absence of significant conformational changes involving protein loops or backbone upon the binding of odorant molecules also has been revealed by the crystal structures of both pOBP and bOBP [38]. Moreover, it has been shown that tryptophan in the pOBP structure is not involved in binding to the odorants 2-isobuthyl-3-methoxypyrazine (IBMP) and DMO by Fourier-transform infrared spectroscopy (FT-IR) and fluorescence spectroscopy [88]. Finally, it was found that the far- and near-UV CD spectra of pOBP at pH 6.6 demonstrate unchanged of the number and positions of the spectral bands compared to those in the presence of DMO, but some difference in the intensity level is observed [85].

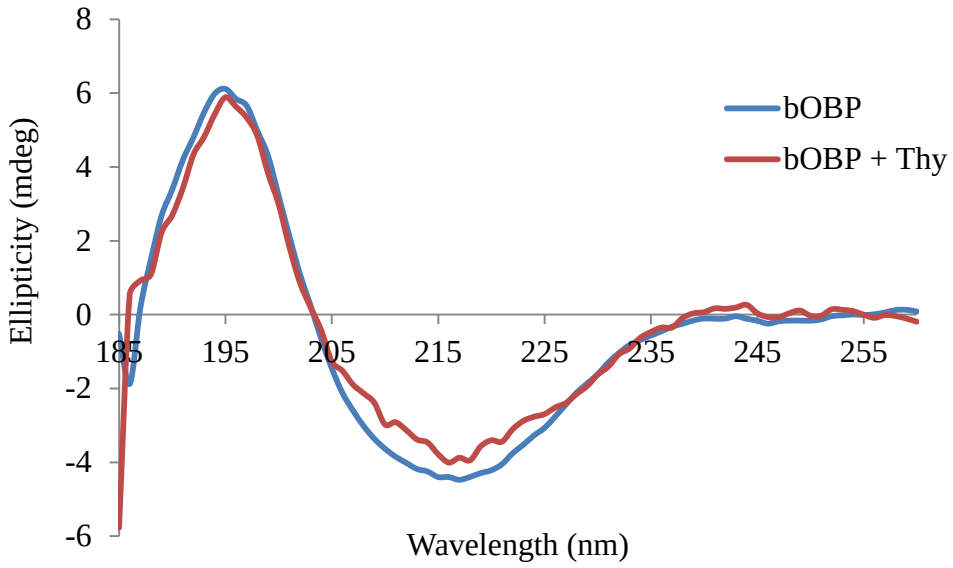

Figure 4.4: Far-UV CD spectra of bOBP in the absence (blue) and presence of thymol (red) demonstrated as ellipticity in millidegrees. *The protein concentration was all 5µM bOBPwt and the ligand concentration was 100µM thymol, which were dissolved in 0.01X PBS with 10µM EDTA supplement, pH 7.4. Data were collected in a cell with 1mm pathlength, T = 20°C.*

4.2 Thermodynamic Information of Protein Unfolding and Binding

4.2.1 Thermal stability

When proteins are folded they have highly chiral secondary structure elements, such as α-helices and β-pleated sheets, which create unique characteristics in the CD spectra (Figure 4.3). When proteins unfold they lose these well-ordered structures and the CD bands alter. The changes in CD spectra obtained as a function of temperature can be used to determine the thermodynamics of unfolding (or more precisely change of state). For example, the midpoint of the unfolding transition (T_m) that is directly related to conformational stability. The enthalpy (ΔH), the free energy (ΔG), the entropy (ΔS) of unfolding, and the dissociation constants (K_d) of interacting proteins, that can also be estimated from data extraction. Additionally, analysis of CD spectra obtained as a function of temperature may be useful in determining whether a protein has unfolding or folding intermediates [89].

The effect of a bound ligand on thermal unfolding of bOBP was investigated with thymol to study the role of the ligand binding interaction on the protein thermal stability. Thermal unfolding of bOBP was carried out by following the far-UV CD signal at 195nm collected every 2°C from 20 to 98°C as shown in Figure 4.5 and 4.6. The thermodynamic parameters of unfolding could be determined from three independent CD measurements. The melting temperature (T_m) is the midpoint of the transition (unfolding curve), which was obtained by either approximately estimating from the first derivative equation of the data by which T_m is represented as the minimum of the curve (Figure 4.7-4.8) or direct fitting the data to the Boltzmann model (Equation 4.1).

$$\mathbf{Y = BP + (TP - BP) / (1 + \exp((T - T_m) / dT))}$$

Equation 4.1: Boltzmann model. Where **BP** is bottom plato, **TP** is top plato, **T** is temperature, and $\mathbf{T_m}$ is melting temperature.

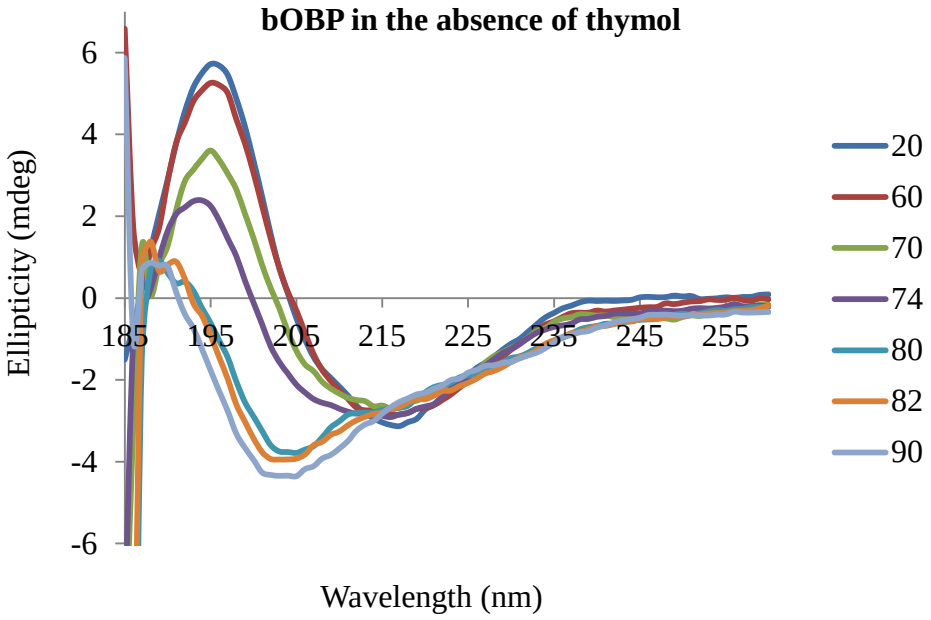

Figure 4.5: Far-UV CD spectra of 5µM bOBP at various temperatures of 20, 60, 70, 74, 80, 82 and 90°C. *The buffer was 0.01X PBS containing 1µM EDTA (pH 7.4).*

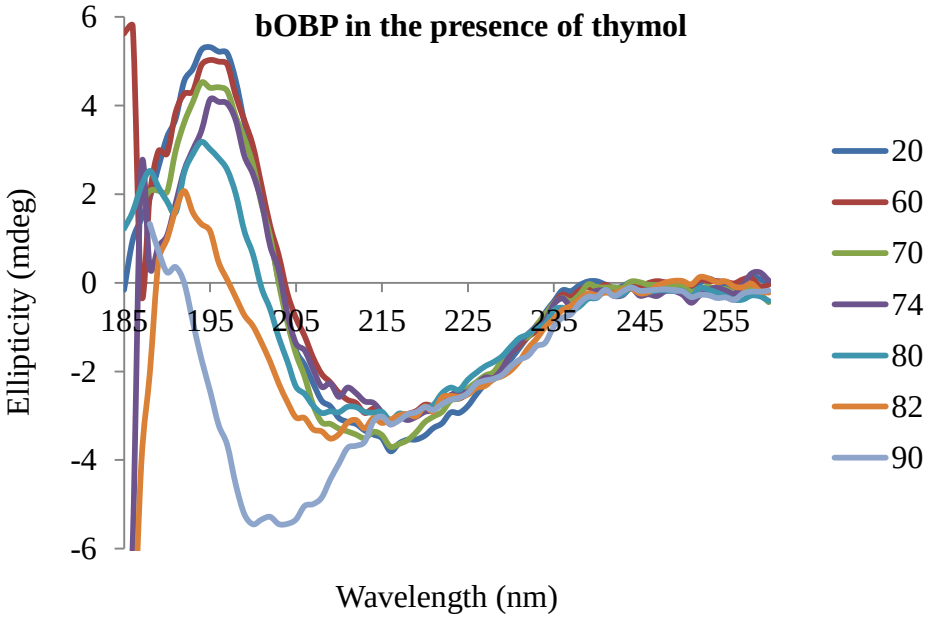

Figure 4.6: Far-UV CD spectra of 5µM bOBP in the presence of 100µM thymol at various temperatures of 20, 60, 70, 74, 80, 82 and 90°C. *The buffer was 0.01X PBS containing 1µM EDTA (pH 7.4).*

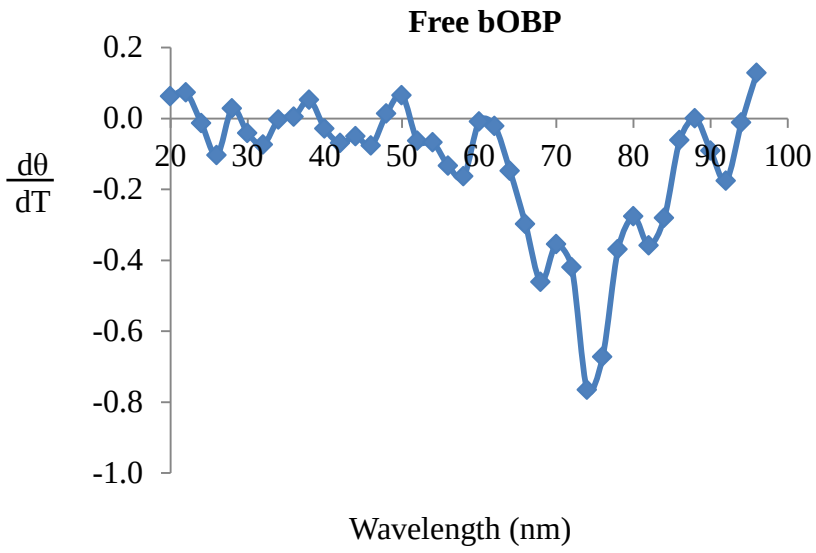

Figure 4.7: First derivatives of 5µM bOBP as a function of the temperature (the data in Figure 4.5 at 195nm). *The minimum corresponds to the midpoints (T_m) of the unfolding/folding curves for the protein.*

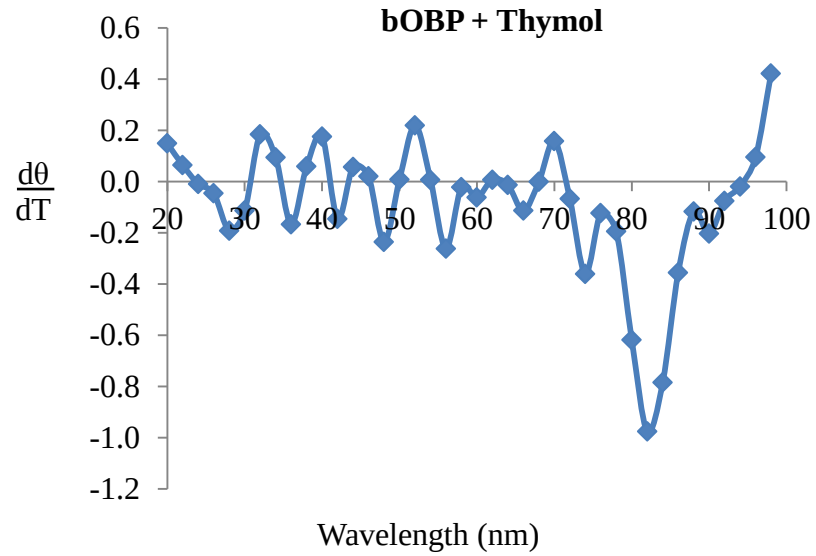

Figure 4.8: First derivatives of 5µM bOBP in the presence of 100µM thymol as a function of the temperature (the data in Figure 4.6 at 195nm). *The minimum corresponds to the midpoints (T_m) of the unfolding/folding curves for the protein-ligand bound complex.*

From calculating T_m by using two different methods, it was found that both methods of calculation gave the same T_m values. It was shown that the equilibrium unfolding transition curves fitting to the Boltzmann equation were sigmoidal (Figure 4.9). The T_m of bOBP in the absence of thymol was 74 ± 0.3°C and significantly shifted towards higher temperature to 82 ± 0.4°C for the one in the presence of thymol. The higher stability of bOBP evidenced by these data could be accounted for by the presence of thymol in the binding cavity of bOBP, which suggested that thymol induced protein stabilization.

Additionally, CD spectroscopy as a function of temperature has also been used to detect temperature-induced effects on structural features. Figure 4.5 and 4.6 showed that the far-UV CD spectra of bOBP in the absence and presence of thymol as a ligand exhibited a maximum at ~195nm and a minimum at ~217nm with the overall maintenance of the β-barrel structure in a large range of different temperatures at which were stable up to 74^{o}C for bOBP and 82^{o}C for thymol-bound bOBP. At temperatures higher than their T_m, it was observed that their secondary structures did not completely convert to random coils, which indicated that some β-sheet structure remained. Thus, although differences in the far-UV CD spectra between the protein in the presence and absence of thymol was not found at 20^{o}C (Figure 4.4), it was clearly seen that differences at 76 - 82^{o}C, which were the temperatures between higher than the T_m of unligated bOBP and the T_m of thymol-bound bOBP.

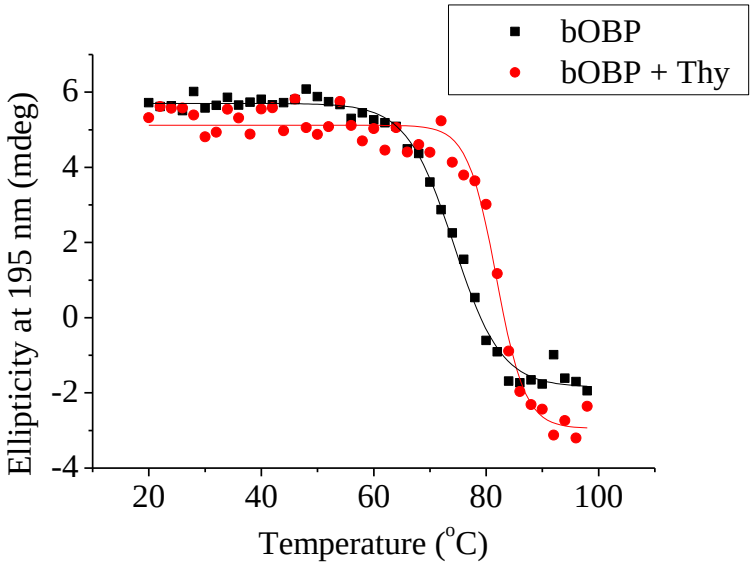

Figure 4.9: Unfolding transition curves of the ellipticity at 195nm for unfolding of bOBP in the absence (black squares) and presence of thymol (red circles) as a function of temperature. *The concentration of protein was 5µM bOBP and the concentration of ligand was 100µM thymol. The reactions were in 0.01X PBS with 10µM EDTA supplement, pH 7.4, recorded by far UV–CD at a thermal scan rate of 45°C/hr from 20 to 98°C during denaturation. The raw data were fit with Boltzmann equation.*

In this experiment, the typical change of ellipticity is shown as a function of temperature for bOBP in the absence and presence of thymol. These were used to determine the thermodynamics of unfolding. It was shown that bOBPwt was highly thermostable with T_m of the unfolding transition of 74 ± 0.3°C in the absence of thymol, which is considerably lower than that observed in the presence of thymol at 82 ± 0.4°C, suggesting a stabilizing role is played by bound thymol. The phenomenon found in this study was similar to those already described for the mutant bOBP that was investigated by using FT-IR and molecular dynamics simulations [64, 90], as well as natural pOBP that was shown by FT-IR and fluorescence spectroscopy [88]. Moreover, the T_m in this finding was in a similar range of temperature as two other reports of thermal denaturation of bOBPwt [63] and pOBP [85]. These were a heating-

induced transition in bOBPwt detected at 75 - 85^{o}C by means of difference infrared spectra, 2D-IR correlation spectroscopy and molecular dynamics simulations [63]. Secondly, the unfolding transition of pOBP has been shown at 69°C by the method of high-sensitivity differential scanning calorimetry (HS-DSC) [85].

It appeared that, similarly to pOBP [88] and the mutant bOBP [64], the secondary structures of unbound and thymol-bound proteins showed a high resistance of its global structural organization to high temperatures, since its overall fold are practically unchanged in a wide range of temperature. The advantageous properties of bOBP shown by these obtained results will allow for a better use of this protein for the design of advanced protein-based biosensors for the detection of compounds.

In next experiments, other thermodynamic parameters of unfolding; the enthalpy (ΔH), the free energy (ΔG), the entropy (ΔS) of unfolding and binding, and the dissociation constant (K_d) for the binding of bOBP to thymol are evaluated.

4.2.2 Enthalpy (ΔH), free energy (ΔG), entropy (ΔS) of unfolding and binding

Following changes in the CD of macromolecules, such as proteins as a function of temperature or denaturant is a very convenient method for obtaining the thermodynamics of unfolding or folding. It is based on the fact that the change in ellipticity is directly proportional to the change in concentration of native and denatured forms [91]. In the simplest case, a molecule undergoes an unfolding transition between two states: folded (F) and unfolded (U).

From the CD spectra of bOBP obtained from section 4.2.1, it appeared that bOBP at high temperature did not have a fully unfolded state. The effect of ligand binding on stability can be modelled by a triangular three-state diagram, which includes a direct path from the folded (F) to the unfolded state (U), and the indirect route *via* the bOBP•Thymol complex (F•L) (Scheme 4.1).

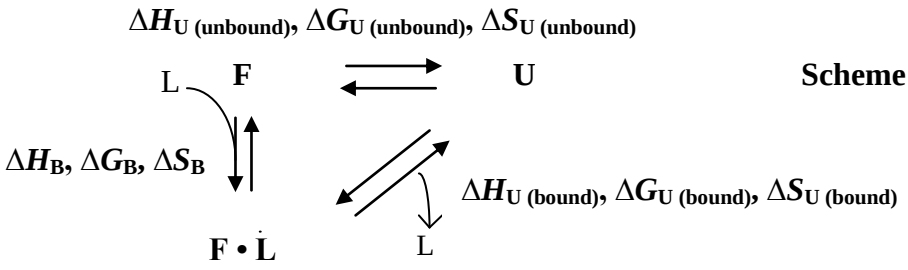

Scheme 4.1

The equilibrium thermodynamic data can be described as shown in Equation 4.2 - 4.4.

Since, $\Delta H_{U\ (unbound)} = \Delta H_B + \Delta H_{U\ (bound)}$

So, $\Delta \boldsymbol{H_B} = \Delta \boldsymbol{H_{U\ (unbound)}} - \Delta \boldsymbol{H_{U\ (bound)}}$ **4.2**

ΔH_B is the enthalpy of binding between bOBPwt and thymol, $\Delta H_{U\ (unbound)}$ is the enthalpy of unfolding for unbound bOBP, and $\Delta H_{U\ (bound)}$ is the enthalpy of unfolding for thymol-bound bOBP.

Likewise, $\Delta \boldsymbol{G_B} = \Delta \boldsymbol{G_{U\ (unbound)}} - \Delta \boldsymbol{G_{U\ (bound)}}$ **4.3**

ΔG_B is the free energy of binding between bOBPwt and thymol, $\Delta G_{U\ (unbound)}$ is the free energy of unfolding for unbound bOBP, and $\Delta G_{U\ (bound)}$ is the free energy of unfolding for thymol-bound bOBP.

And, $\Delta \boldsymbol{S_B} = \Delta \boldsymbol{S_{U\ (unbound)}} - \Delta \boldsymbol{S_{U\ (bound)}}$ **4.4**

ΔS_B is the entropy of binding between bOBPwt and thymol, $\Delta S_{U\ (unbound)}$ is the entropy of unfolding for unbound bOBP, and $\Delta S_{U\ (bound)}$ is the entropy of unfolding for thymol-bound bOBP.

For the purposes of thermodynamic calculations, bOBP was assumed to have the simple two-state transition upon heating as shown in Scheme 4.2.

$$\mathbf{F} \xrightarrow{\boldsymbol{K_U}} \mathbf{U}$$

Scheme 4.2

K_U is the equilibrium constant of unfolding at a given temperature.

$K_U = [U] / [F]$

[F] and [U] are the concentrations of the folded and unfolded forms, respectively.

If α is defined as the fraction folded at a given temperature,

$\alpha = [F] / [F] + [U]$

The concentrations can be written in terms of the ellipticity

$$\boldsymbol{K_U = (1 - \alpha) / \alpha} \qquad \textbf{4.5}$$

$$\boldsymbol{\alpha = (\theta_t - \theta_U) / (\theta_F - \theta_U)} \qquad \textbf{4.6}$$

θ_t is the observed ellipticity at any temperature, θ_F is the ellipticity of the fully folded form and θ_U is the ellipticity of the unfolded form [89, 91].

Additionally, the relationship between free energy (ΔG), enthalpy (ΔH), entropy (ΔS) and the equilibrium constant (K) for a chemical reaction at a specific temperature (T):

$$\boldsymbol{\Delta G = -R\,T \ln K = \Delta H - T\Delta S} \qquad \textbf{4.7}$$

R is the gas constant that equal to 8.314 J/mol·K, and T is the absolute temperature (Kelvin).

A process at constant temperature and pressure will be spontaneous in the direction in which free energy decreases ($-\Delta G$). When Equation 4.7 is rearranged to remove ΔG, $\ln K$ is expressed in terms of ΔH, ΔS and T only:

$$\boldsymbol{\ln K = \frac{-\Delta H}{R \cdot T} + \frac{\Delta S}{R}} \qquad \textbf{4.8}$$

During protein folding, the process is considered to have a *favourable enthalpy change* ($\Delta H < 0$), as the amino acid residues come close together so forming non-covalent bonds. Denaturation only occurs when ΔG is negative, with which ΔH and ΔS are generally both positive [92, 93]. In order to analyse free energy (ΔG), enthalpic (ΔH), and entropic (ΔS) effects on the unfolded state of bOBP in the absence and presence of thymol as a function of temperature, those three independent CD data sets of section 4.2.1 were used to obtain mean values of these thermodynamic parameters.

First, ΔH of unfolding (ΔH_U) was determined by using the van't Hoff plot, that is the natural logarithm (ln) of the equilibrium constant of unfolding (K_U) was plotted as a function of 1/T where T is the absolute temperature (Kelvin). The plot should result in a straight line with a slope equal to ($-\Delta H/R$). Thus, enthalpy, ΔH, is determined from the slope, but entropy, ΔS, is normally calculated from the Equation 4.8 instead of the graph. This is because the intercept of the y-axis appears when the ratio (1/T) = 0 (that is when T = ∞) [89]. K_U were calculated based on the fraction folded data (α) by using Equation 4.5, with which α were determined by fitting the experimentally observed values of the change in ellipticity as a function of temperature (data of Figure 4.7) to Equation 4.6. The K_U values could only be accurately determined through the transition region as shown in Figure 4.10-4.11. Additionally, ΔH of binding between bOBPwt and thymol (ΔH_B) was determined from Equation 4.2; $\Delta H_B = \Delta H_{U\ (unbound)} - \Delta H_{U\ (bound)}$, The resulting values of ΔH are collected in Table 4.1.

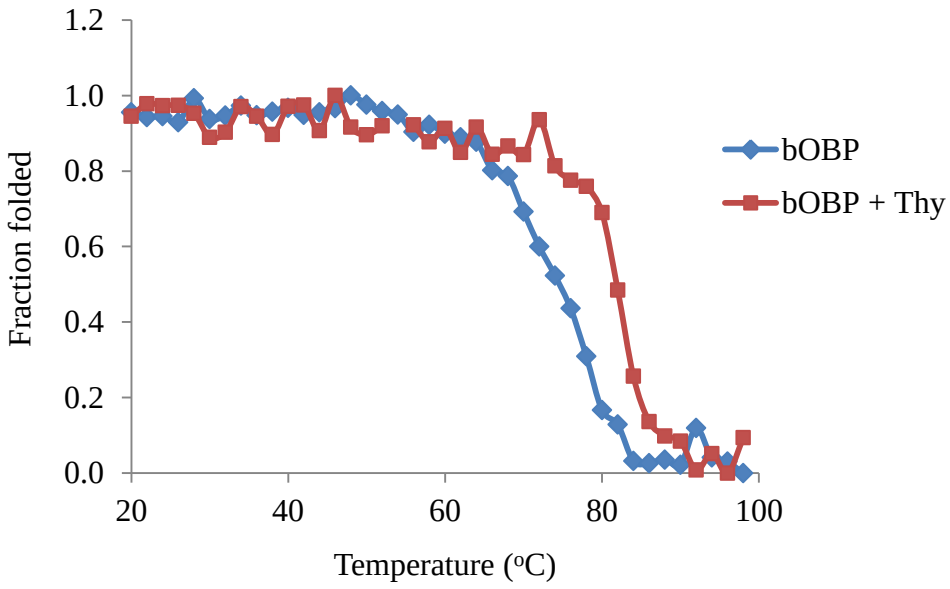

Figure 4.10: Change in fraction folded (α); $\alpha = (\theta_{obs} - \theta_{unfold})/(\theta_{fold} - \theta_{unfold})$ of bOBP in the absence (blue diamond) and presence of thymol (red square) from the change in ellipticity as a function of temperature. *Fraction folded data were used to calculate equilibrium constant of unfolding (K_U). The protein concentration was 5μM bOBPwt and the ligand concentration was 100μM thymol. The reactions were in 0.01X PBS with 10μM EDTA supplement, pH 7.4.*

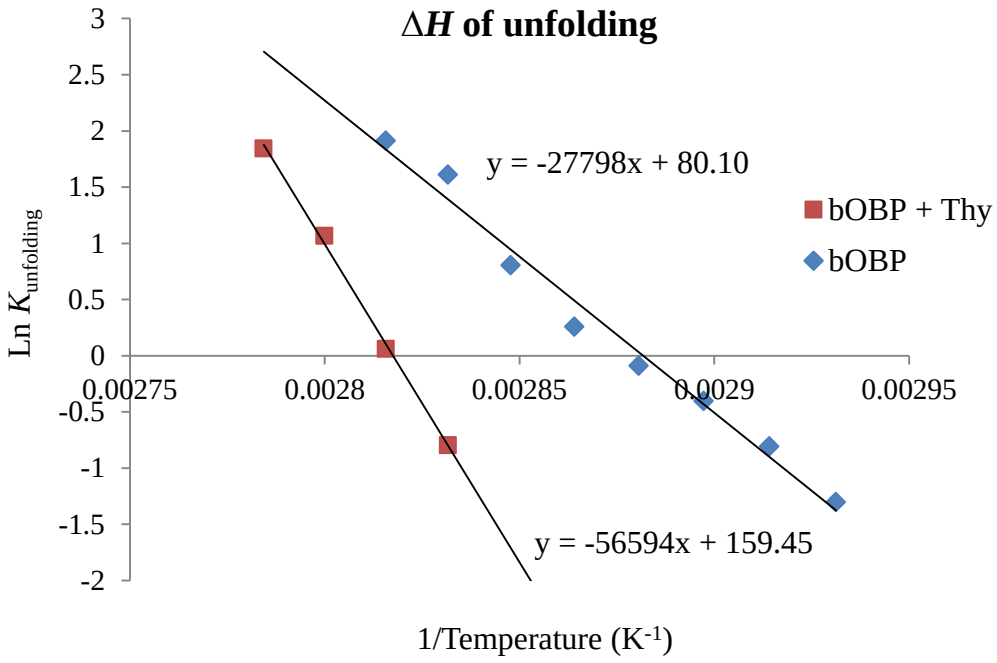

Figure 4.11: Enthalpies of unfolding (ΔH_U) for bOBP in the absence (blue diamond) and presence of thymol (red square) from the change in ellipticity as a function of temperature. *Van't Hoff plot of the thermal unfolding data for bOBP was created. The unfolding equilibrium constants were calculated according to Equation 4.5 (K_U = unfolded/folded) from the α data attained in Figure 4.10.*

Table 4.1: Summary of enthalpies of unfolding (ΔH_U) for bOBP in the absence and presence of thymol, and enthalpy of binding (ΔH_B) between bOBPwt and thymol determined from the van't Hoff analysis (Figure 4.11). *The change in ellipticity as a function of temperature was monitored by CD. The protein concentration was 5μM bOBPwt and the ligand concentration was 100μM thymol. The reactions were in 0.01X PBS with 10μM EDTA supplement, pH 7.4. Each value of ΔH is the average of three independent determinations.*

Thermodynamic parameters	ΔH (kJ/mol)
Unfolding of bOBP in the absence of thymol	217 ± 26
Unfolding of bOBP in the presence of thymol	451 ± 17
Binding of bOBP and thymol	-234 ± 31

Next, free energies of unfolding (ΔG_U) for bOBP in the absence and presence of thymol were studied. Analysis of thermal unfolding exhibited a decreasing linear plot of ΔG_U as a function of temperature in the transition zone. It was found that the CD data at lower temperatures did not contribute to a linear line or to unfolding. This is due to the limitation of the detecting instrument that was unable to distinguish very small changes of unfolding at low temperatures. So, only data within the temperature range of the linear part and affecting unfolding were analyzed. Then, the data above 62°C for unbound bOBP and above 76°C for that in the presence of thymol were used in calculating ΔG_U of bOBP in the absence and presence of thymol based on Equation 4.7; $\Delta G = - R T \ln K$. The ΔG_U results were shown as values of temperature dependence (Figure 4.12) that ΔG_U of the both systems decreased during the unfolding reactions. In detail, $\Delta G_{U\ (unbound)}$ and $\Delta G_{U\ (bound)}$ were positive (ΔG_U more than 0) when less than 74°C for unbound bOBP and less than 82°C for in the presence of thymol. When T was more than T_m, ΔG_U was negative (ΔG_U less than 0). This suggested that when T was less than T_m, unfolding reactions of unbound and thymol-bound bOBP were endergonic and non-spontaneous (or unfavourable), and became exergonic and spontaneous (or favourable), when T was more than T_m. In addition, ΔG of binding between bOBPwt and thymol (ΔG_B) was determined from Equation 4.3; $\Delta G_B = \Delta G_{U\ (unbound)} - \Delta G_{U\ (bound)}$, by which ΔG_U were obtained from data in Figure 4.12. Thus, the temperature dependence of ΔG_B was calculated and found to be linear (Figure 4.13). ΔG_B was shown to have negative values (ΔG_B less than 0) with a tendency to be positive, pointing out that the binding of bOBP and thymol was prone to be non-spontaneous (unfavourable) reaction at higher temperature. This is because the protein had more unfolded fraction, so the binding site to thymol was less existed.

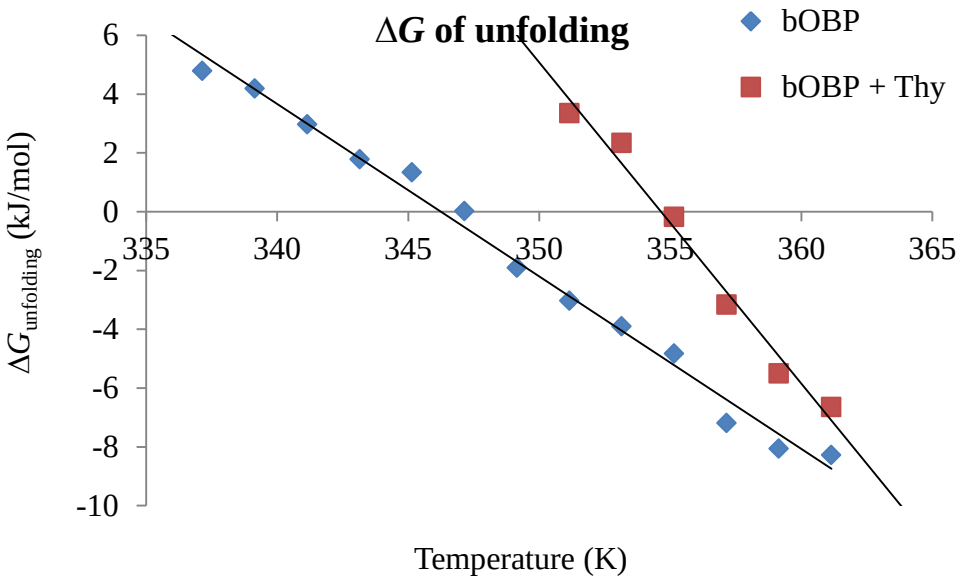

Figure 4.12: Free energies of unfolding (ΔG_U) for bOBP in the absence (blue diamond) and presence of thymol (red square) from the change in ellipticity as a function of temperature. *ΔG_U were calculated from the data (Figure 4.9) above 62°C for unbound bOBP and above 76°C for that in the presence of thymol using Equation 4.7; $\Delta G = -R\,T\,ln\,K$.*

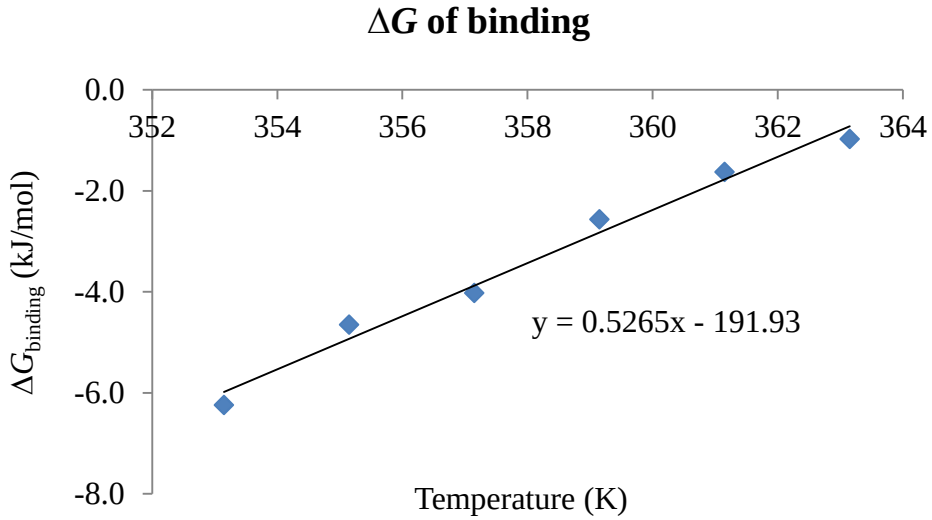

Figure 4.13: Plot of linear dependence of ΔG of binding (ΔG_B) between bOBPwt and thymol as a function of temperature; $\Delta G_B = \Delta G_{U\ (unbound)} - \Delta G_{U\ (bound)}$. *$\Delta G_U$ were from data in Figure 4.12.*

Entropy is a quantitative measure of the amount of disorder in a system. The entropy of the universe increases or remains contant for every change that occurs. This means that whenever something (a system) is organized, then there is an activity happening somewhere else (the surroundings) that produces more disorder. Entropies of unfolding (ΔS_U) for bOBP in the absence and presence of thymol, and entropy of binding (ΔS_B) between bOBPwt and thymol were estimated. By using Equation 4.7; $\Delta G = \Delta H - T\Delta S$, ΔS_U was derived by using ΔH_U and ΔG_U data in Table 4.1 and Figure 4.12. While ΔS_B was the difference of ΔS_U between unbound and thymol-bound bOBP; $\Delta S_B = \Delta S_{U\ unbound} - \Delta S_{U\ bound}$. The results illustrated in Figure 4.14 were that $\Delta S_{U\ (unbound)}$ and $\Delta S_{U\ (bound)}$ were positive (ΔS_U more than 0), indicating high extents of disorder in the system. This represented that the reactions of the unfolding for both unbound and thymol-bound bOBP were the processes that produced more disorder. Each unfolded protein molecule adopted multiple conformations, so making the systems disordered. Additionally, as the walls of the cavities of bOBP are largely comprised of hydrophobic residues [54], the positive ΔS also suggested hydrophobic interactions, which were attributed to the protein stability, were main driving forces in protein unfolding to thymol. This was in agreement with the spectroscopic and molecular dynamics simulation data, which revealed that the hydrophobic regions of the protein matrix are an important factor for the protein stability and integrity [64, 94]. Moreover, it pointed to situations that minimized the area of contact between H_2O and non-polar, i.e. hydrocarbon, regions of the protein, that was achieved by clustering non polar groups together [95-97]. Furthermore, ΔS_B was found to be negative (ΔS_B less than 0) (Figure 4.14), implying that the binding process between bOBPwt and thymol resulted in the more orderly state due to the reduced conformational freedom.

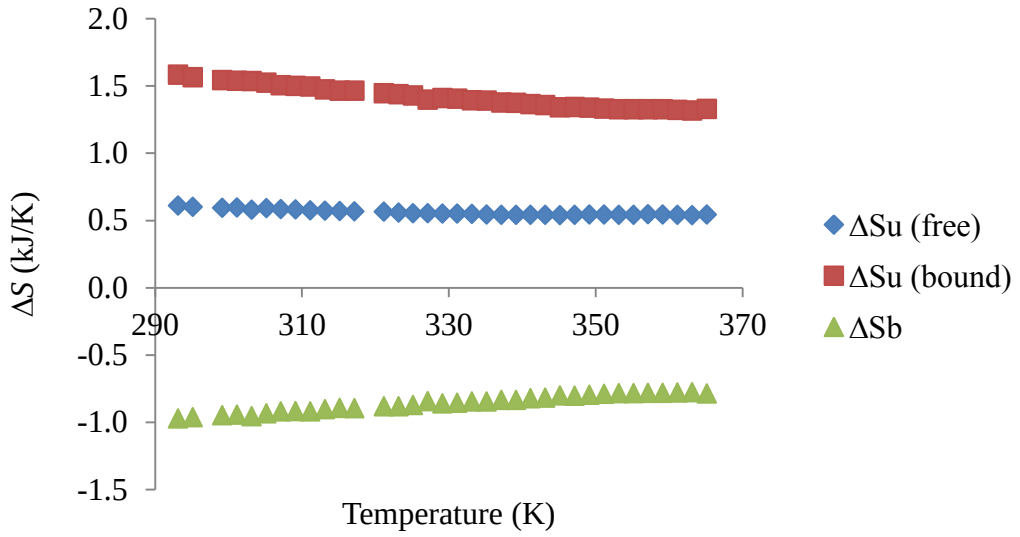

Figure 4.14: Entropies of unfolding (ΔS_U) for bOBP in the absence (blue diamond) and presence of thymol (red square), and Entropy of binding (ΔS_B) between bOBPwt and thymol (green triangle) from the change in ellipticity as a function of temperature. *The calculation was based on Equation 4.4 and 4.7; $\Delta G = \Delta H - T\Delta S$ and $\Delta S_B = \Delta S_{U\,(unbound)} - \Delta S_{U\,(bound)}$.*

4.2.3 Dissociation constants (K_d) of binding between bOBP and thymol

The direct assessment of bOBP-thymol interaction carried out by CD yielded the values of binding parameters (ΔG_b). This value can serve in calculating the dissociation constant, K_d, of binding.

$$\Delta G_b = -R\,T \ln K_b \qquad 4.9$$

K_b is the binding constant of bOBPwt and thymol interaction, whereas $K_b = 1/K_d$.

The K_d value for thymol binding to the bOBPwt were estimated by using Equation 4.9 at which the ΔG_b was derived from the linear dependence plot in Figure 4.13. Thus, the K_d value of binding between bOBP and thymol was found to be 0.75µM. In the following chapter, the labelling of the cysteine residues is described.

In overall conclusion for the relationship of ΔH, ΔG, ΔS for the unfolding of bOBP in the absence and presence of thymol, and for the binding of bOBP and thymol, CD measurements indicated that the unfolding of bOBP in the absence and presence of thymol were entropically driven ($+\Delta S_U$) and energetically favourable ($-\Delta G_U$). The positive ΔH and ΔS in both cases were attributed to the release of ordered water molecules and the associated entropy gain (due to the hydrophobic effect). The data were consistent with the notion that exposing of the hydrophobic core of the β-barrel structure was the main driving force for bOBP thermal unfolding. The results implied systems, that strongly distorted the protein, had net unfavourable ΔH as the result of molecular strain, primarily associated with the bonding destacking, so ΔS were net favourable.

While the binding interaction of bOBPwt with thymol was enthalpically driven ($-\Delta H_B$) with an unfavourable change of entropy ($-\Delta S_B$). Therefore, it can be concluded that the mechanism of binding of thymol to bOBP is not dominated by a hydrophobic effect related to any change in the hydration state of protein and ligand groups but, most likely, is driven by van der Waals and polar interactions, and hydrogen bonding. This finding is in agreement with that of pOBP either binding to IBMP (−97 kJ/mol) or DMO (−88 kJ/mol), which was characterized by isothermal titration calorimetry (ITC) [85].

CHAPTER 5

CHARACTERIZATION OF THE RECOMBINANT bOBPs WITH DTNB AND IANBD AMIDE

The previous chapter described the purification of single site cysteine mutants of bOBP. Cysteine is very attractive for site-specific conjugation due to its low frequency of occurrence and is high reactivity as a nucleophile. Introduction of this residue can be achieved by site-directed mutagenesis, most often without perturbing the protein's function. The site-specific covalent labelling of proteins through cysteine residue with fluorophores and other moieties has permitted the development of an abundance of detection methods for biosensing [98, 99]. Such an approach is particularly effective when the cysteine residue is on the surface of the protein.

Figure 5.1 is a simplified model showing the overview of labelling and ligand binding to bOBP. A reporting probe is site-specifically conjugated to the cysteine residue on bOBP via covalent bonding. A targeted ligand is then recognised and bound inside internal cavity of bOBP binding site while the probe is still present at the attached position. The protein undergoes a conformational change, which results in an optical change (either absorbance or fluorescence emission signal). This event demonstrates the benefit of this type of specific labelling in creating reversibility of sensing, since the probe is fixed on the protein either with ligand bound or not bound, making the protein biosensor reusable.

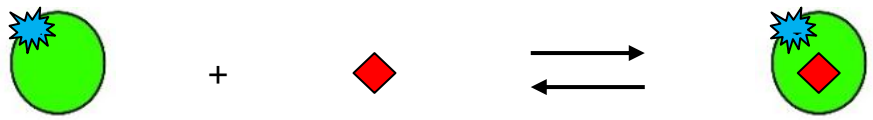

Probe labelled bOBP Target Detection of optical change

Figure 5.1: Simplified model showing the overview of a reporting probe labelling and ligand binding to bOBP. *OBPs (●), 1-AMA (✸), ligands (◆).*

The five recombinant bOBPs; WT, I22C, S24C, F54C, and F91C were characterized by labelling with a number of probes in order to identify those that showed good properties. Several approaches were applied to understand the reactivity of the cysteine residues. These included calculation of the solvent accessible surface area (SASA), reactivity with Ellman's reagent, and labelling efficiency with IANBD amide.

5.1 Calculation of the Solvent Accessible Surface Areas (SASA) of Cysteine Residues in the Recombinant bOBPs

The hydrophobic amino acids in the internal buried cavity of the protein core pay an effective role in protein folding. Information about SASA of the amino acid sequence of proteins is useful in many applications in protein design and structural biology. The calculation of SASA is a geometric measure of the extent to which an amino acid interacts with the solvent and the protein core, that is naturally proportional to the surface area exposed to these environments. The method of calculating SASA typically exploits the 'rolling ball' algorithm developed by Shrake & Rupley in 1973 at which uses a sphere of solvent with a particular radius to probe the surface of the molecule by rolling over the van der Waals surface of the molecule and monitoring the areas which contact the sphere. Basically, a probe of radius 1.4 Å is used to simulate a water molecule, and calculated for the surface contact area. The contact area is the part

of any exposed residue that is capable of making contact with the probe (Figure 5.2). Unit of SASA is usually measured as square Ångstroms [100, 101].

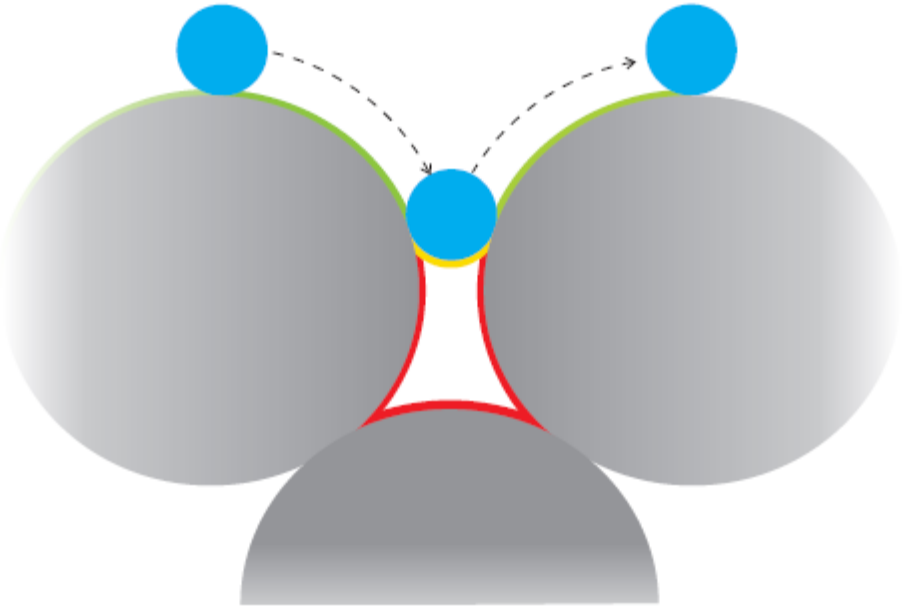

Figure 5.2: Principle of the calculation of solvent accessible surface area. *A probe (blue) is 'rolled' over the Van der Waals surface of the amino acid residue. The surface areas which make contact with the probe are that accessible to solvent are called SASA (green). The surface areas which are not accessible to solvent (red) are called non-contact surfaces. The re-entrant area which combines surface contact areas is shown in yellow.*

In this experiment, the five recombinant bOBPs; WT, I22C, S24C, F54C, and F91C were characterized the binding interaction with a number of ligands at their labelling positions. There are two factors determining labelling efficiency: inherent reactivity and SASA. In this experiment, the likelihood of being labelled was determined from estimation of the SASA at their cysteine residue of the bOBPs, which provided some information about how much the labelling residue exposed to the environment and interacted with the solvent upon binding to some ligand(s). This could imply how well each different bOBP mutant would be labelled.

Eight different files available in PDB database were used to construct the three-dimensional (3D) models of bOBP-WT, bOBP-I22C, bOBP-S24C, bOBP-F54C, and bOBP-F91C in complexes with each of eight different ligands using the SwissPdb Viewer. The SASA for each recombinant bOBPs was calculated and weighted relative to the size of the residue, which was the specific labelling position of the mutated cysteine residue using UCSF Chimera program. Table 5.1 gives the details about the 3D structures of bOBP complexed with various ligands, which were used in the calculation of SASA at the specific labelling position for the recombinant bOBPs.

The result from Figure 5.3 demonstrated that position 24 gave the lowest SASA suggesting its buried existence, while position 91 showed the most significantly different than other mutants with having the highest SASA, particularly when binding to unknown atom or ion (UNX) that was small molecular weight. The order of the cysteine-mutated residues from the highest to the lowest SASA was 91C, 54C, 22C, and 24C. This may influence how readily they react with fluorescent labels.

Table 5.1: Summary of the 3D structures used in the calculation of SASA of the specific cysteine residues in the recombinant bOBPs.

No. of binding ligand	PDB ID	Ligand	Formula	Short name	Reference
1	1G85	1-Octen-3-ol	$C_8 H_{16} O$	3OL	[54]
	1GT5	Benzophenone	$C_{13} H_{10} O$	BZQ	[38]
	1PBO	4-Butyl-5-propyl-1,3-selenazol-2-amine	$C_{10} H_{18} N_2 Se$	SES	[77]
	1GT4	Undecanal	$C_{11} H_{22} O$	UNA	[38]
	1OBP	Unknown atom or ion	X	UNX	[53]
2	1HN2	1-Octen-3-ol	$C_8 H_{16} O$	3OL	[54]
		1-Aminoanthracene	$C_{14} H_{11} N$	ANC	
	1GT3	1-Octen-3-ol	$C_8 H_{16} O$	3OL	[38]
		2,6-Dimethyl-7-octen-2-ol	$C_{10} H_{20} O$	DHM	
3	1GT1	1-Octen-3-ol	$C_8 H_{16} O$	3OL	[38]
		1-Aminoanthracene	$C_{14} H_{11} N$	ANC	
		2-Isobutyl-3-methoxypyrazine	$C_9 H_{14} N_2 O$	PRZ	

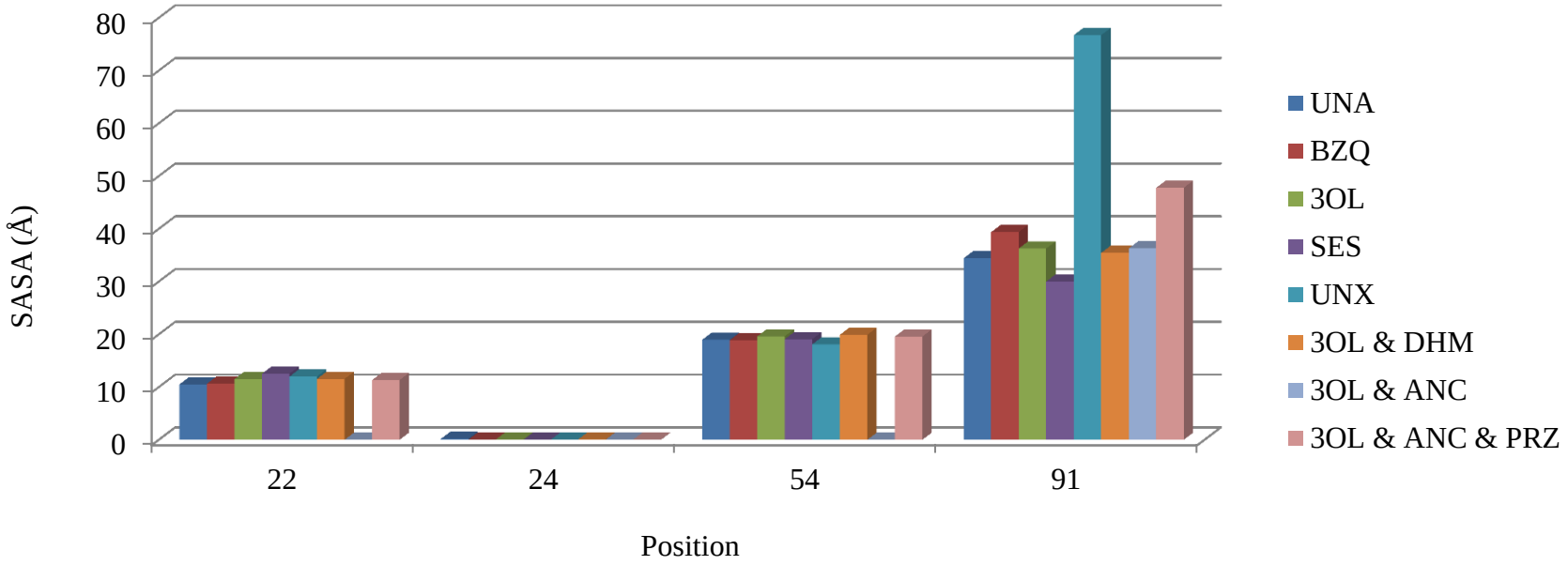

Figure 5.3: SASA of the specific residues in the recombinant bOBPs complexed with eight different ligands. *The analysis was undertaken by Swiss-Pdb Viewer and UCSF Chimera programs.*

5.2 Quantification of Free Thiol Groups Based on the Reaction with Ellman's Reagent

Ellman's reagent or DTNB (5,5'-dithiobis-(2-nitrobenzoic acid)); MW $C_{14}H_8N_2O_8S_2$ is a chemical used for quantitating the number or concentration of thiol groups or sulfhydryl groups in a sample [102]. The reaction of the thiol with DTNB involves producing the mixed disulfide and 2-nitro-5-thiobenzoic acid (TNB) that ionizes to the TNB^{2-} dianion in water at neutral and alkaline conditions (Figure 5.4). This reaction is rapid and stoichiometric, with the presence of one mole of thiol generating one mole of TNB. This TNB^{2-} ion gives a yellow colour that is quantified by the absorbance at 412 nm and has different molar extinction coefficient (ε) in various solvents as shown in Table 5.2.

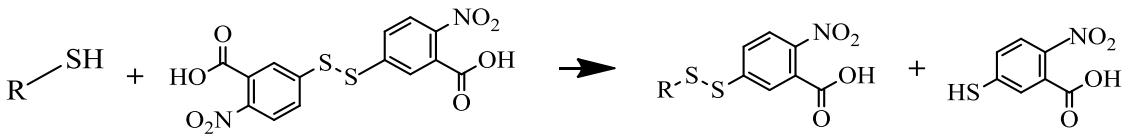

Thiol **DTNB** **Mixed disulfide** **TNB**

Figure 5.4: Reaction of DTNB with a thiol (R-SH)

Table 5.2: Molar extinction coefficients of Ellman's Reagent in various solvents [103].

Solvent	ε at 412 nm
2% SDS	12,500
0.1 M phosphate, pH 8.0, 1 mM EDTA	14,150
Buffered 6 M guanidine hydrochloride	13,700
6 M guanidine hydrochloride	13,880
8 M urea	14,290

Sulfhydryl groups can be estimated in a sample by comparison to a standard curve composed of known concentrations of a sulfhydryl-containing compound such as cysteine. Alternatively, sulfhydryl groups can also be quantitated by reference to the ε of TNB.

Firstly, it was found that there was no reaction of all five native recombinant proteins with DTNB solution. Instead of changing to the yellow colour of TNB^{2-} as expected, the transparent colour of DTNB solution became cloudy and the reactions were precipitated, despite varying the concentration of DTNB (10 – 100 µM) and PBS (0.01 – 1X) in the presence of 10 µM bOBPs, which indicated that the DTNB solution could not access the thiol groups on the proteins.

Hence, it is necessary to expose thiol groups, which are buried in the interior of the protein. The denaturation process induced by 8M urea (in PBS, pH 7.4, containing 1mM EDTA) was accomplished and found turning to yellow colour of the reaction consisted of 10µM bOBPs, 8M urea buffer, 100µM DTNB, and 1% ethanol, which indicated exposure of the free thiol groups. The reactions of the thiol with DTNB solution in the denaturing condition were found to be fast and stable, that was completed in few minutes and did not change over time. The yellow colour of TNB^{2-} was quantified by the absorbance measurement at 412nm. The absorbance values of each mutant bOBP allowed calculation of their thiol concentration based on the Beer-Lambert's law (Equation 5.1) using the molar extinction coefficient of TNB^{2-} in this buffer system at 412nm = 14,290 $M^{-1}cm^{-1}$. From solving the equation 5.1, the concentration of free thiol in each mutant bOBP was therefore determined as shown in Table 5.3, and indicated that each mutant bOBP had a comparable concentration of free thiol and this is consistent with the introduction of a single cysteine residue into each recombinant protein mutant. Additionally, the stoichiometric binding between bOBP and DTNB compound appeared to be 1:1.

$$A = \varepsilon_\lambda c l$$

Equation 5.1: Beer-Lambert's Law. *Where **A** is absorbance, **ε** is extinction coefficient of the chemical species, **c** is concentration of the species, **l** is pathlength of the light, and **λ** is wavelengt.*

Table 5.3: Concentration of thiol in each 10 µM mutant bOBP by the Ellman's assay. *The calculation was based on Beer-Lambert's law (Equation 5.1) using the molar extinction coefficient of TNB at 412 nm (14,290 $M^{-1}cm^{-1}$) in 8 M urea buffer condition together with their absorbance at 412 nm.*

Residue	SH content (per monomer)
WT	0.6
22C	1.2
24C	1.2
54C	1.2
91C	1.3

5.3 Characterization of the Reaction of the Recombinant bOBPs with IANBD Amide

A challenge for the development of effective fluorescent protein-based biosensors is the signal transduction of the binding events, which is a significant determinant in the performance of the biosensors. With the advance in fluorescence technology, fluorescent probes have become an essential tool in biological fields that are invaluable for exploring the domain function, and structure variation in local regions within a single macromolecule, such as DNA or protein. They are widely used instead of radioactive probe owing to their preferable advantages, including its easier handling, higher stability, lower total costs, re-readability, and fast detection [104].

Types of detection consist of a conventional immunoassay and a molecularly integrated assay (Figure 5.5). The conventional immunoassay is a multistep sandwich analysis, which involves sample labeling. The target molecule must support two distinct binding sites, and separation of free and bound molecules is required after each step. Whereas the advanced assay has molecularly integrated the recognition and signaling events by the attachment of one or more fluorescent reporter probe(s) to the recognition element that allows the probe(s) to respond to analyte binding. This requires a fluorophore to possess emission properties which are sensitive to changes in the local environment induced by binding to the target molecule [105]. The detection can be typically performed by Förster resonance energy transfer (FRET) [106, 107], the formation of a nonfluorescent complex [108], fluorescence anisotropy [109], or more relevant to this project, the change of emission intensity of a single environmentally sensitive fluorophore in the presence of the analyte.

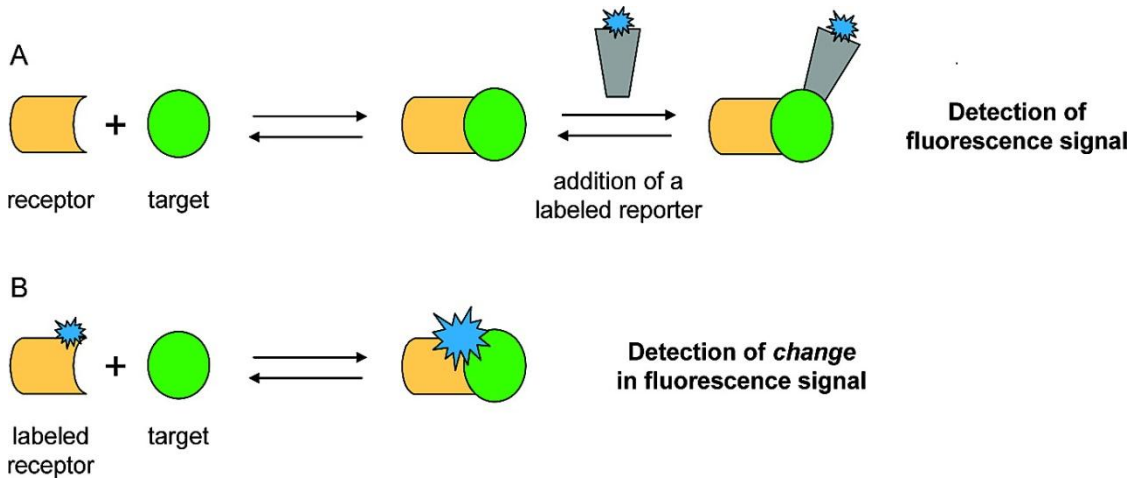

Figure 5.5: Types of detection of fluorescence signal for protein quantification. *(A) A traditional sandwich assay relies on a labeled reporter molecule for detection. (B) A molecularly integrated assay of the recognition and reporting functions provides a homogeneous detection [105]. This image has been reproduced with the permission of the rights holder, American Chemical Society.*

Binding of a ligand molecule to a protein molecule can lead to protein structural changes that involve domain rearrangement [110], conformational changes of secondary structures [111], and residue re-orientation in the local binding site. Fluorophores located where the environmental change occurred upon ligand binding, results in the modulation of its fluorescence intensity that can be monitored as a function of ligand concentration, allowing detection and quantification of an analyte of interest. Therefore, the position of the fluorophore where the conformational changes occurred is crucial for the ligand-binding detection.

Among fluorescent probes, a class of fluorescent moieties called environmentally sensitive fluorophores offers an effective way for targeting the specific region of protein and yielding informative data on micro-environmental changes of the region. Environmentally sensitive fluorophores are a special class of chromophores that have spectroscopic behaviour that is dependent on the physicochemical properties of the surrounding environment. Numerous reports have used them to study biochemical functions that are related to conformational changes, such as ligand binding.

The widely used site-specific covalent labelling of IANBD amide was chosen as a fluorescent reporter probe (Fig. 5.5b) for sensing in this project because of its thiol-reactive property. The examples of thiols reacting with this probe include cysteine, and 2-mercaptoethanol. A schematic diagram shows the reaction of the IANBD amide fluorophore (its full structure shown in Figure 2.3) with thiol group of cysteine residue on protein molecule making the conjugation of NBD with thioether (NBD・thioether) by the covalent link of thioether bond (Figure 5.6). In addition, IANBD is an environmentally sensitive fluorophore, which emits no significant fluorescent before conjugating with a thiol group. Therefore, labelling with IANBD amide fluorescent probe was not only to detect the presence of an amount of materials, but also indicate response to conformational and environmental changes of the labelled protein upon interaction with small molecules, i.e. ligand binding.

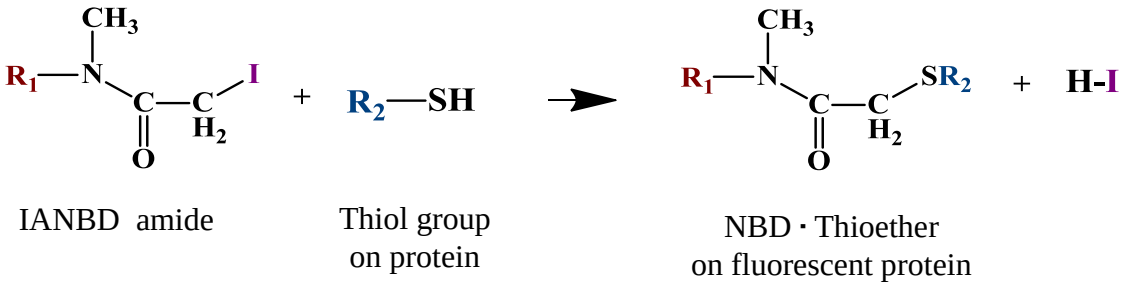

Figure 5.6: Reaction of IANBD amide with thiol group on protein molecule

In these following experiments, IANBD amide was investigated to see if it could be a possible good reporting probe for engineering bOBP biosensors. The characterization of the ligand binding interaction between the recombinant bOBP and the fluorescent IANBD amide has been performed.

5.3.1 Reaction of IANBD amide with thiol

IANBD amide (its structure shown in Figure 2.3), a thiol-reactive fluorescent probe, is known to emit no significant fluorescent before conjugating with a thiol group in solution, and therefore less background fluorescence is supposedly produced by the unreacted IANBD amide molecules.

A control experiment was performed in order to investigate the binding of IANBD amide as a thiol-reactive fluorescent probe with 2-mercaptoethanol as a thiol. The various concentrations of IANBD amide were conjugated with the excess 2-mercaptoethanol. Their fluorescence intensities were detected at 480 nm for excitation wavelength and at 550 nm for maximum emission wavelength.

The result in Figure 5.7 showed that the fluorescence emission intensity increased upon the concentration of conjugated NBD, indicating binding of IANBD to thiol group of 2-mercaptoethanol and generating the conjugated NBD, which confirmed that IANBD amide is a thiol-reactive fluorophore. However, it was found that at high

concentrations, the fluorescence intensities were not proportional to the concentrations of the conjugated fluorophore. The distortion of the curve shape by decreasing intensity of the emitted light in this experiment could have a contribution from an inner filtering effect, arising from high concentrations of the fluorophore making the intensity of the excitation light not constant throughout the solution. As a result, only a small percentage of the excitation light reached the fluorophores that emit the declined photons for the detection system. It was found that there was no inner filter effect at IANBD ≤ 26µM as shown by a linear curve in Figure 5.7 (inset).

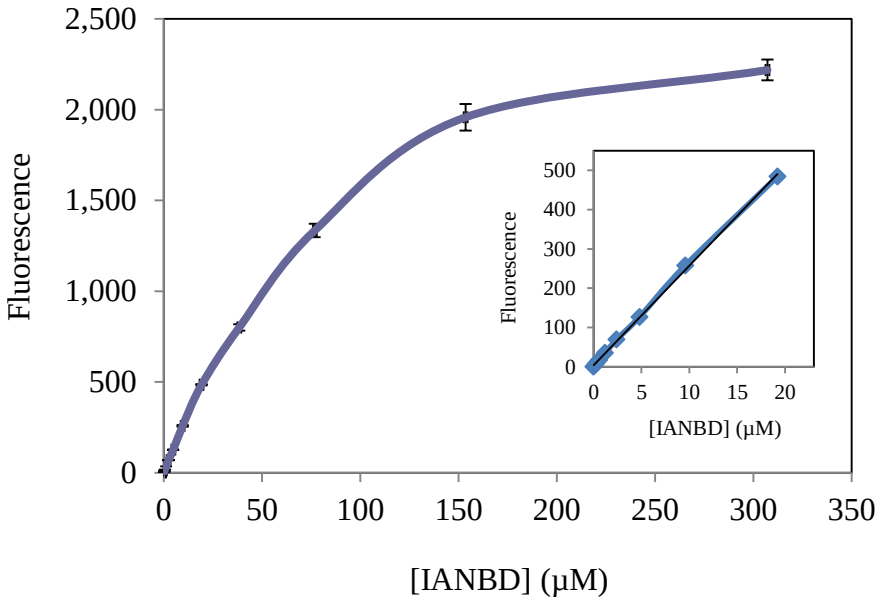

Figure 5.7: Fluorescence of IANBD amide in the presence of thiol. *The curve shows inner filter effect when IANBD amide concentrations were >26µM.* ***The various*** *concentrations of IANBD amide ranging from 0 to 307.2 µM were conjugated with the corresponding 10-fold molar excess 2-mercaptoethanol. The reaction was carried out for 1hr in PBS with 10mM EDTA supplement, pH 7.4 with 1% DMSO.* ***The*** *fluorescence excitation and emission were 480 nm and 550 nm, respectively. Inset: linear curve of IANBD amide in the presence of thiol shows no inner filter effect when IANBD amide was ≤ 26µM.*

5.3.2 Molar binding ratio of IANBD amide and bOBPwt

Conceptually, an environmentally-sensitive fluorophore is a reporter for binding between a ligand molecule with a fluorescently labelled protein, which can be due to a direct effect of its interaction with the ligand, or an indirect effect through a protein conformational change.

It is known that IANBD amide is a thiol-reactive fluorescent probe that can be attached to site-specifically mutated cysteine residues in ligand binding proteins e.g. periplasmic binding protein (PBP) [112-114]. These labelled proteins show ligand dependent changes in the fluorescence of the NBD group.

Likewise, it is proposed that the cysteine mutants of bOBP are specifically labelled with the thiol reactive probe IANBD by forming covalent bond with cysteine residues on the protein molecule. In this experiment, the extent of the interactions of wild-type bOBP (which does not contain cysteine residue) and IANBD amide as a ligand were evaluated by determining the molar binding ratio of IANBD amide and the WT protein, for which the value was expected to be approximately zero.

The molar binding ratio represents the average number of the fluorescent probe molecules conjugated to each protein molecule. The C_f / C_P molar ratio is the ratio of the binding interaction between fluorophore and protein concentrations, which can be determined based on the Beer-Lambert's Law (Equation 5.2). Two parameters are needed: the molar extinction coefficients of the IANBD amide (given in the handbook of manufacturer) is 25,000 $M^{-1}cm^{-1}$ at 480 nm, and the molar extinction coefficient of 47,000 $M^{-1}cm^{-1}$/ bOBP dimer at 280 nm [54].

The experiment was carried out by incubating 100μM bOBPwt with a 10-fold molar excess of IANBD amide, followed by removing the excess unbound fluorophore in the reaction in order to decrease non-specific binding, and leave only the fluorescent probe that conjugated to bOBPwt. The absorbance at 480 and 280nm of the binding solution was measured to determine the concentration of the fluorophore and the protein after binding and removing excess IANBD amide.

$$\textbf{Fluorophore binding ratio} = \frac{\textbf{Concentration of Fluorophore}}{\textbf{Concentration of Protein}} = \frac{A_{480} / \varepsilon_{480}}{A_{280} / \varepsilon_{280}}$$

Equation 5.2: Fluorophore binding ratio. *Where **A** is absorbance at a certain wavelength and ε is extinction coefficient at a certain wavelength for the fluorophore or protein.*

The result from the calculation of the average molar binding ratio of the interaction between IANBD amide and the wild type bOBP was 0.27 ± 0.01, indicating that the interaction between the IANBD amide and bOBPwt was existed and was significant. This could be due to the IANBD amide non-site specific covalently reacting with other residues (such as methionine [115], histidine [115], and tyrosine [116]) inside the ligand binding cavity of bOBP. However, it might be a non-covalent complex being formed, so the next experiment involving the reaction of IANBD amide with wild type bOBP was performed in order to examine any non-covalent interactions of the IANBD amide with the protein.

5.3.3 Reaction of IANBD amide with bOBPwt

The formation of non-covalent bonding in the interaction of the IANBD amide fluorescent probe with bOBP was investigated by eliminating the non-site specifically covalent bonding in the reaction of IANBD amide with 2-mercaptoethanol, and then evaluating any non-covalent interaction of the IANBD amide with the wild type bOBP that might occur. A binding study with constant conjugated NBD concentration and variable bOBPwt concentration was thus performed. 2µM IANBD amide was covalently conjugated with the 10-fold excess molar 2-mercaptoethanol (20µM), and titrated with increasing bOBPwt concentrations from 0 to 40.96µM.

The fluorescence intensity at 550nm as a function of bOBPwt concentration at constant conjugated NBD was plotted. The result in Figure 5.8 showed the increase of IANBD amide fluorescence emission intensity in the presence of the wild type bOBP upon excitation at 480nm, indicating non-covalent bonding existed in the interaction between IANBD amide and bOBP, as they could form a complex, resulting in an enhancement of the fluorescence emission as the protein concentrations increased until all of the fluorophore was bound to the protein.

A saturation binding curve was derived by fitting to hyperbolic equation (Equation 5.3) to determine the equilibrium dissociation constant (K_d) value of non-covalently bound complex of bOBP and IANBD amide by which K_d = 25 ± 6 µM was obtained. The F_{max} (maximal fluorescence value of bOBPwt bound conjugated NBD: F_I) was found to be 748µM^{-1}, whereas fluorescence value of IANBD(SH) ($F_{I\text{-}P}$) was 26µM^{-1} (derived from the section 5.3.1: Reaction of IANBD amide with thiol), making µM Fluorescence (F_I / $F_{I\text{-}P}$) = 29-fold enhancement.

$$\mathbf{F} = \frac{\boldsymbol{F_{max}} \mathbf{*\ [bOBP]}}{\boldsymbol{K_d} \mathbf{+\ [bOBP]}}$$

Equation 5.3: Hyperbolic equation.

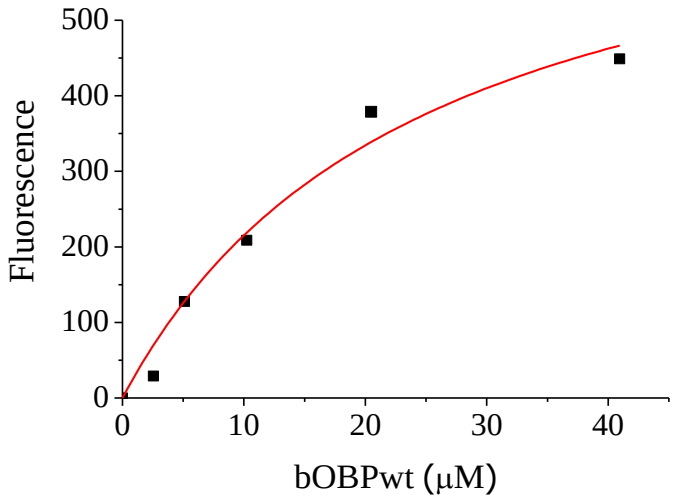

Figure 5.8: Binding curve of non-covalently bound complex of bOBPwt and conjugated IANBD amide. *2μM IANBD amide was conjugated with 20μM 2-mercaptoethanol, and titrated with increasing bOBPwt concentrations ranging from 0 to 40.96μM. The reaction was in PBS with 10mM EDTA supplement, pH 7.4 with 1% DMSO. The fluorescence excitation and emission were 480nm and 550nm, respectively.*

Although four cysteine bOBP mutants were made and characterised, the non-covalent binding of IANBD amide made it difficult to distinguish ligand dependent conformational changes from ligand dependent displacement. Therefore, no further work was carried out on IANBD/thiol mutants and a simpler fluorophore that provided ligand displacement was studied. The following chapter describe a ligand displacement sensing with 1-aminoanthracene (1-AMA) as a fluorescent reporter molecule.

CHAPTER 6

FLUORESCENCE AND ABSORBANCE SPECTROSCOPY OF bOBP-LIGAND INTEREACTIONS

6.1 Fluorescence-Binding Assay

Biomolecules such as proteins and nucleic acids can be labelled with optical probes to allow for their detection. Covalent labelling is by the reaction of an appropriately functionalized dye molecule with a reactive group on the protein or other biomolecule. However, the binding of IANBD to bOBP described in Chapter 4 showed that a mixture of covalent and non-covalent bonding was occurring.

In some cases, non-covalent label is known to bind and yield a fluorescent complex. A non-protein example of this is staining DNA with ethidium bromide or SYBR Gold. Although the interactions arising from non-covalent labelling are considerably less stable than the covalent linkages, the important benefit of non-covalent labelling is that it affects the functional activity of the biomolecule to a lesser extent. This is because the interactions happen at a faster rate and at a physiological pH range. Additionally, purification steps are generally unnecessary when the stoichiometry of the complex is known. Finally, non-covalent labels regularly are shielded by the biomolecule from those quenching effects [117-119].

1-aminoanthracene (1-AMA) is a polarity-sensitive hydrophobic probe that has been used previously to investigate binding in the lipocalin family of protein cavities as well as to study interaction between these different proteins and their ligands, particularly odorant binding proteins (OBPs) and hydrophobic ligands such as 2-iso-butyl-3-metoxypyrazine (IBMP), dihydromyrcenol (DHM) or benzophenone (BZP) [38, 46, 54, 65, 87, 88, 90, 120-123]. This fluorescent ligand as a substitute for the

tritium-labelled 2-isobuthyl-3-methoxypyrazine (PYR) is often used to monitor the functional state of OBPs and is also applied in competitive binding assays [88, 124].

A simplified model of competitive binding strategy is illustrated in Figure 6.1. In general, 1-AMA shows enhanced fluorescence intensity when complexed with OBPs. When hydrophobic ligands are added to OBPs/1-AMA complex, bound 1-AMA is displaced by these ligands in competitive binding assays. Binding of these ligands to the proteins is indicated by a decrease in the fluorescence intensity of bound 1-AMA. This allows a fluorescence assay based on 1-AMA and bOBP should be useful for compound screening and hence biosensor engineering.

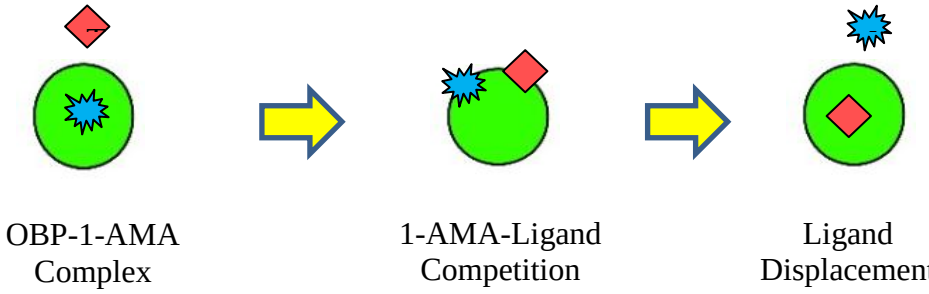

Figure 6.1: Simplified model of competitive binding strategy. *OBPs (●), 1-AMA (✸), ligands (◆).*

The three-dimensional structure of the 1-AMA/bOBP complex determined by x-ray crystallography is illustrated in Figure 6.2, revealing two very well ordered 1-AMA molecules in the buried cavities [54] where the natural ligand (1-octen-3-ol) binds [46, 53]. Two molecules of 1-AMA are bound per dimer, that is one to each bOBP β-barrel [54]. These β-barrels are known to be the general binding site of bOBP [54] as similarly in pOBP [48, 59].

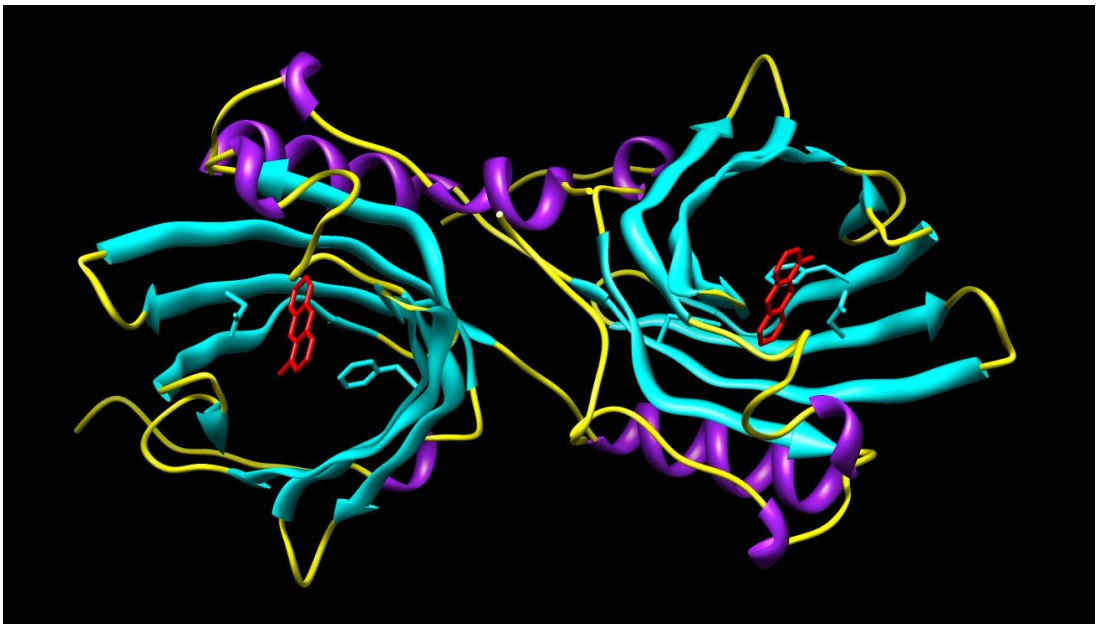

Figure 6.2: Three-dimensional structure of 1-AMA/bOBP complex. *Two 1-AMA molecules are bound in the internal binding site of bOBP.*

6.1.1 A binding assay based on 1-AMA

The ligand, 1-aminoanthracene (1-AMA) (its structure shown in Figure 2.4) has been demonstrated in the binding in the internal cavities of the bOBP protein, and used for measurement of the bOBP functionality [54]. Thus, the recombinant bOBPwt was characterized in its binding interaction with 1-AMA.

The maximum wavelengths of excitation and emission spectra for the bOBP/1-AMA complex were monitored and the result was that the bound complex exhibited a fluorescence maximum emission wavelength at 490nm with a 390nm maximum excitation wavelength (Figure 6.3 – 6.4). The position of the 1-AMA emission peak shifted from 570nm to 490nm in binding to bOBP, as also found in [125].

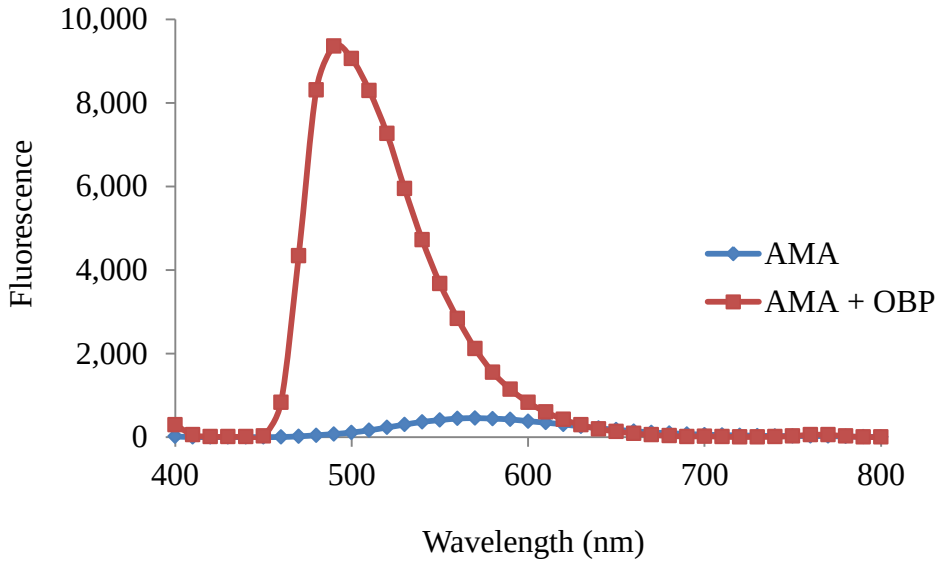

Figure 6.3: Fluorescence emission spectra of unbound 1-AMA (blue diamond) and 1-AMA complexed with bOBPwt (red square). *Excitation wavelength was 390nm. bOBPwt was 100µM and 1-AMA 100µM in both cases. The reactions were in PBS with 1mM EDTA supplement, pH 7.4.*

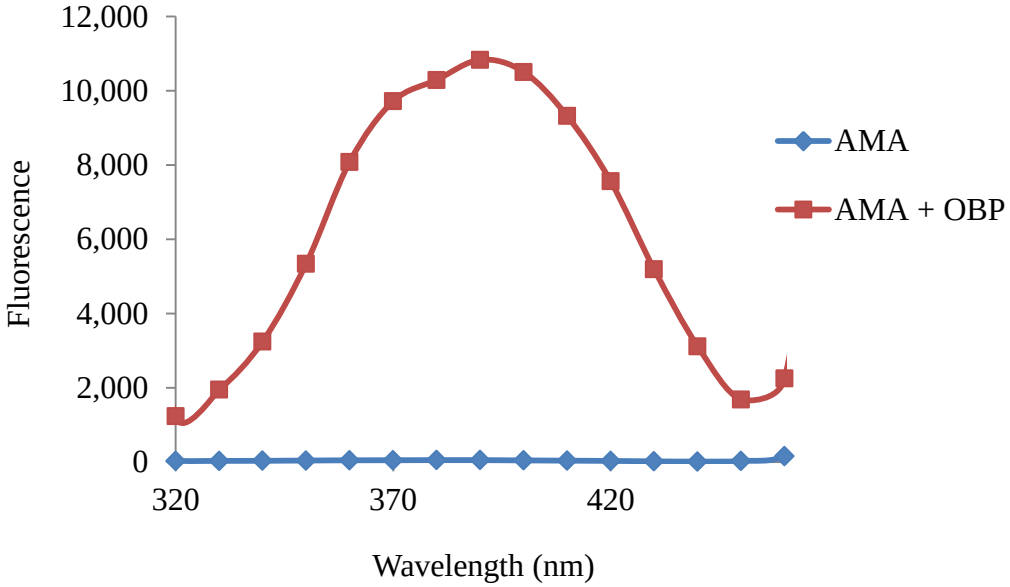

Figure 6.4: Fluorescence excitation spectra of unbound 1-AMA (blue diamond) and 1-AMA complexed with bOBPwt (red square). *Emission wavelength was 490nm. bOBPwt was 100µM and 1-AMA 100µM in both cases. The reactions were in PBS with 1mM EDTA supplement, pH 7.4.*

The binding affinity of 1-AMA for the recombinant bOBPwt was determined by direct titration of 0.5µM of bOBPwt using 1-AMA concentrations that ranged from 0 to 12.8µM. The result indicated that the increase in fluorescence signal of 1-AMA upon complexation to the protein was the result of the formation of the bOBPwt/1-AMA complex (Figure 6.5; blue point). Corrected emission fluorescence intensity of the recombinant bOBPwt with 1-AMA was obtained from fluorescence intensities of 1-AMA bound to bOBP when corrected for contributions from unbound 1-AMA (Figure 6.6). The titration curve of the bOBPwt with 1-AMA was used to determine their equilibrium dissociation constant (K_d) of the 1-AMA/bOBPwt complex using a single-site specific binding model (Equation 6.1).

$$\mathbf{Y} = \frac{\boldsymbol{B}_{\mathbf{max}} * \mathbf{X}}{\boldsymbol{K}_{\mathbf{d}} + \mathbf{X}}$$

Equation 6.1: Single-site specific binding model. *Where Y is the corrected fluorescence intensity, B_{max} is the maximal Y value, X is the concentration of 1-AMA, and K_d is the concentration of 1-AMA required to reach half-maximal binding.*

It was found that the dose-response curve gave a K_d value of 0.16 ± 0.023 µM for 1-AMA to bOBP, indicating bOBP is functional and able to bind 1-AMA. This value is comparable with the one of Mazzini *et al*. 2007 (0.23 ± 0.01 µM) [87]. Typical values that have been reported by others are between 0.66 - 1µM for either recombinant or natural bOBPwt [38, 46, 54, 62, 126, 127].

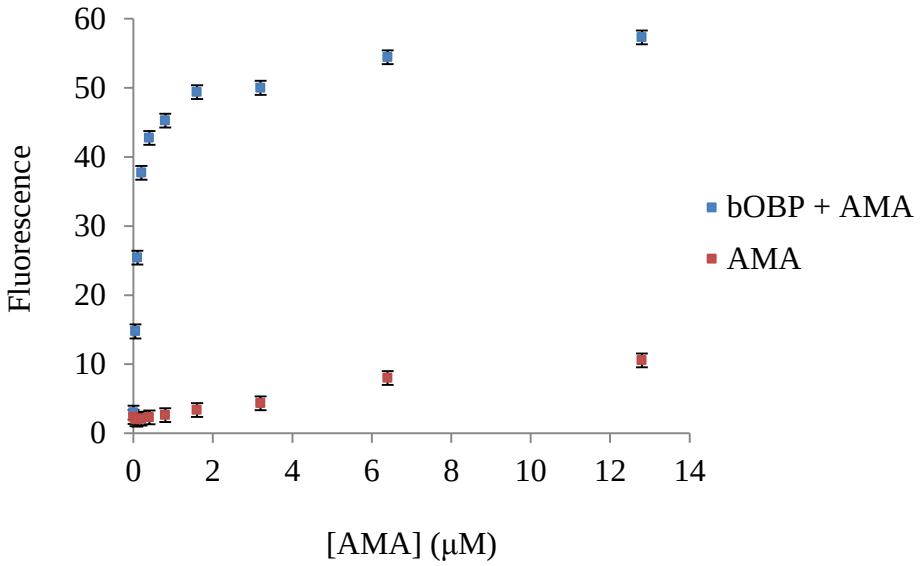

Figure 6.5: Fluorescence binding curve of the recombinant bOBPwt with the ligand 1-AMA (blue point). *0.5µM bOBPwt monomer concentration was titrated with 1-AMA from 0 to 12.8µM in PBS with 1mM EDTA supplement, pH 7.4, with 0.1% DMSO. Fluorescence intensity of 1-AMA was measured at 490nm with excitation at 390nm, 1 hour after addition of the probe to the protein. Unbound 1-AMA (red point) was represented as a background.*

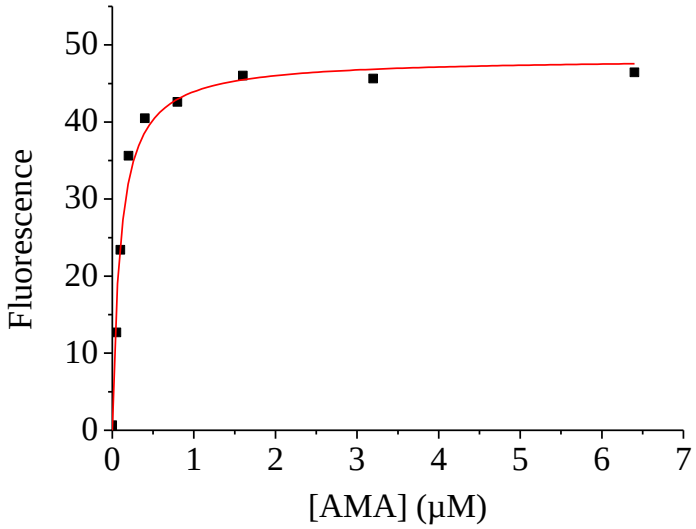

Figure 6.6: Corrected emission fluorescence intensity of the recombinant bOBPwt with 1-AMA. *The curve was obtained from intensities of bOBP/1-AMA complex (in Figure 6.5) with subtraction of unbound 1-AMA background.*

6.1.2 Competitive binding assays with 1-AMA

Since x-ray crystallography experiments demonstrated that 1-AMA binds in the internal β-barrels of bOBP (Figure 6.2) as well as the fluorescence binding assays that showed bOBP dimer binds two 1-AMA molecules, then competitive binding of other ligand should displace the 1-AMA and so reduce its fluorescence [54].

Competitive titrations between 1-AMA and several known or possible ligands, thymol, bromocresol green, malachite green, and methyl salicylate, were set up to determine their binding affinities. In the competitive binding assays, a fixed concentration of 1μM bOBPwt was incubated with a fixed amount of 1μM 1-AMA in the presence of increasing concentrations of each ligand (0–100μM) in the reaction containing PBS with 1mM EDTA supplement, pH 7.4 with the final concentration of 0.1% (V/V) DMSO solvent and 0.1% (V/V) absolute ethanol. The decrease of competitive 1-AMA fluorescence at 490nm was recorded as a function of ligand concentration.

It was found that the fluorescence intensities decreased on the addition of thymol, bromocresol green, and malachite green, in a hyperbolic fashion (Figure 6.7; A-C).

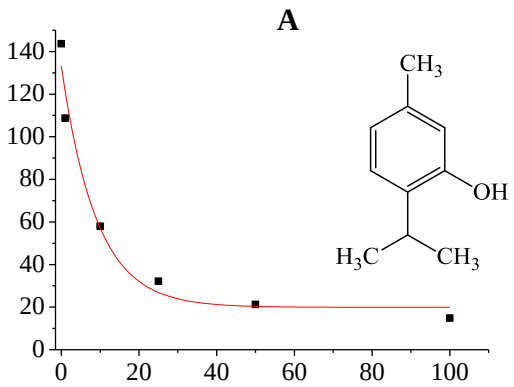

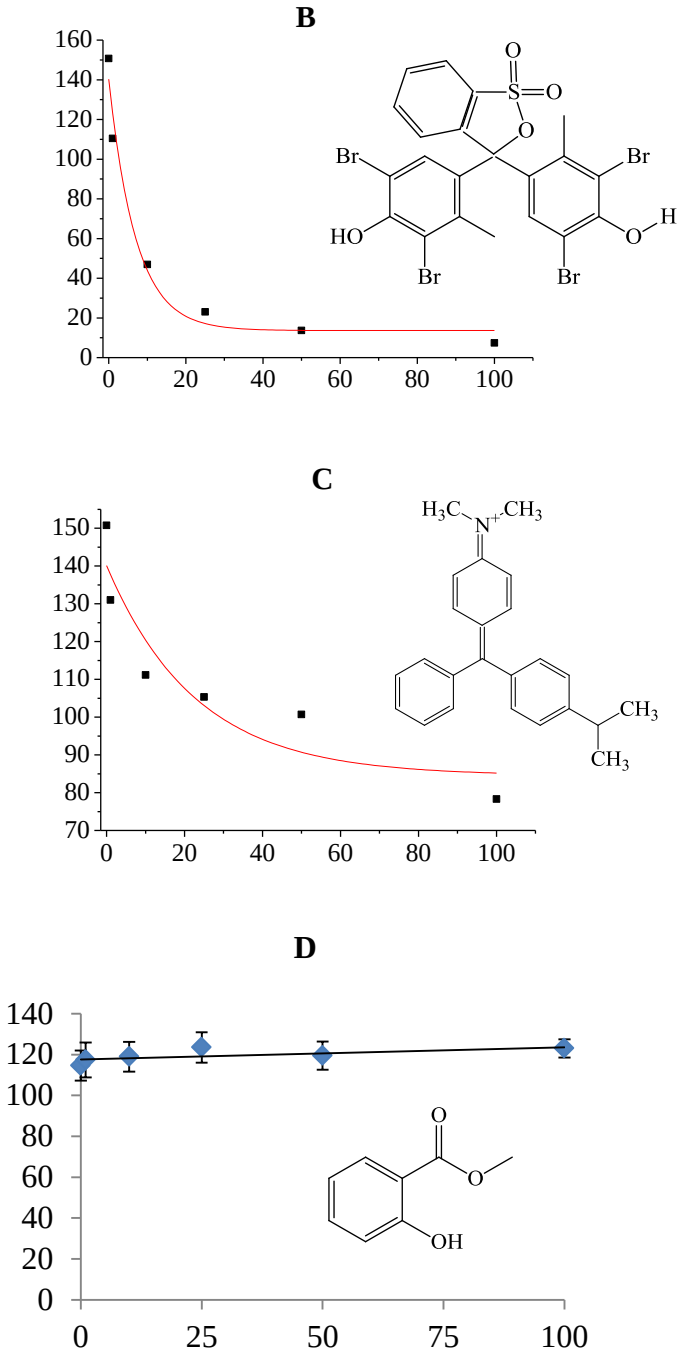

Figure 6.7: Competitive binding curves of various ligands with 1-AMA on bOBP. *The fluorescence of 1-AMA decreases when displaced by the ligands; (A) Thymol, (B) Bromocresol green, (C) Malachite green, and (D) Methyl salicylate. Y-axis is fluorescence intensity of bound 1-AMA at 490nm. X-axis is the micromolar concentration of total ligand competing for binding. bOBP and 1-AMA were used at 1 μM concentration.*

The fluorescent emission data obtained were transformed into the fractional occupancy (***f***), the concentration of protein-ligand complexes in the total protein concentration by using Equation 6.2.

$$f = \frac{F\text{-}Fo}{Fmax\text{-}Fo} \qquad \textbf{6.2}$$

Where ***f*** is fraction of ligand binding sites filled with ligand, **F** is fluorescence intensity, $\mathbf{F_o}$ is fluorescence intensity in the absence of ligand, and $\mathbf{F_{max}}$ is fluorescence intensity in the excess of ligand.

The dependence of ***f*** on ligand concentration was used to determine the apparent K_d (K_d^{app}) for each ligand from the single-site specific binding equation (Equation 6.1). The corrected K_d value (K_d^{corr}) for each ligand was then calculated from the K_d^{app} using the formula [54] shown in Equation 6.3 with K_d of 1-AMA for bOBP was 0.16 μM, and the 1-AMA concentration was 1 μM.

$$\boldsymbol{K_d^{corr} = K_d^{app} * \frac{1}{1 + (1 / K_d^{AMA} * [AMA])}} \qquad \textbf{6.3}$$

Where $\boldsymbol{K_d^{AMA}}$ is the dissociation constant of the 1-AMA/OBP complex.

The results of the K_d^{app} and K_d^{corr} values for thymol, bromocresol green, and malachite green are listed in Table 6.1, and the values indicated that 1-AMA was the best ligand. Thymol and bromocresol green had comparable affinity constant values to bOBPwt, although both are very different in their chemical structures. The K_d value of thymol for bOBP was 0.58 ± 0.28 μM, which is in agreement with the compounds listed as 'strong ligands' for bOBP usually bind with K_d between 0.1 and 1 μM [36]. Surprisingly, it was found that methyl salicylate that is a wintergreen-scented chemical used to provide fragrance to various products, did not show competitive displacement with 1-AMA to bOBPwt as shown in Figure 5.21; D. Thus, no special characteristic could be attributed to the good binders upon interaction with all ligands [38].

Table 6.1: Apparent dissociation constants (K_d^{app}) and Equilibrium dissociation constants (K_d^{corr}) values of ligands for bOBPwt derived from competitive binding assays with 1-AMA. *Each value of K_d is the average of a minimum of three and a maximum of thirteen (thymol) independent determinations.*

Ligand	K_d^{app} (µM)	K_d^{corr} (µM)
Thymol	4.17 ± 2.04	0.58 ± 0.28
Bromocresol green	3.25 ± 0.51	0.45 ± 0.07
Malachite green	5.86 ± 3.18	0.81 ± 0.48

6.1.3 Dual ligand titration with 1-AMA

All of previous OBPs/1-AMA reports determine K_d values of a system in which two alternative substrates compete for the same protein-binding site by titrating the fixed concentrations of protein and 1-AMA at 1:1, and then varying concentrations of another ligand competitor.

In this study, the analysis of the effect of two ligands, 1-AMA and another ligand competitor in competitive binding assay was presented in order to estimate the equilibrium K_d value of ligand with improved accuracy compared to typical methods that fix 1-AMA concentration. The experimental set up involved with titrating a fixed concentration of 0.5µM bOBPwt with varying 1-AMA and thymol concentrations. The procedure was performed by the addition of a concentration of thymol in a set of a standard single ligand titration of 0.5µM bOBPwt with 1-AMA ranging from 0–12.8µM. The concentration of thymol used in each set of experiments was 0, 0.1, 10, 25, 50, and 100µM.

The titration curves between the fluorescence intensities of 1-AMA/ bOBPwt complex with the presence of each thymol concentration against the concentrations of 1-AMA were plotted (Figure 6.8) and used to determine the K_d values of the 1-AMA/ bOBPwt complexes based on the single-site specific binding model (Equation 6.1). Next, the curve of -log K_d of 1-AMA with the presence of each thymol concentration was plotted against their corresponding thymol concentrations (Figure 6.9). The equilibrium K_d value for thymol from the dual ligand titrations was analysed based on global nonlinear regression method of Lew and Angus (Equation 6.4) [79].

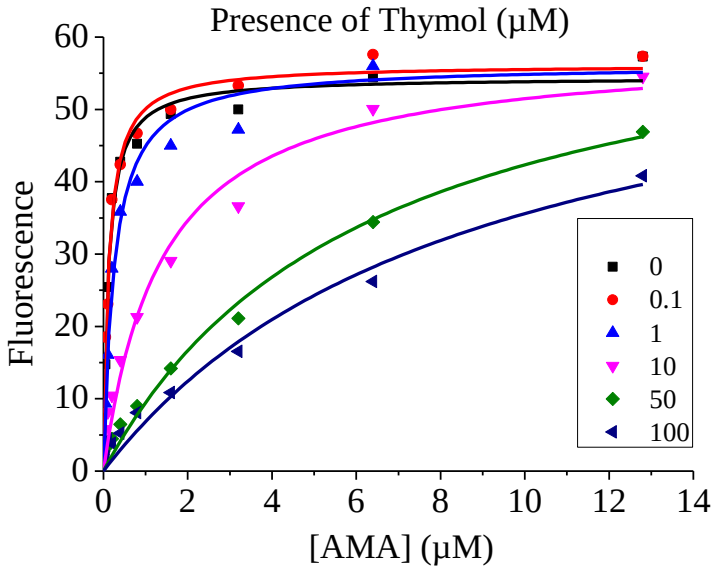

Figure 6.8: Dual ligand titration using 1-AMA and thymol. *Standard titration assays were to add thymol to bOBPwt in the presence of increasing amounts of 1-AMA. The concentrations of thymol used in these experiments were 0, 0.1, 1, 10, 50, 100µM. The data for each titration curve of the bOBPwt with 1-AMA was used to determine the K_d value of the 1-AMA/bOBPwt complex with the presence of each thymol concentration based on the single-site specific binding model (Equation 6.1).*

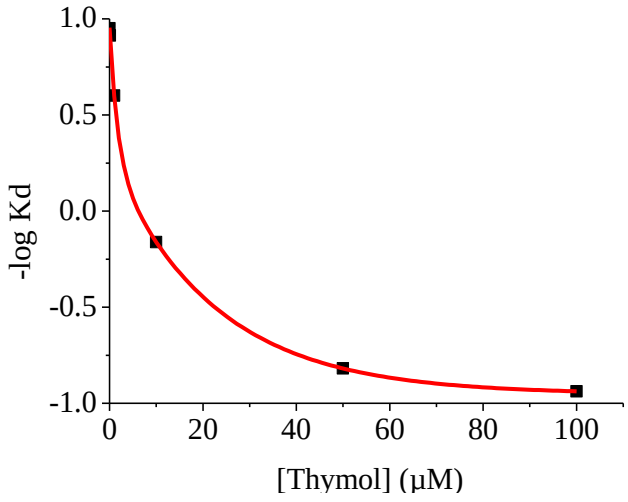

Figure 6.9: Plot of -log K_d of 1-AMA with the presence of various thymol concentrations against their corresponding thymol concentrations. *This plot was used for determining the equilibrium K_d value for thymol from the dual ligand titrations. The calculation was based on global nonlinear regression method of Lew and Angus; -log K_d^{AMA} = - log ([L] + $10^{log\ (Kd)}$) + C (Equation 6.4) [79], by using either SciDAVis or Prism 5.0 software.*

$$\textbf{- log } K_d^{\textbf{AMA}} \textbf{ = - log ([L] + 10}^{\textbf{log (Kd)}}\textbf{) + C} \qquad \textbf{6.4}$$

Where K_d^{AMA} are dissociation constants of 1-AMA at various concentrations of antagonist (including 0), [L] is the antagonist concentration corresponding to K_d^{AMA}, K_d is dissociation constant of antagonist, and C is a constant value [79].

The data shown in Figure 6.9 were calculated using either SciDAVis or Prism 5.0 software. The K_d value of thymol for bOBPwt was found to be 1.03 ± 0.153 µM, which is slightly different from that obtained with single ligand titrations (0.58 ± 0.28 µM) and that determined by CD spectroscopy (0.75 µM).

In order to illustrate the competitive type of ligands and 1-AMA for binding to bOBP, the double reciprocal plot has been applied; this is used to distinguish competitive, non-competitive, and uncompetitive ligands. It is created by taking the reciprocal of both sides of hyperbolic binding function (Equation 6.1).

Thus, the data of dual ligand titration using 1-AMA and thymol (Figure 6.8) was used to produce the double reciprocal curves whereby 1/ [1-AMA] was plotted against -1/ [Thymol]. It was shown that each line of thymol concentration has the same y-intercept, but there were different slopes and x-intercepts between the data sets (Figure 6.10). The pattern of lines was in accordance with a model in which the binding of 1-AMA and thymol was competitive for binding to bOBPwt, since the maximum concentration of thymol bound is unaffected by competitive inhibitors.

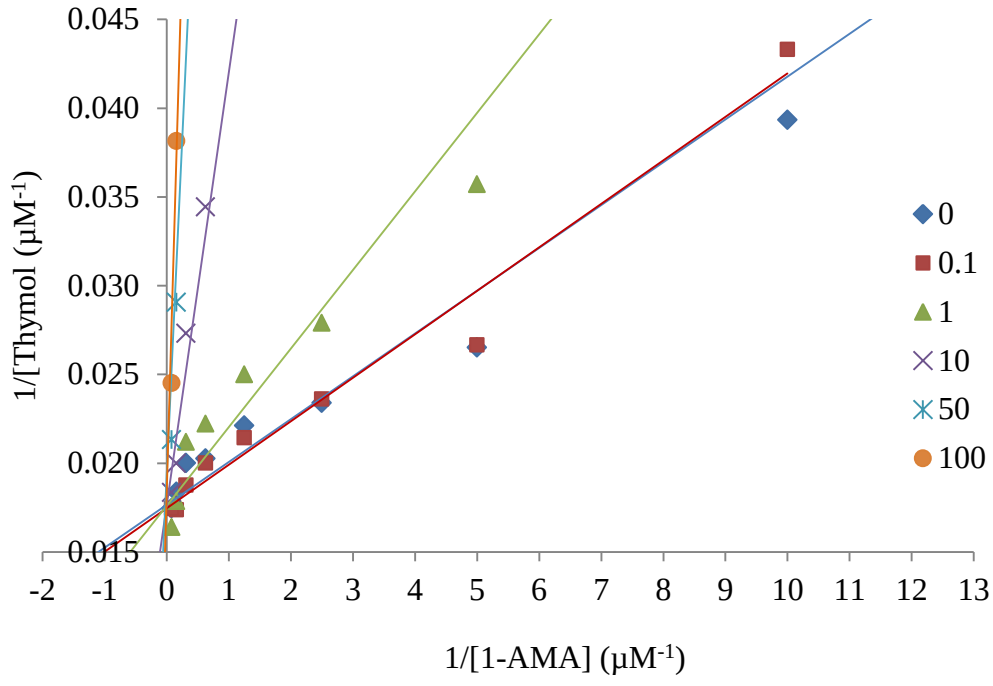

Figure 6.10: Double-reciprocal plots showing competitive type of reversible ligand inhibitor.

In conclusion, the functionality of bOBPwt was analysed by binding assays with 1-AMA, and resulting in a good affinity with the K_d value of 0.16 ± 0.023 μM. Four different ligands, namely thymol, bromocresol green, malachite green, and methyl salicylate were investigated in competitive ligand-binding experiments with the purified recombinant bOBP. Most of the ligands examined were found to be good ligands with the K_d values in the micromolar range, but methyl salicylate was found not to bind to this protein. The significant differences of ligand binding affinity confirmed the broad binding specificity of OBPs. Finally, the data showed that the fluorescent ligand 1-AMA is a suitable ligand used to observe the functionality of bOBP through fluorescence analysis, and also indicated the possibility of using 1-AMA with the competitive binding strategy as a probe in building biosensors based on this recombinant bOBPwt that have applications in ligand discrimination for pre-screening some chemical substances.

6.2 Absorbance-Binding Assay

It has been shown in Section 6.1 that the strategy of competitive displacement labelling of 1-AMA was successful. Thus in this experiment, the light absorption characteristics based on this competitive strategy were investigated in order to find a chromophore that could be used as a probe other than the fluorophore 1-AMA that although it is sensitive, can photobleach.

Fifteen chromophores in the laboratory including DTNB, bromocresol green, cibacron blue, thionin, benzohydroxamic acid, nickel(II) chloride, p-nitroaniline, potassium permanganate, 1,2-phenylenediamine dihydrochloride, potassium chromate, 3,4-dinitrotoluene, copper(II) nitrate, iodine, 4-nitrophenol, and 1-AMA, were then screened to examine for the binding property to bOBP by changes in their UV–vis absorption spectra. It was found that some of them, for example bromocresol green (BG), bound to bOBP as the absoption spectra increased with increasing protein concentration, as seen by the peak at 625nm (Figure 6.11). Likewise, Figure 6.12 illustrates the increase in absorbance at 625nm of bromocresol green as a function of

bOBP concentration indicated the increase in the amount of the bromocresol green/ bOBPwt complex before reaching to the binding saturation. In addition, this curve also provided information about the stoichiometric binding ratio between bOBP and bromocresol green, which was found to be 1.25: 2.

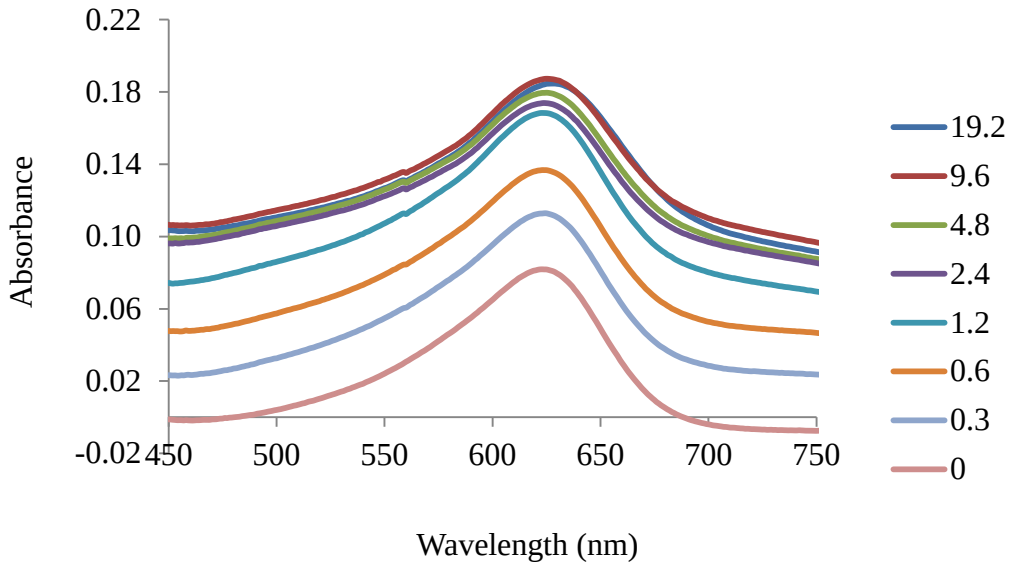

Figure 6.11: Titration absorption spectra of binding 2µM bromocresol green to various concentrations of bOBPwt ranging from 0-19.2 µM. *The reaction was in PBS with 1mM EDTA supplement, pH 7.4 with 1%DMSO.*

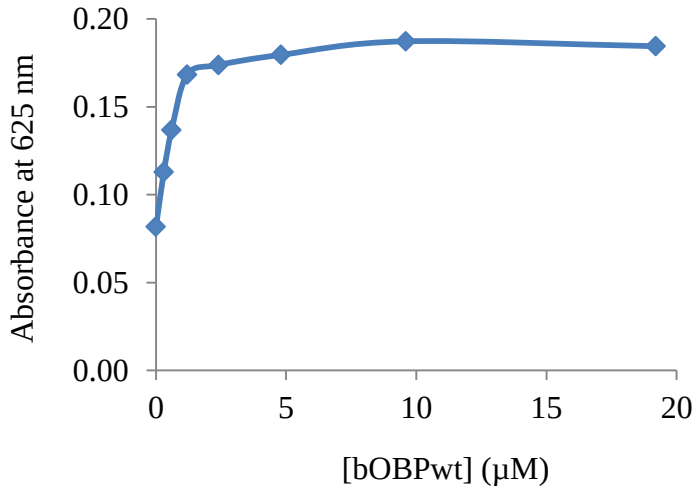

Figure 6.12: Absorbance titration curve at 625nm of binding of bromocresol green to bOBPwt in PBS with 1mM EDTA supplement, pH 7.4. *Bromocresol green concentration was fixed at 2μM and the bOBPwt concentrations were varied from 0 to 19.2μM.*

Those chromophores (including bromocresol green) that bound bOBPwt were then tested in competitive binding assays. The displacement of bromocresol green by various thymol concentrations with 1.25μM bOBPwt was executed. The absorbance at 625nm of bromocresol green bound to bOBP was measured as a function of thymol concentration. It was found that none of the probes were displaced by thymol in competitive binding, as their absorbance didn't drop (Figure 6.13). The result was confirmed by repeating the assays, in which the protein concentration was increased up to 12.5-100μM, the amount of bromocresol green was raised up to 20-100μM and the thymol concentration was widely varied at 0.0001-100μM, irrespective of a 1-hour incubation time.

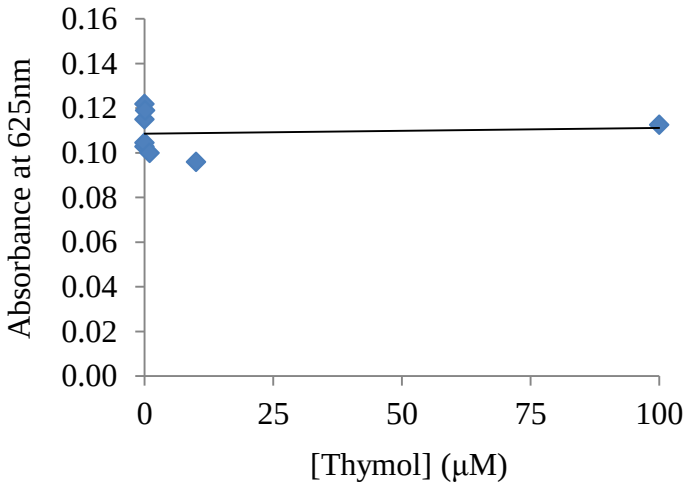

Figure 6.13: Competitive binding curve between 2μM bromocresol green and various thymol concentrations on 1.25μM bOBPwt. *The absorbance at 625nm of bromocresol green bound to bOBP is plotted as a function of the concentration of thymol.*

Therefore, those chromophores were checked for their ability to be displaced for bOBP when the fluorophore 1-AMA was used as a probe in this competition. The displacement of 1µM bromocresol green bound to 1µM bOBP was carried out when 100µM 1-AMA was added to the bOBP/BG complex. Competitive binding of 1-AMA to the protein was then reported by analyzing the fluorescence emission intensity at 490nm of bound 1-AMA. As shown in Figure 6.14, it was found that the increase of fluorescence signal in the displacement reaction of 1µM bOBP + 1µM BG + 100µM 1-AMA when compared to the background reaction of 1µM bOBP + 1µM BG. This indicated that the bound BG was released from the binding site on bOBP, and displaced by 1-AMA. Conversely, the displacement of 1µM 1-AMA bound to 1µM bOBP by 100µM bromocresol green was also performed and found the releasing of bound 1-AMA. As shown in Figure 6.15, the fluorescence of 1-AMA bound to bOBP in the displacement reaction of 1µM bOBP + 1µM 1-AMA + 100µM BG decreased when compared to the background reaction of 1µM bOBP + 1µM 1-AMA.

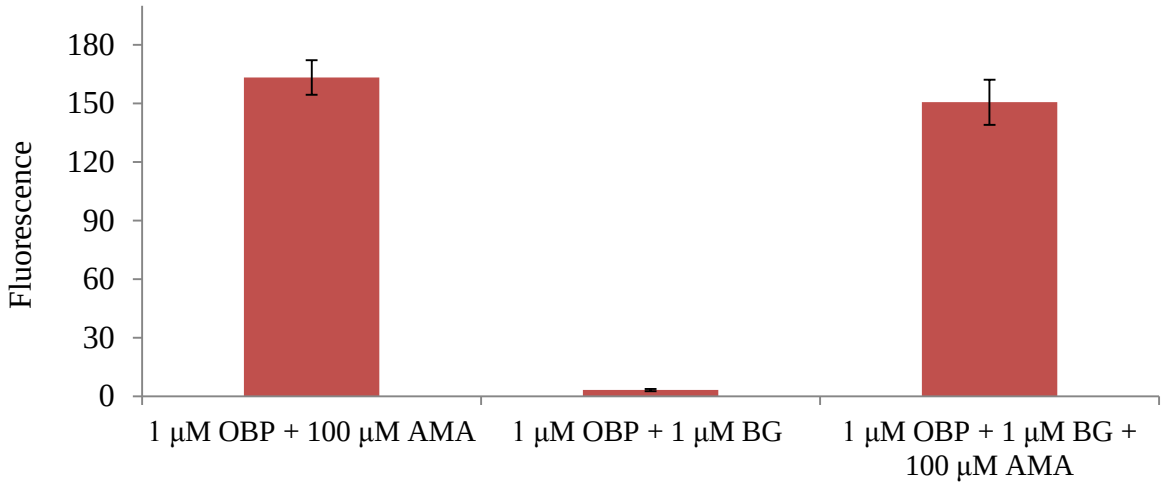

Figure 6.14: Bromocresol green displacement by 1-AMA (1µM bOBP + 1µM bromocresol green + 100µM 1-AMA). *Two reactions, including 1µM bOBP + 100µM 1-AMA and 1µM bOBP + 1µM bromocresol green, were represented as backgrounds. Fluorescence emission intensities of bound 1-AMA were measured at 490nm with excitation at 390nm.*

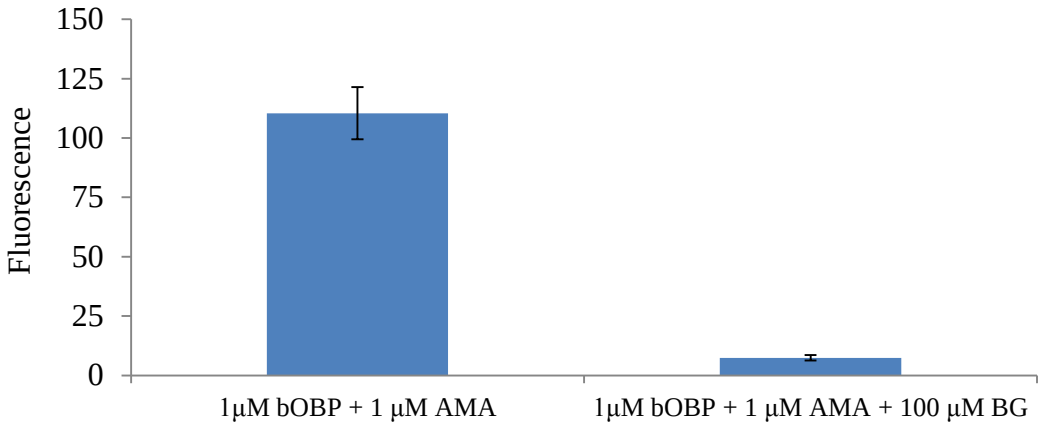

Figure 6.15: 1-AMA displacement by bromocresol green (1µM bOBP + 1µM 1-AMA + 100µM bromocresol green). *The reaction of 1µM bOBP + 1µM 1-AMA was represented as background. Fluorescence emission intensities of bound 1-AMA were measured at 490nm with excitation at 390nm.*

The results from the competitive binding assays of bromocresol green to bOBP by using the fluorophore 1-AMA as a probe indicated that bromocresol green had the ability to bind, release and displace on bOBP, at which its K_d value and that of malachite green, another chromophore were then reported in Section 6.1. However, bromocresol green couldn't be used as a probe in the competitive binding assays due to inability to detect absorbance change during the displacement. This is because the signal from absorption spectroscopy is low when compared to that of fluorescence. Fluorescence labelling techniques offers a much greater sensitivity as well as application range than the measurements based on absorption [117, 119, 128]. They have become increasingly popular in the labelling field in recent years, since they require just a small amount of samples to be labelled [119].

In conclusion, a number of chromophores in the laboratory have been investigated the ability to be used as a probe in the competitive binding to bOBP based on absorbance spectrophotometry, and found that none of them gave a signal in the displacement analysis. Thus, the fluorophore 1-AMA has been used to detect ligand binding events for bOBP biosensors in this study.

CHAPTER 7

IMMOBILIZATION OF bOBP ON SOLID SURFACES

In chapter 6, 1-AMA was shown to be a useful probe for sensing with bOBP in a competitive binding strategy. In this chapter, immobilization of bOBP on different polymer surfaces is demonstrated.

Immobilization is perhaps the biggest challenge in the development of a biosensor. Since one of problems is that many proteins undergo irreversible conformational changes upon binding to surfaces, causing denaturation of a proportion of the protein at the surface or having a random surface orientation resulting in a portion of the protein being orientated such that it is non-functional. Another problem is leaching of the bound protein. Thus, protein immobilization on solid supports, while potentially preserving function over a long period of time is widely used in biosensor applications [129].

In addition to implanted biosensors, immobilization is also essential for ones operating in on-line system for continuous sensing. For instance, glucose binding polypeptide elements were immobilized in a polyacrylamide hydrogel matrix placed on the tip of an optical fibre for continuous glucose monitoring [130]. Recombinant *E. coli* were immobilized on antibody modified solid substrates and used as disposable or multiple bioluminescent sensors [131]. These make the choice of the surface material an important factor to consider.

A variety of methods are available for immobilizing proteins, with the coupling chemistry often being classified into three major groups. (i) The most commonly used method relies on the nonspecific physical adsorption of the protein to a solid support through electrostatic and hydrophobic interactions [132]. Typical surfaces include membranes made of polyvinylidene difluoride (PVDF), nylon, polyethersulfone (PES), and nitrocellulose. Non-covalent binding of proteins is simple and may allow the conformation of the immobilized protein to remain intact [133]. Additionally, it has a particularly low background on glass surface, with high capacity and retention of protein activity [134]. However, this method gives random orientation [133, 135], leading to the possibility of protein denaturation on the surface or perhaps desorption under assay or storage conditions [136].

The direct adsorption of proteins in polymer (polyvinyl chloride and polystyrene) 96-well microplates is very well established in Enzyme-Linked Immunosorbent Assay (ELISA) owing to its simplicity and automatization [137]. For example, the detection and quantitative assay of plant viruses that are involved with virus in the test sample is selectively trapped and immobilized by specific antibody adsorbed on a polystyrene microtitre plates [138, 139]. In an attempt to increase the yield per plate, decrease reaction volumes, and thereby operating cost per plate, formats of the 384 and 1536-well microplates have been then developed. 1536-well plate are called “High throughput screening” (HTS) approach because of being conducted by dedicated robotic systems. The next generation assay platform of a novel microfluidic ELISA microplate that has been applied for the unparalleled assay performances was designed by connecting a microfluidic channel to each well of a 96-well micro-titter plate where binding events occur [140].

Interestingly, a leading trend in protein microarray development is the shift from planar substrates to three-dimensional materials [141, 142]. Instead of immobilizing only in the two dimensions available on a planar substrate, the additional capture molecules can be immobilized within the depth of the three dimensional support [143]. Commercially available examples of the protein microarray approach employ nitrocellulose pads fixed onto the surface of a glass supported FAST™ slide and PATH™ slide, or three-dimensional hydrophilic polyacrylamide surfaced HydroGel™ slides.

(ii) Covalent linkage through a specific chemical reaction with reactive groups within proteins has also been used to immobilize proteins to chemically activated surfaces containing complementary reactive groups such as aldehyde, epoxy, amine, and active esters [144-146], for example epoxysilane coated slide (Figure 7.1). This stable bond formation permits somewhat random orientation of immobilized protein [135]. Furthermore, chemical modification of proteins results in loss of function and low immobilization efficiency [133].

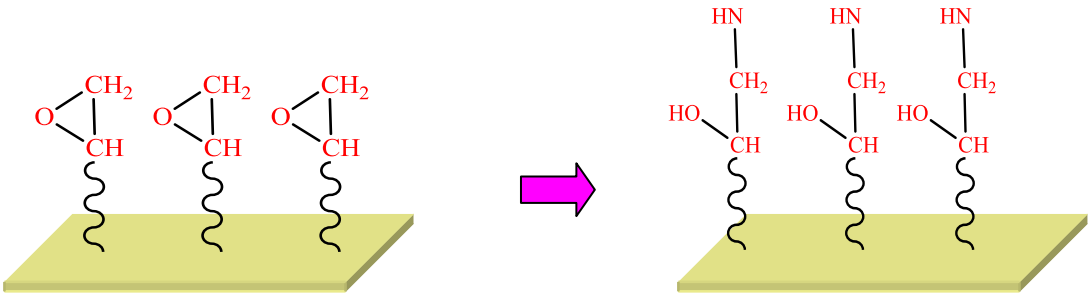

Figure 7.1: Schematic representation of an amino group coupling to epoxysilane coated slide [147].

(iii) Another type of protein immobilization has been achieved by the affinity tag method such as the streptavidin-biotin interaction (streptavidin slide) [148-150]. Biotinylation or bio-tag of proteins through the use of peptide tags can occur either *in vivo* or *in vitro* [151]. One is an *in vivo* genetic introduction of the natural biotinylated protein (biotin carboxyl carrier protein, BCCP) with more than 87 amino acids [152] to fuse with the target protein in bacteria. The other is an *in vitro* chemical modification with biotin derivative [153]. The other example of the recombinant tag methods is the polyhistidine tagged protein and nickel modified surfaces (Ni-NTA coated microtitre plate) [150, 154]. The protein tag carrying methods require a genetic modification of each prospective target [155]. They create a stable linkage and bind protein specifically in a reproducible orientation [133], improving the functionality and accessibility of immobilized proteins [156-158].

It is believed that an oriented immobilization provides a superior binding mode as compared to random immobilisation as it is thought to lead to better retention of function [159-161]. However, no actual improvement in performance was detected in some instances [162, 163]. In addition, there are some reports of low and non-homogeneous protein deposition [164], lower binding affinities or reduced specificities with modified antibodies [162, 165], changes in specificity and affinity of the capture antibody [150], expensive and time consuming manipulations of ligands [162, 163], and in the case of single histidine tags, they are prone to leaching [166].

7.1 Screening of Solid Surfaces for Immobilization of bOBP

The properties of the support will play crucial roles in the quality and performance of the immobilized bOBP biosensors. Firstly, polymer supports for the bOBP biosensors were examined for their biocompatibility with bOBP function using 1-AMA as a probe. Ten different commercially available solid supports were selected to represent different coupling chemistries. These included epoxysilane coated slide, polyvinylidene difluoride (PVDF) membranes (hydrophobic and hydrophilic type), glass fibre membrane, nylon membranes (neutral and positively charge), polyethersulfone (PES) membrane, nickel coated plate, mixed cellulose ester (MCE) membrane, and nitrocellulose membrane. The details of the ten different substrates used to immobilize bOBP such as their trade names, wettability, pore sizes, and particularly binding mechanisms are shown in Table 7.1. These surfaces were evaluated by measuring the signal to background ratios (S/B). Signal was defined as the fluorescence intensity from immobilizing 100µM bOBP and treating with 100µM 1-AMA, while the background was the fluorescence intensity after treating the material with 100µM 1-AMA.

It was found that most of the supports gave a high background, presumably due to adsorption of 1-AMA. Polymer surfaces made of nitrocellulose or MCE exhibited the best S/B (Figure 7.2), indicating that immobilization on these membranes allowed bOBP to retain its ability to bind 1-AMA as seen by the enhancement of 1-AMA fluorescence. Due to its ready availability, the nitrocellulose membrane was then used for immobilizing the bOBP in this project.

Table 7.1: Information of the ten different commercially available solid surfaces used to immobilize bOBP.

No.	Substrates	Forms of surface	Trade Name	Wettability	Pore Size (µM)	Binding mechanism
1	Epoxysilane coated	Slide	Nexterion® Slide E	Hydrophobic	-	Covalent binding
2	Polyvinylidene difluoride (PVDF)	Membrane	Immobilon-P	Hydrophobic	0.45	Adsorption
3	Polyvinylidene difluoride (PVDF)	Membrane	Millipore	Hydrophilic	0.45	Adsorption
4	Glass fibre	Membrane	Metrigard	Hydrophilic	0.50	Adsorption
5	Nylon - neutral charge	Membrane	Hybond-N	Hydrophilic	0.45	Adsorption
6	Nylon - positive charge	Membrane	Nytran SPC	Hydrophilic	0.45	Adsorption
7	Polyethersulfone *(*PES)	Membrane	Supor-200	Hydrophilic	0.20	Adsorption
8	Nickel coated	96-well	HIS-Select® High Capacity	-	-	Affinity binding
9	Mixed cellulose ester (MCE)	microtitreplate	Millipore	Hydrophilic	0.45	Adsorption
10	Nitrocellulose	Membrane	Protran™ (Whatman)	Hydrophilic	0.45	Adsorption

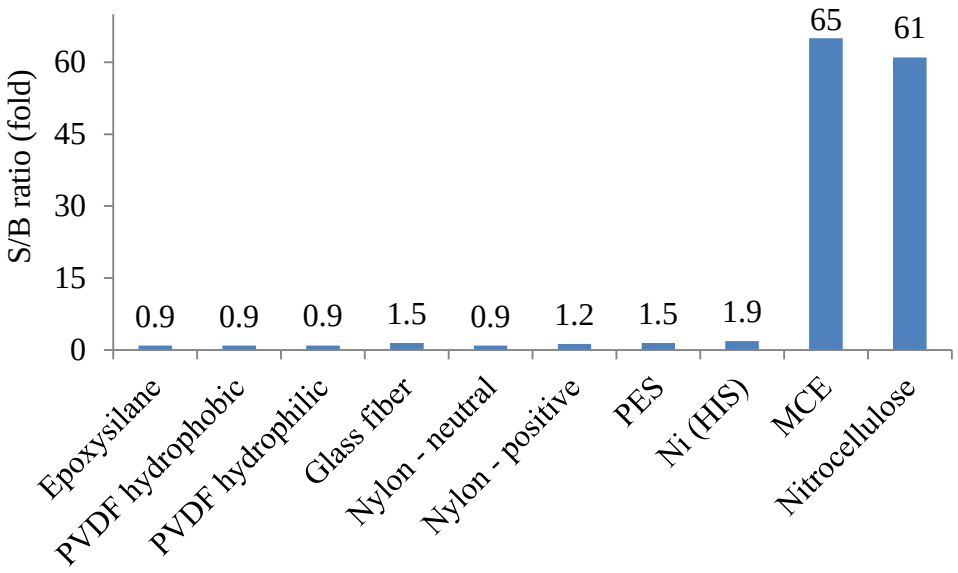

Figure 7.2: Signal to background ratio of the immobilization on ten different commercially available solid supports. *Signal is defined as the fluorescence intensity from the material after treating with 25µl of 100µM bOBP for 5min and rinsing with 25µl of PBS solution containing 1mM EDTA, pH 7.4, then followed by treating with 25µl of 100µM 1-AMA for 5min and rinsing with 25µl of PBS solution containing 1mM EDTA, pH 7.4. While the background is that after treating with 25µl of 100µM 1-AMA for 5min and rinsing with 25µl of PBS solution containing 1mM EDTA, pH 7.4.*

The nitrocellulose layer immobilizes proteins through physical non-covalent adsorption in a non-orientated but irreversible and quantitative manner, resulting in reproducible results. Figure 7.3 illustrates the 3-D micro-porous matrix (sponge structure) of nitrocellulose membrane that provides a much larger surface area for protein binding compared with 2-D surfaces. It is because protein can be deposited for many layers through matrix in comparison to just one layer on the surface of an impermeable support. This 3-D micro-porous surface also serves as an environment for immobilized protein molecules that is the most similar to that in free solution. This helps to preserve the protein conformation and then retains biological activity. In addition, Protran™ is a hydrophilic material that is expected not to bind 1-AMA, which is a hydrophobic molecule. As a result, it gave the lowest background signal, therefore showed the highest S/B among the supports [147, 167-169].

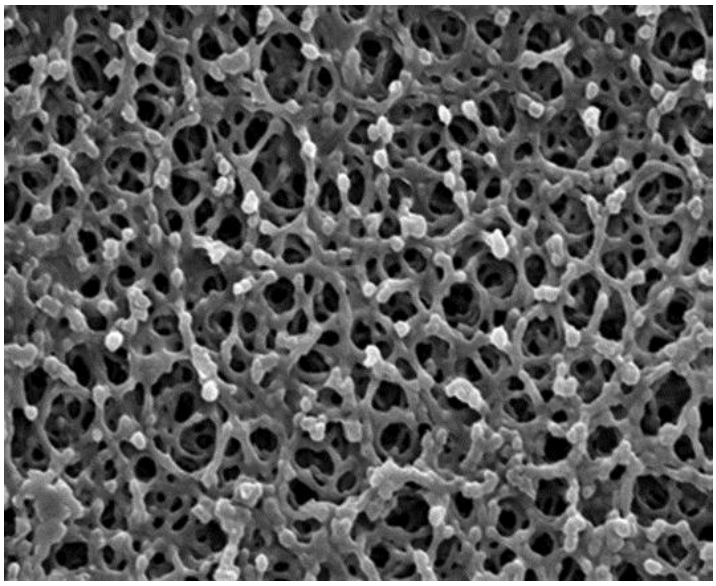

Figure 7.3: Nitrocellulose surface demonstrating microporous 3-D matrix. *The structure responsible for the high-binding capacity of nitrocellulose was imaged by means of scanning electron microscopy. This image is taken from reference [167].*

7.2 Amount of bOBP Immobilized on Nitrocellulose

In order to determine the extent of protein binding to the nitrocellulose membrane, 25µl of bOBP solution with various concentrations ranging from 0 - 100µM was adsorbed on the membrane for 5min. The volume and A_{280} of the bOBP solution were then measured before and after adsorption. It is noted that the volume and A_{280} of the bOBP solution before and after protein immobilization referred to those of the total protein applied to nitrocellulose and the unbound protein, respectively.

The concentration in µM of unbound protein was then calculated by using Equation 7.1.

$$\mu M(\text{unbound}) = \frac{A280(\text{after}) * \mu M(\text{total})}{A280(\text{before})} \quad 7.1$$

Next, the concentrations in µM of the total and unbound protein were converted into nmole by using Equation 7.2.

$$\text{nmole} = \frac{\mu M * \mu l * 1{,}000}{1{,}000{,}000} \quad 7.2$$

Therefore, nmole of the immobilized protein were obtained from the subtraction of nmole between the total and unbound protein as shown in Equation 7.3.

$$\text{nmole(immobilized)} = \text{nmole(total)} - \text{nmole(unbound)} \quad 7.3$$

The calculated result was plotted as a Langmuir Isotherm of the amount of bOBP (nmol) immobilized on nitrocellulose as a function of the total protein applied (Figure 7.4 and Equation 7.4).

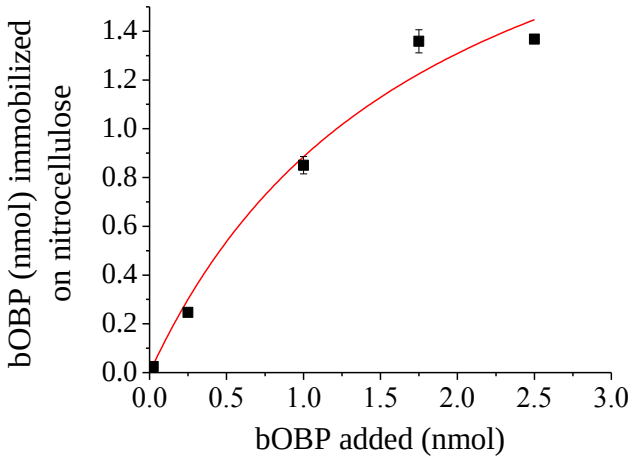

Figure 7.4: Amount of bOBP (nmol) immobilized on nitrocellulose as a function of the total protein applied. *The Protran^{TM} nitrocellulose membrane with 0.5-cm diameter was placed in 25µl of bOBP solution with each concentration of 0, 1, 10, 40, 70 and 100µM, and allowed binding for 5min. The volume and OD_{280} of the bOBP solution before and after immobilization were then measured and calculated.*

$$\text{Bound} = \frac{\text{Bmax} * \text{X}}{\text{Kd} + \text{X}} \qquad 7.4$$

Where *Bound* is the amount of bOBP (nmol) bound to nitrocellulose, B_{max} is the maximum amount of bOBP (nmol) bound to nitrocellulose that is equivalent to 2.5nmol, X is the amount of bOBP (nmol) added to nitrocellulose, and K_d is the amount of bOBP added required to reach half-maximal binding of bOBP to nitrocellulose that is equivalent to 1.8nmol.

7.3 Titration of bOBP and 1-AMA on Nitrocellulose

As the membrane contained both bOBP and 1-AMA, the fluorescence response of the protein biosensor system is expected to be influenced by their respective concentrations. Titrations of the concentrations of bOBP and 1-AMA were therefore carried out on nitrocellulose in order to illustrate their optimum operating concentrations immobilized on nitrocellulose for the bOBP biosensor.

The nitrocellulose membrane was incubated with a concentration of bOBP solution (0, 1, 10, 40, 70, 100µM) for 5min and rinsed with PBS solution containing 1mM EDTA, pH 7.4. Each concentration of the immobilized bOBP was then immersed in a concentration of 1-AMA solution (0, 1, 10, 40, 70, 100µM) for 5min and washed with PBS solution containing 1mM EDTA, pH 7.4. The effect of these factors was then investigated on analytical fluorescence signal at 490nm with excitation at 390nm.

It was found that increasing the concentrations of bOBP and 1-AMA resulted in an increase in the fluorescence signal as a hyperbolic function shown in Figure 7.5. The fluorescence response that may imply the sensitivity of the biosensor indicated the amount of the functional bOBP/1-AMA complex formed. The maximum fluorescence intensity was demonstrated at the concentrations of 100µM bOBP and 100µM 1-AMA (corresponding to 1.4nmol of bOBP immobilized on 0.5-cm diameter nitrocellulose) in PBS containing 1mM EDTA, pH 7.4 with 0.1% DMSO. Therefore, 100µM bOBP and 100µM 1-AMA as the reagent phase were selected and used for subsequent studies on nitrocellulose membrane.

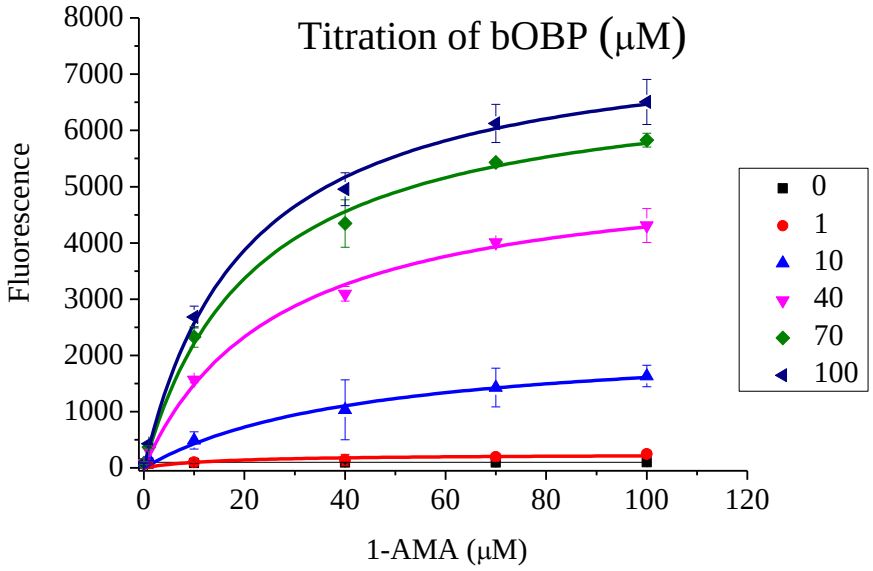

Figure 7.5: Fluorescence titration curve of bOBP with 1-AMA on nitrocellulose membrane. *The Protran™ nitrocellulose membrane (0.5-cm diameter) was placed in 25µl of a concentration of bOBP solution (0, 1, 10, 40, 70, 100µM) for 5min and washed with 25µl of PBS solution containing 1mM EDTA, pH 7.4. Each concentration of the immobilized bOBP was then incubated with 25µl of a concentration of 1-AMA solution (0, 1, 10, 40, 70, 100µM) for 5min and washed with 25µl of PBS solution containing 1mM EDTA, pH 7.4. Fluorescence measurement was recorded at 490nm with excitation at 390nm.*

7.4 Amount of Functional bOBP Immobilized on Nitrocellulose

The quantity of functional bOBP immobilized on nitrocellulose was determined by relating the fluorescence intensity upon the stoichiometric binding of bOBP with 1-AMA on nitrocellulose and that in the solution phase. The fluorescence calibration curve of that in the solution phase was carried out by incubating the binding reactions of 1-AMA and bOBP with the stoichiometric final concentration of 0, 1, 10, 40, 70, and 100µM for 5min at room temperature. The fluorescence emission intensity at 490nm was recorded at a fixed excitation wavelength of 390nm. The fluorescence

intensities of the bOBP·AMA complex formation were then corrected by subtracting that of the backgrounds of both bOBP and 1-AMA individually at their corresponding concentrations. This calibration curve of that in the solution phase was found to be linear from 0 to 70µM of bOBP and 1-AMA (Figure 7.6), with a slope of 129μM^{-1}.

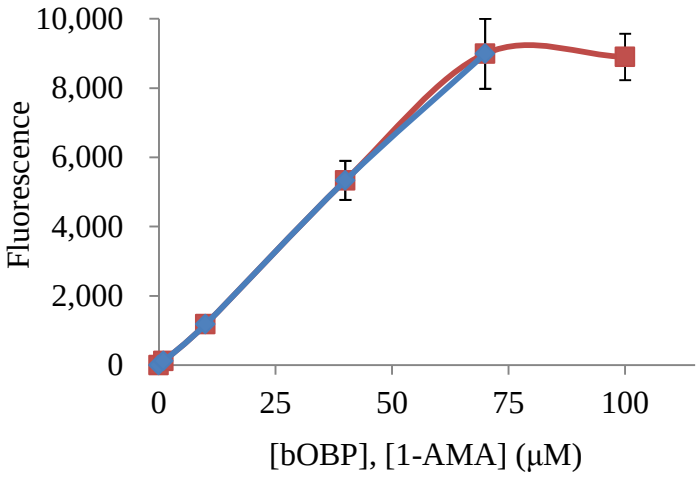

Figure 7.6: Fluorescence calibration curve of the bOBP/1-AMA binding reaction in solution phase. *The linear curve (blue line) is the proportional relationship of the fluorescence intensity and the stoichiometric bOBP and 1-AMA concentrations at 0, 1, 10, 40 and 70µM. The red curve shows the inner filter effect occurred at >70µM stoichiometric bOBP and 1-AMA concentrations It is noted that the inner filtering effect will present when absorbance of the solution is greater than 0.2.*

The concentration of functional bOBP applied to nitrocellulose was then determined from the slope of the calibration curve in Figure 7.6 Next, the amount in nmole of total functional bOBP applied to nitrocellulose was calculated by using Equation 7.5.

$$\text{nmole of total functional protein} = \frac{\mu M(\text{functional}) * \mu l(\text{total}) * 1{,}000}{1{,}000{,}000} \qquad 7.5$$

Finally, the amount in nmole of functional bOBP immobilized on nitrocellulose was therefore obtained by using the Langmuir Isotherm of Equation 7.4. Figure 7.7 showed this result plotted as a curve of the amount of functional bOBP (nmol) immobilized on nitrocellulose relative to the stoichiometric bOBP and 1-AMA concentrations that were applied to the nitrocellulose membrane.

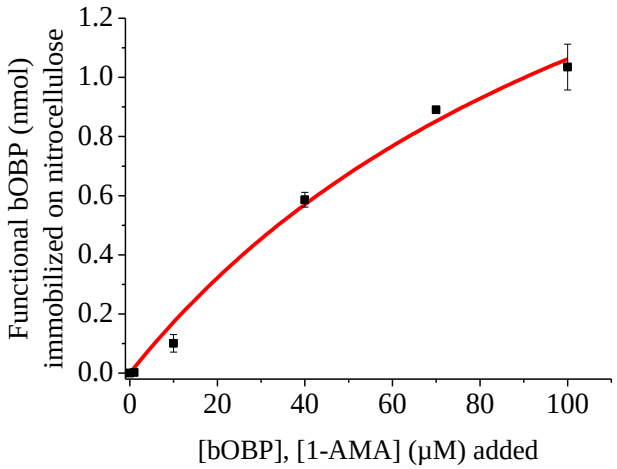

Figure 7.7: Amount of functional bOBP (nmol) immobilized on nitrocellulose relative to the stoichiometric bOBP and 1-AMA concentrations that were applied to the nitrocellulose membrane. *The Protran™ nitrocellulose membrane with 0.5-cm diameter was immersed into 25µl of a concentration of bOBP solution (0, 1, 10, 40, 70 and 100µM) for 5min, and washed with 25µl of PBS solution containing 1mM EDTA, pH 7.4. 25µl of the stoichiometric 1-AMA was then added to the membranes for 5min, and washed again with 25µl of PBS solution containing 1mM EDTA, pH 7.4. The membranes were measured the emission intensity at 490nm with a SPECTRAmax GEMINI XS spectrofluorometer at a fixed excitation wavelength of 390nm.*

From section 7.2 - 7.4, it was found that at 2.5nmol (or 100µM) of total protein applied yielded greater amount of bOBP immobilized on 0.5-cm diameter nitrocellulose (1.4 ± 0.01 nmol) than other concentrations used (Figure 7.4), which was calculated as 7 ± 0.1 nmol bOBP per cm^2 of membrane, and had 55 ± 1% of bOBP immobilized on nitrocellulose relative to total protein applied (Figure 7.8). Additionally, it was found that the reaction comprising of 100µM bOBP (2.5nmol) and 100µM 1-AMA exhibited the highest fluorescence intensity (Figure 7.5) as well as the highest quantity of functional bOBP immobilized on 0.5-cm diameter nitrocellulose (1 ± 0.1 nmol) among other stoichiometric compositions of bOBP and 1-AMA (Figure 7.7). This reaction composition on the membrane yielded 5 ± 0.4 nmol of functional bOBP per cm^2 of membrane, which equaled to 41 ± 3% of functional bOBP immobilized on nitrocellulose relative to total protein applied. In order to easily see the comparison of the amounts of the total and the functional bOBP immobilized on nitrocellulose relative to the amounts added, both curves of section 7.2 (Figure 7.4) and section 7.4 (Figure 7.7) were plotted in the same graph as shown in Figure 7.8.

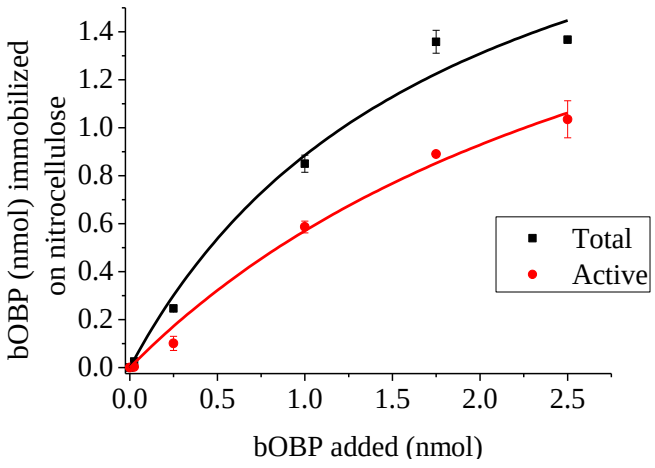

Figure 7.8: Amounts of bOBP (nmol) immobilized on nitrocellulose membrane relative to the total bOBP applied. *Total immobilized bOBP is represented as black squares, and the functional immobilized bOBP is represented as red circles.*

7.5 Effect of Immobilization Method for bOBP and 1-AMA on Nitrocellulose

It is expected that the method of immobilization of bOBP and 1-AMA on nitrocellulose is a factor affecting the fluorescence response of the protein biosensor. In this experiment, two different methods of immobilizing bOBP and 1-AMA on nitrocellulose were examined in order to obtain the optimum immobilization method for the bOBP biosensor.

The first method was individual immobilization of bOBP and 1-AMA step by step as the same as previously treated in section 7.1 – 7.4. The nitrocellulose membrane was immersed in 100µM bOBP solution for 5min and washed with PBS solution containing 1mM EDTA, pH 7.4. The immobilized bOBP was then immersed in 100µM 1-AMA solution for 5min and washed again with PBS solution containing 1mM EDTA, pH 7.4. The second method was the immobilization of bOBP/1-AMA complex by which the solution of 100µM bOBP/100µM 1-AMA mixture was used in adsorption to nitrocellulose for 5min. Then the membrane was washed with PBS solution containing 1mM EDTA, pH 7.4. The influence of this factor was evaluated by measuring S/B ratio with which all three different backgrounds, including PBS (containing 1mM EDTA, pH 7.4), 100µM 1-AMA, and 100µM bOBP backgrounds were considered in this matter.

The result demonstrated in Figure 7.9 that immobilization of bOBP/1-AMA complex gave approximately two-fold better S/B ratio than individual immobilization of bOBP and 1-AMA for all three backgrounds, indicating higher amount of the bound protein immobilized on nitrocellulose due to more conformational stabilization induced by 1-AMA, and/or higher amount of functional protein immobilized on nitrocellulose due to the better binding capability of solution-phase protein to 1-AMA. Therefore, incubation of nitrocellulose with the complex of bOBP and 1-AMA solution was used as the immobilization method for bOBP biosensors. The extent of the functional bOBP on nitrocellulose immobilized by this method was found to be 1.4 ± 0.1 nmol per 0.5-

cm diameter disk, or 7 ± 0.4 nmol per cm^2 of membrane, which was equivalent to 54 ± 3% of functional bOBP immobilized on nitrocellulose relative to total protein applied.

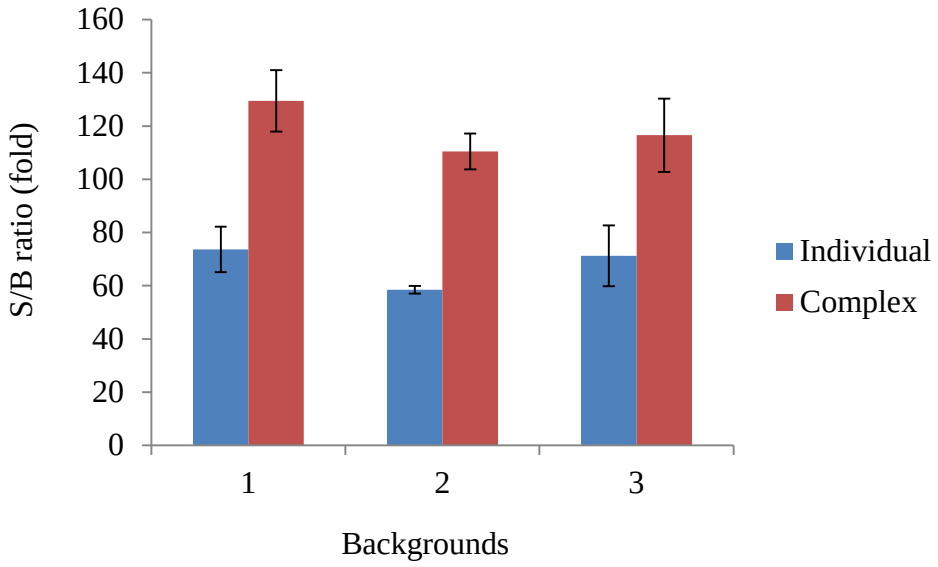

Figure 7.9: S/B ratio showing the effect of the two different immobilization methods on nitrocellulose for three different backgrounds. *The first method was individual immobilization of 100µM bOBP and 100µM 1-AMA step by step on nitrocellulose. The second method was the immobilization of 100µM bOBP/100µM 1-AMA complex on nitrocellulose. Background no.1 is PBS (containing 1mM EDTA, pH 7.4) background (0µM bOBP and 0µM 1-AMA); Background no.2 is 1-AMA background (0µM bOBP and 100µM 1-AMA); and Background no.3 is bOBP background (100µM bOBP + 0µM 1-AMA). The emission fluorescence intensity at 490nm was measured by the SPECTRAmax GEMINI XS spectrofluorometer with excitation at 390nm.*

Based on the results in this chapter, nitrocellulose was chosen as the best membrane for immobilization and the next chapter describes the development of a fibre-optic sensor.

CHAPTER 8

DEVELOPMENT OF FIBRE-OPTIC SENSOR BASED ON bOBP

In chapters 6 and 7, the sensing of bOBP both in solution and when immobilized using the microtiter plate spectrofluorimeter for detection was demonstrated. In this chapter, the development of the immobilized bOBP sensing format into a fibre-optic sensor is described.

The microplate format is not suitable for either remote or continuous monitoring, thus optical fibre was selected as the signal transducer for engineering bOBP biosensors as they have been widely used in optical sensing, for example the measurement of change in absorption or emission [170].

An optical fibre is a long, thin, flexible, and transparent strand made of glass (silica) or plastic about the diameter of a human hair (Figure 8.1A). Optical fibres consist of core and cladding, the core is center of the fibre where the light is transmitted, and the cladding is material around the core where the light reflects back into the core. Protective coating is plastic or acrylate coating that surrounds the cladding protecting the fibre from damage and moisture (Figure 8.1B) [171].

Optical fibres transmit light between the two ends of the fibre since the light waves are propagated along the fibre by total internal reflection (TIR) as illustrated in Figure 8.2 [172-174]. TIR occurs when $n_1 > n_2$ [175], and when light enters the core of the optical fibre and strikes the core/cladding interface at an angle θ, such that $\sin\theta > n_2/n_1$ [174], where n_1, n_2 are refractive indexes of the core and cladding, respectively, and θ is an angle made by the incident ray.

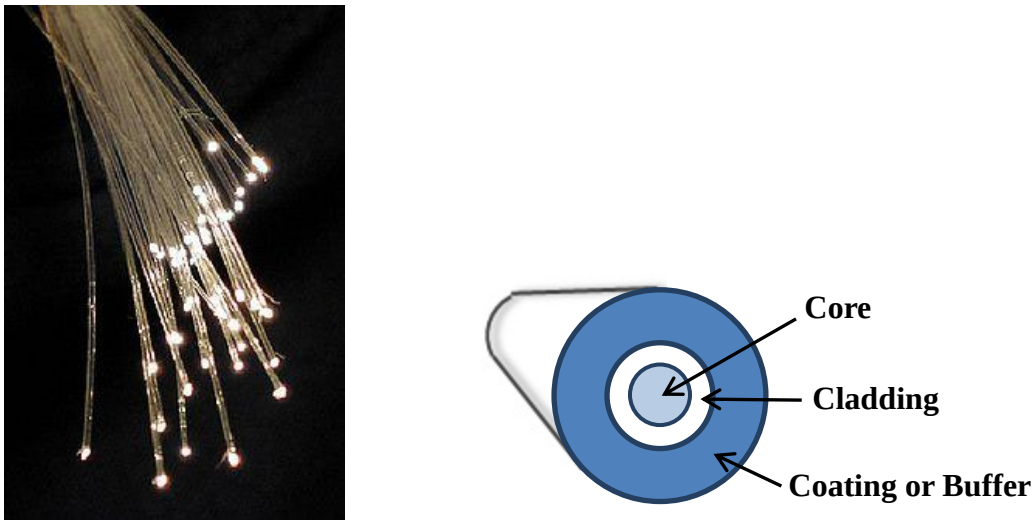

Figure 8.1: Optical fibre. (A) Image of a bundle of optical fibres [176], (B) Components of an optical fibre. *Core - centre of the glass fibre where the light travels; Cladding - Outer glass material around the core where the light reflects back into the core.; Protective coating - Plastic or acrylate coating that surrounds the cladding protecting the fibre from damage and moisture [171].*

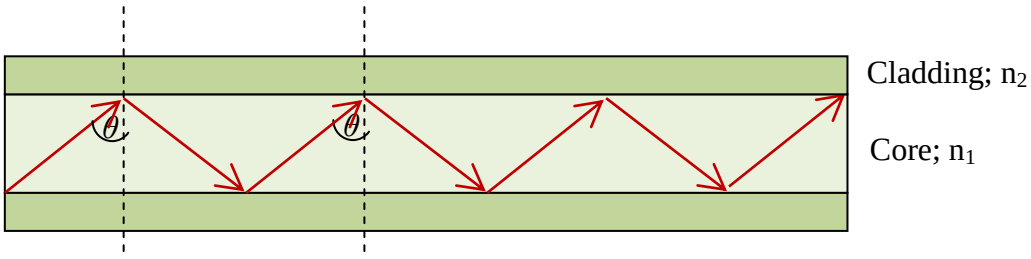

Figure 8.2: Illustration of total internal reflection in a single-core optical fibre, showing the trajectory for bound rays. *The ray of light will be reflected back into the core then experiencing total internal reflection at $n_1 > n_2$ as well as at $\sin\theta > n_2/n_1$, where n_1, n_2 are refractive indexes of the core and cladding, respectively, and θ is an angle made by the incident ray [174, 175].*

Fibre optics refers to the technology that uses optical fibres to carry digital information over long distances. Fibre optic systems have many attractive properties that are superior to electrical systems. These include improved system performance with a larger amount of bandwidth, and lower signal attenuation (loss) over a greater distance at faster speeds. They can be used in harsh environments and are immune to noise including electrical noise, electromagnetic interference [EMI] and radio-frequency interference [RFI], making them ideal for real-time use. In addition, they are intrinsically safe, chemically inert, non-toxic, non-conductive, and non-flammable due to no electrical power needed. Other advantages include reduced size and weight, taking up less space in the ground. Next, they have environmental protection that is resistant to radiation and corrosion, and temperature variations. Finally, they are overall system economy. However, they are expensive to install, fragile and difficult to splice [177].

Fibre optic cables are widely used in telecommunications and computer networking as a replacement for conventional metal (copper) wires. Optical fibres are also employed in other applications, including medical imaging, mechanical engineering inspection, plumbing inspection, lasers, and sensors [173, 178]. One particularly useful feature of their applications is fibre-optic sensors that can provide remote sensing.

Fibre-optic sensors typically comprise a light source, optical fibre, detector, and transducer (Figure 8.3), and can be used in association with different types of spectroscopic technique, of which the most common are absorption and fluorescence [172].

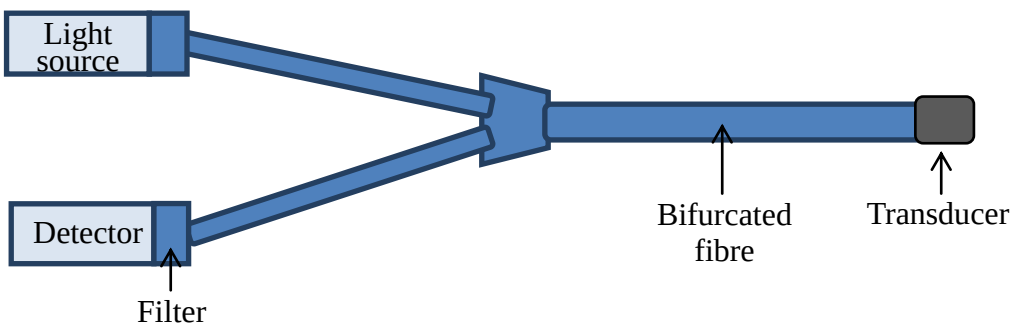

Figure 8.3: Schematic representation of a fibre-optic biosensor. *Optical fibres guide the light from the source to a sample located at the tip of an optical fibre. This light will then be filtered and delivered to the detector located remotely.*

Fibre-optic sensors can be basically divided into two groups: intrinsic or extrinsic (Figure 8.4). In an intrinsic fibre-optic sensor, sensing takes place on the surface of the fibre itself [179]. The cladding is stripped from the fibre and sensing dye or fluorophore immobilized on the surface of the core [170]. An example of this type of sensor is a chemical sensor for the detection of cocaine by using a fluorescent molecularly imprinted polymer (MIP) covalently attached to the core of an optical fibre (Figure 8.5A). The sensor showed an increase in fluorescence intensity in response to cocaine in the concentration range of 0 - 500µM in aqueous acetonitrile mixtures with good reproducibility over one month [180].

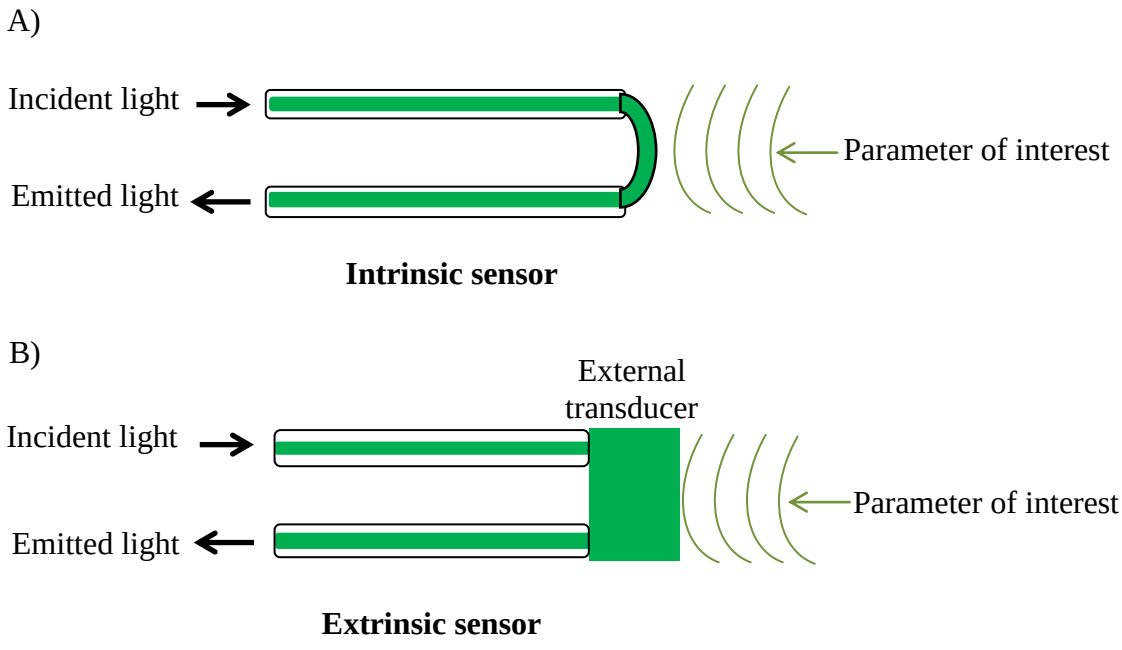

Figure 8.4: Two basic types of fibre-optic sensors. (A) Intrinsic devices sense directly on the fibre itself, whereas (B) Extrinsic devices relay via a transducer.

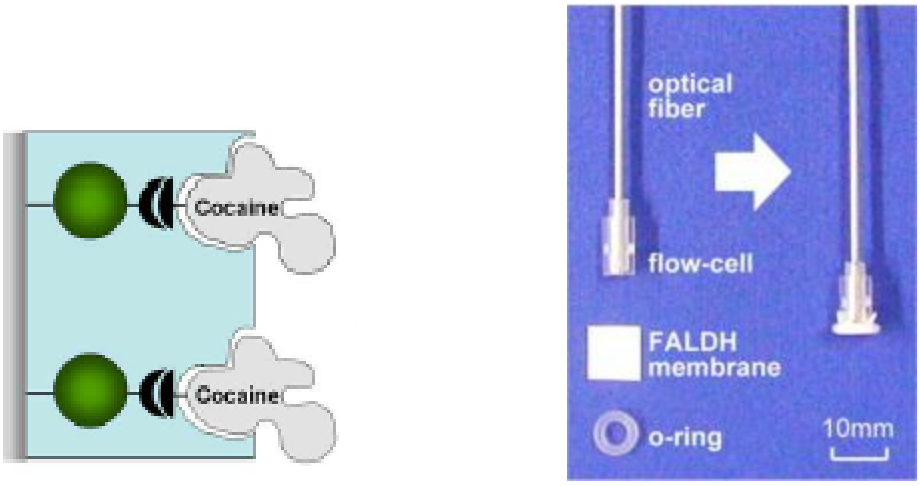

(A) **(B)**

Figure 8.5: Designs of intrinsic (A) and extrinsic (B) fibre-optic sensors. *(A) Intrinsic fluorescence-based optical fibre sensor for cocaine using a molecularly imprinted polymer (MIP) as the recognition element. A MIP was attached to the surface of the optical fibre for cocaine sensing [180]. This image has been reproduced with the permission of the rights holder, IEEE. (B) Biochemical gas sensor (bio-sniffer) for ultrahigh-sensitivity gaseous formaldehyde monitoring. A flow cell with FALDH immobilized PTFE membrane was attached onto the optical fibre probe with having the phosphate buffer containing NAD(+) circulation [181]. This image has been reproduced with the permission of the rights holder, Elsevier.*

In an extrinsic fibre optic sensor, the sensing occurs in a region outside the fibre that is on a transducer, and the optical fibre transmits light to and from the sensing location [182]. Various types of membrane support have been utilized to attach to the external transducer including nitrocellulose, polyvinylchloride, polyamide, silicone, etc [183]. For example, the construction of an ultrahigh-sensitive fibre-optic biochemical gas sensor (bio-sniffer) for continuous monitoring of indoor gaseous formaldehyde that was measured as fluorescence of nicotinamide adenine dinucleotide (NADH), which is the product of formaldehyde dehydrogenase (FALDH) reaction. The bio-sniffer device was built by attaching a flow cell with a FALDH immobilized PTFE membrane onto

the optical fibre probe, with which phosphate buffer containing NAD(+) was circulated inside the flow cell (Figure 8.5B).

$$\text{Formaldehyde} + NAD^{+} + H_2O \xrightarrow{\text{FALDH}} \text{Formic acid} + NADH + H^{+}$$

The calibration range of the FALDH bio-sniffer for formaldehyde concentration was from 2.5ppb to 10ppm, which covers the guideline value of the World Health Organization (80 ppb) [181].

One of the major advantages of this type of sensor is that it permits sample analysis to be done over long distances and this has important implications for field monitoring, for example in potentially explosive situations where electrochemical equipment would present a hazard [170, 173]. Additionally, they can be easily miniaturized and integrated for the determination of different target compounds, which could benefit in a wide range of application fields, including industrial process, environmental monitoring, food processing, DNA analysis, drug discovery, and medical diagnostics, as well as in protection against bioterrorism [173]. However, the main drawback is possibility of photobleaching or indicator wash out. Others can be limited availability of optimized commercial accessories, as well as limited stability of the immobilized biological component, however this would also be a hindrance for other types of transducer [172].

Fibre-optic biosensors are under continuous research and development in order to improve the sensors' performance, such as selectivity, stability, leaching, response time, repeatability, in some cases reversibility, and particularly sensitivity; several papers reported sensors with detection limits comparable to more sophisticated large bench-top analytical instrumentation. Therefore, immobilization protocols have been a common focus for this area [173, 184].

8.1 Construction of Fibre-Optic Biosensor Based on bOBP

The sensing of bOBP in solution and immobilized formats on a 96-well plate reader was described in chapters 6 and 7. The next step was the development of a fibre-optic biosensor based on bOBP that could be used for testing of samples.

The fibre-optic biosensor based on bOBP was constructed as shown in Figure 8.6. This is an extrinsic sensor with bOBP immobilized on a nitrocellulose membrane disk and mounted to the front surface of the probe at the end of a bifurcated bundle of optical fibres that was in turn connected to the light source and the spectrometer. Light from the LLS-385 light-emitting diode (LED) light source (at 385nm) was directed through one leg of a bifurcated bundle of optical fibres to the probe tip where the bOBP is immobilized on a membrane disk. The light intensity emitted by the bOBP immobilized membrane was monitored by transmission through the second leg of silica fibre and reflecting onto the 2048-element CCD array detector system of a HR2000 high-resolution spectrometer covering a wavelength range of 200nm to 643nm, with a 50µm entrance slit and an L2 detector collection lens. The HR2000 spectrometer was connected to a laptop with the supplied SpectraSuite software. The fluorescence emission signal was collected at 490nm. The integration time was set at 1 second.

All experiments were carried out in the dark in order to avoid ambient light interference. For the reduction of possible photobleaching of 1-AMA, the light source was switched on only when readings were being taken.

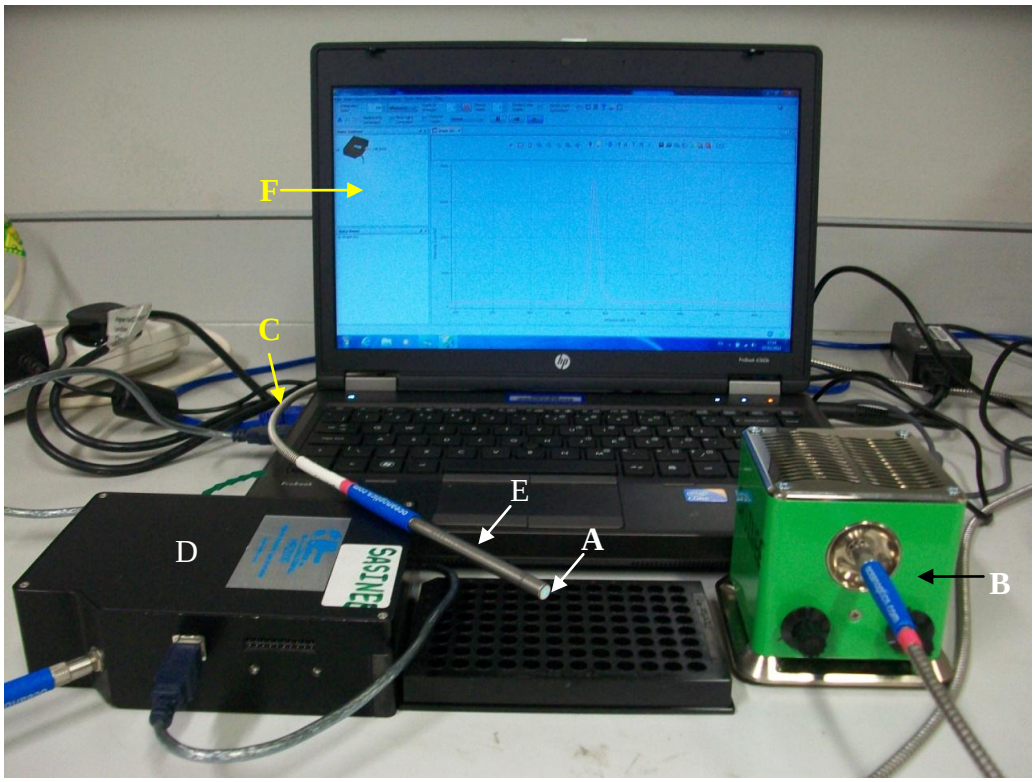

Figure 8.6: Fibre-optic biosensor setup. *The instrumental configuration consisted of (A) bOBP immobilized membrane. (B) LED light source (LLS-385, Ocean Optics; 3.86mW at 385nm). (C) Bundle of 7 pure silica optical fibres in a stainless steel ferrule (6 illumination fibres around 1 read fibre) (Ocean Optics; 2m long, 400µm diameter). (D) 2048-element CCD array detector system (Sony, product no. ILX511) of a high-resolution spectrometer (HR2000, Ocean Optics). (E) Reflection probe (Ocean Optics; 76.2mm long for probe ferrule), and (F) Laptop (HP 6360b) with SpectraSuite software.*

8.2 Signal to Background Ratio of Fibre-Optic Biosensor Based on bOBP

The fibre-optic bOBP biosensor initially had its S/B ratio determined for based on three different backgrounds, which were PBS containing 1mM EDTA (pH 7.4), 1-AMA, and bOBP. The fibre-optic bOBP biosensor was compared to both the solution measurements and the membrane bound protein in a microplate reader.

The results of S/B ratio range for all three different bOBP biosensing formats concerning their three different backgrounds were collected in Table 8.1, and Figure 8.7 was presented in order to easily see the comparison among them and moreover the effect of backgrounds on bOBP biosensing formats was also shown. It was found that based on all three different backgrounds, the S/B ratios obtained using the fibre-optic system were lower than that obtained using the microplate reader by about a factor of three. In addition, there was no effect of different backgrounds on S/B ratios obtained from biosensing formats of bOBP immobilized membrane on microplate reader as well as the fibre-optic biosensor. However, it was found that for the solution phase format, the high 1-AMA background contributed to approximately two-fold lower S/B ratio than the other two backgrounds.

Table 8.1: Range of S/B ratios obtained from three different bOBP biosensing formats regarding their three different backgrounds. *bOBP solution phase in microplate spectrofluorometric format contained 100µ1 of 1µM bOBP/1µM 1-AMA mixture, bOBP immobilized membrane in microplate spectrofluorometric format and fibre-optic biosensor format contained 25µ1 of 100µM bOBP/25µ1 of 100µM 1-AMA mixture.*

Background	S/B ratio (fold) of bOBP biosensing formats		
	Solution phase	Immobilized membrane	Fibre-optic biosensor
PBS	60 - 79	118 - 147	29 - 44
1-AMA	25 - 36	98 - 118	36 - 62
bOBP	54 - 83	91 - 134	28 - 52

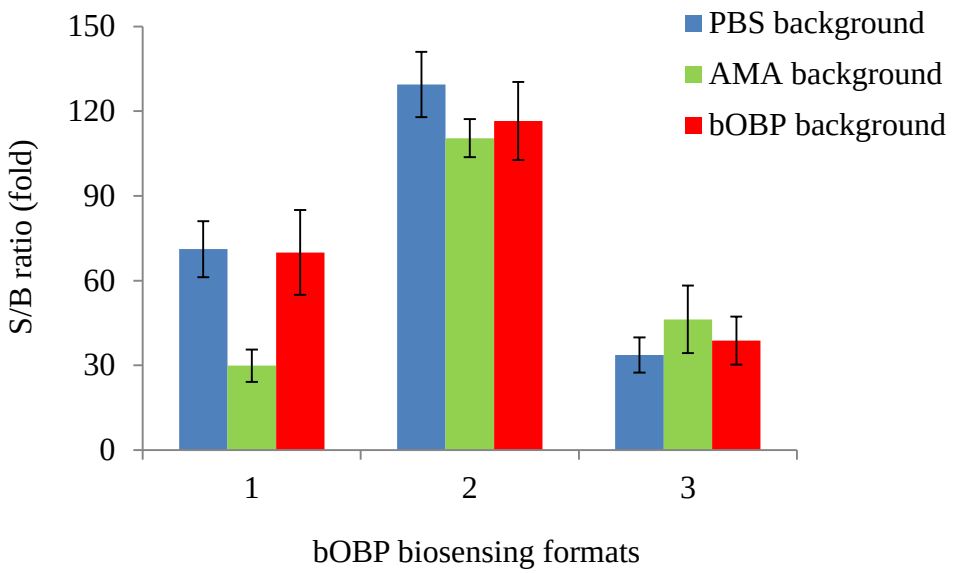

Figure 8.7: Comparison of S/B ratios obtained using three different bOBP biosensing formats for their three different backgrounds. *bOBP sensing format no.1 is solution-phase protein on microplate spectrofluorometer (100µ1 of 1µM bOBP/1µM 1-AMA mixture; n=3), bOBP sensing format no.2 is protein immobilized membrane on microplate spectrofluorometer (25µ1 of 100µM bOBP/25µ1 of 100µM 1-AMA mixture; n=6), and bOBP sensing format no.3 is fibre-optic biosensor with protein immobilized membrane attachment (25µ1 of 100µM bOBP/25µ1 of 100µM 1-AMA mixture; n=6).*

8.3 Limit-of-Detection (LOD) of Fibre-Optic Biosensor Based on bOBP for Liquid-Phase Thymol

The limit-of-detection (LOD) for thymol in the liquid phase was determined to provide a quantitative comparison of the utility of the fibre-optic bOBP biosensor with other two bOBP biosensing formats. The competitive binding assays with thymol in the liquid phase have been accomplished on the solution-phase and the immobilized protein. Different concentrations of thymol solution ranging from 0-100µM were added to each biosensing formats in triplicate and then incubated for 1 hour at room temperature.

The effect of thymol concentration on the response of these biosensing formats was shown in Figure 8.8, showing average fluorescence plotted in relation to the concentration of thymol in the liquid phase. The response curves of all three different bOBP biosensing formats to thymol in the liquid phase showed quenching of the fluorescence signal that increased with increasing concentrations of thymol, indicating the increasing amounts of thymol binding to bOBP. The LODs to thymol in the liquid phase were found to be 0.5 ± 0.2 µM, 5 ± 2 µM, and 14 ± 6 µM for solution, immobilized, and fibre-optic formats, respectively. The LOD is defined as the concentration of thymol required to produce a decrease in fluorescence signal that yields a signal-to-noise (S/N) ratio of 3 where the noise is taken as the standard deviation of the intensity for five separate measurements of a blank (without thymol). The one-sided *t*-test was then used to check and confirm the statistically significant difference of blank signal and LOD signal where p-value is not more than 0.05.

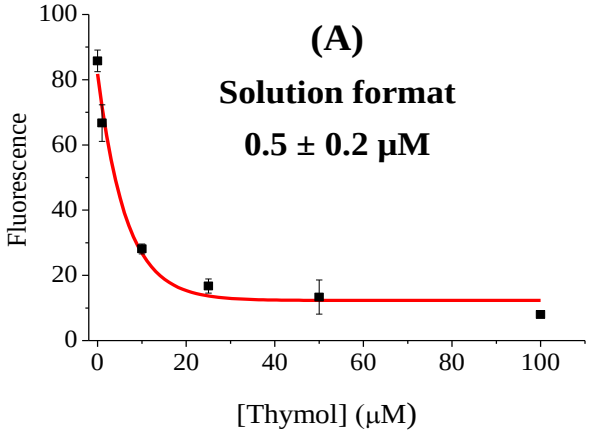
(A)
Solution format
0.5 ± 0.2 µM
Fluorescence
[Thymol] (µM)
0
20
40
60
80
100

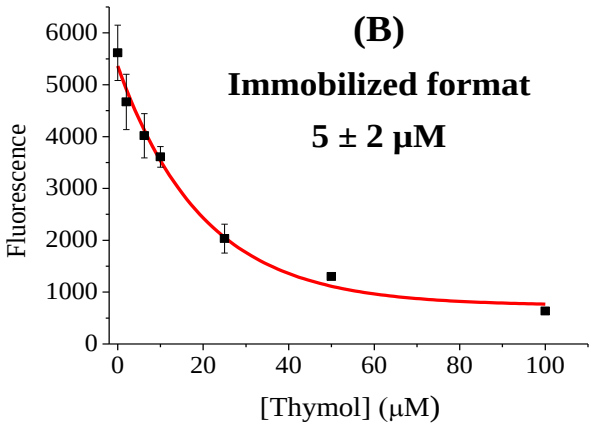
(B)
Immobilized format
5 ± 2 µM
Fluorescence
[Thymol] (µM)
0
1000
2000
3000
4000
5000
6000
0
20
40
60
80
100

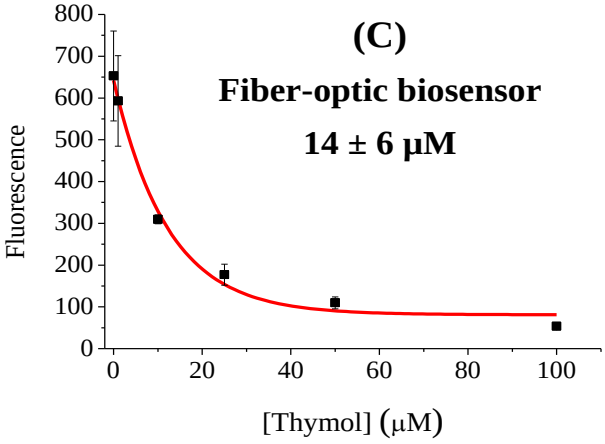
(C)
Fiber-optic biosensor
14 ± 6 µM
Fluorescence
[Thymol] (µM)
0
100
200
300
400
500
600
700
800
0
20
40
60
80
100

Figure 8.8: Response curve and LOD of three different bOBP biosensing formats for liquid phase thymol. *Different concentrations of thymol solution ranging from 0-100µM were added to each biosensing formats in triplicate and incubated for 1 hour at room temperature. The 1-AMA fluorescence signal was then measured at 490nm emission. (A) bOBP solution phase using microplate reader (100µ1 of 1µM bOBP and 1µM 1-AMA; 10 independent determinations). (B) bOBP immobilized membrane using microplate reader (25µ1 of 100µM bOBP/25µ1 of 100µM 1-AMA mixture; 9 independent determinations) and (C) Fibre-optic biosensor with bOBP immobilized membrane attachment (25µ1 of 100µM bOBP/25µ1 of 100µM 1-AMA mixture; 8 independent determinations).*

The immobilized protein formats (Figure 8.8B and 8.8C) showed LOD values that were poorer than that obtained for the free protein in solution by about a factor of ten (Figure 8.8A). This might be due to the effect of a higher background from membrane scattering. In addition, the fibre-optic system exhibited approximately three-fold reduced sensitivity when compared to that obtained from the microplate reader; this is likely to be a result of different configurations of optical detection.

The current fibre-optic bOBP biosensor has a LOD of 14 ± 6 µM, which can be compared with U.S. Environmental Protection Agency mammalian toxicity data for thymol as shown in Table 8.2 [185]. The LOD for the bOBP biosensor is still significantly lower than the LD50 for inhaled thymol (33 µM).

Table 8.2: Mammalian toxicity data for thymol [185].

Acute toxicity	LD_{50}	MRID NO.*
Oral	640 mg/kg (4 mM)	National Library of Medicine SIS ChemiID Plus; NIOSH RTECS; Stammati et.al, 1999; Aldrich Chemical Corp. MSDS
Dermal	1,049 mg/kg (7 mM)	EPA Thymol RED; ERMA (2005)
Inhalation	>5 mg/l (33 µM)	Food and Drug Administration, April 10, 1997, NADA, Freedom of Information Summary, p3

** Note that: Master Record Identification Number (MRID NO.) is a unique cataloging number assigned to an individual pesticide study at the time of its submission to the Agency [186]*.

8.4 Ability to Sense Thymol Vapour of Fibre-Optic Biosensor Based on bOBP

The ability to sense thymol vapour of the fibre-optic biosensor based on bOBP was then investigated. A simple preliminary experiment was set up by 0.5-cm bOBP immobilized nitrocellulose membrane disk containing 25µ1 of 100µM bOBP/25µ1 of 100µM 1-AMA mixture that was stuck at the lid of a 0.5-ml tube was incubated in triplicate for 1 hr at room temperature with thymol vapour produced from different concentrations of 50µl thymol solution ranging from 0-25mM at the bottom of the tube. Thymol solution was dissolved in PBS containing 1mM EDTA (pH 7.4) that had 0.1% ethanol final concentration. Blank comprised of five separate measurements of the bOBP immobilized membrane at the top of the tube incubating with 50µl of PBS containing 1mM EDTA (pH 7.4) and 0.1% ethanol at the bottom of the tube. The bOBP immobilized membrane was then attached to the edge of the fibre bundle, and the emission fluorescence intensity was measured at 490nm.

A response curve of the fibre-optic bOBP biosensor to thymol vapour in Figure 8.9 showed that the 1-AMA signal significantly decreased as thymol concentration was increased indicating the increasing amounts of thymol vapour binding to bOBP. However, the LOD to thymol vapour by using this biosensor for detection could not yet be reported correctly from this non-equilibrium experimental set-up. Therefore, the next experiment was performed in order to investigate the construction of a closed equilibrium system for the quantification of thymol vapour.

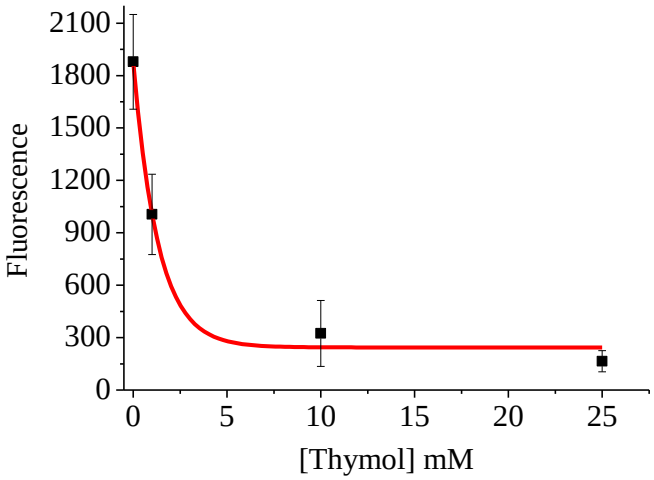

Figure 8.9: Response curve of fibre-optic biosensor based on bOBP for thymol vapour. *0.5-cm bOBP immobilized nitrocellulose membrane disk at the lid of a 0.5-ml tube was incubated in triplicate for 1 hr at room temperature with thymol vapour produced from different concentrations of 50µl thymol solution ranging from 0-25mM at the bottom of the tube. The bOBP immobilized membrane was then attached to the edge of the fibre bundle, and the emission fluorescence intensity was measured at 490nm.*

8.5 Analysis of Thymol Vapour by Fibre-Optic Biosensor based on bOBP

The construction of the equilibrium system for the quantification of thymol vapour was planned by the fibre-optic probe consisting of one bOBP immobilized membrane inserted into one neck of a closed 2-neck round bottom flask in order to continuously monitor fluorescence changes as increasing concentrations of thymol vapour that will be injected into another neck of the flask. This meant that only one immobilized membrane will be used in monitoring changes of concentrations of thymol vapour throughout the experiment, and then one membrane (that also contained 1-AMA) must be measured or excited the 1-AMA fluorescence by the LED light source for at least five times (for five different concentrations of thymol vapour) during the experiment.

Therefore in this experiment, the photostability of the bOBP immobilized membrane was investigated by monitoring %fluorescence remaining of the bOBP immobilized membrane containing 25µ1 of 100µM bOBP/25µ1 of 100µM 1-AMA mixture that was mounted to the reflection probe at the end of the fibre bundle, and flashed using the fibre-optic system (Figure 8.6). The experiment was carried out in the dark room in order to avoid ambient light interference. The LLS-385 LED light source (Ocean Optics; 3.86mW at 385nm) excited the membrane at 385nm, and was switched on only when readings were being taken. The emission fluorescence signal was collected at 490nm. The integration time was set at 1 second.

The result shown in Figure 8.10 was %fluorescence remaining of the bOBP immobilized membrane was significantly decreased after the light exposures by having less than 40% at four shots, indicating photobleaching of the bOBP immobilized membrane caused by exposure to high level of near-UV radiation from the light source of the fibre-optic system. Even though the intensity of light that exposed to the immobilized membrane was reduced to the minimum level, photobleaching was still existent. It is noted that 1-sec integration time has already been the minimum and optimum level. On the contrary, Figure 8.11 showed there was no photobleaching of the bOBP immobilized membrane when using microplate reader

(SPECTRAmax^{TM} GEMINI XS spectrofluorometer) for detection as %fluorescence remaining of the immobilized membrane was comparable at illumination of 2, 5, 7, and 61 times.

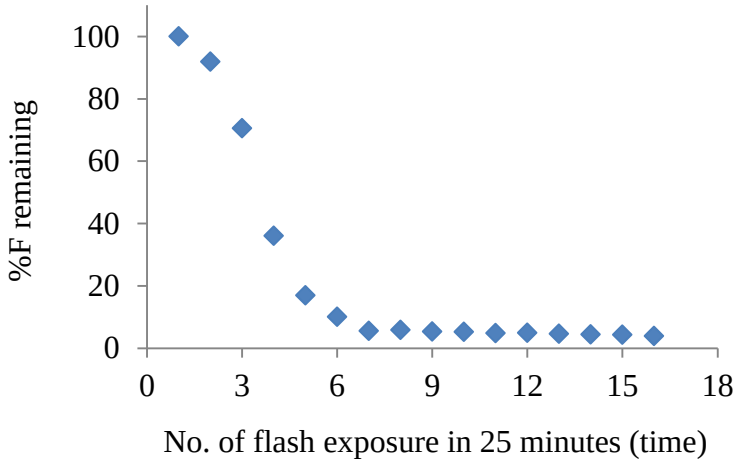

Figure 8.10: %Fluorescence remaining of bOBP immobilized membrane that was monitored by using the fibre-optic system. *%fluorescence remaining of the bOBP immobilized membrane containing 25µ1 of 100µM bOBP/25µ1 of 100µM 1-AMA mixture was mounted to the reflection probe at the end of the fibre bundle was illuminated using the fibre-optic system. The LLS-385 LED light source (Ocean Optics; 3.86mW at 385nm) excited the membrane at 385nm, and was switched on just only when readings were being taken. The emission fluorescence signal was collected at 490nm. The integration time was set at 1 second.*

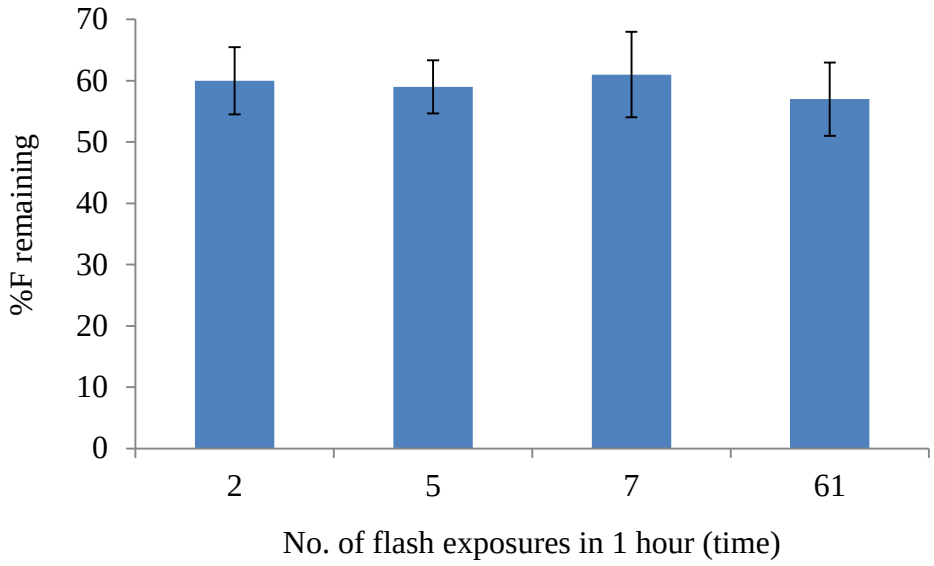

Figure 8.11: %Fluorescence remaining of bOBP immobilized membrane that was monitored by using SPECTRAmax™ GEMINI XS spectrofluorometer. *%fluorescence remaining of the bOBP immobilized membrane containing 25µ1 of 100µM bOBP/25µ1 of 100µM 1-AMA mixture was illuminated using the microplate reader at 390nm excitation and at 490nm emission with 9-nm bandwidth. General photometric performance of SPECTRAmax™ GEMINI XS microplate reader included xenon flash lamp (1 joule/flash) as a light source, photomultiplier (R-3896) as a detector, and approximately 0.16 second read time. Data points were collected for 1 hour as follow: 2-flash exposure was at time 0 and 1 hour; 5-flash exposure was at time 0 and then every 15 minutes; 7-flash exposure was at time 0 and then every 10 minutes; and 61-flash exposure was at time 0 and then every 1 minute.*

Nevertheless, after discussing the photobleaching problem caused by the fibre-optic system with the senior business development manager from Ocean Optics Inc. (Dr. Nick Barnett), it was more likely due to the too small-sized entrance slit (50μm) of the HR2000 spectrometer; hence a higher LED intensity than was necessary was causing the photobleaching. Consequently, one of the main further optimization of this fibre-optic bOBP biosensor will importantly be reconfiguration of HR2000 with a larger entrance slit. Alternatively, a neutral density filter could be used to reduce the intensity of the excitation light. Moreover, the use of a more robust photostable fluorophores e.g. Alexa Fluors or DyLight Fluors may be tried.

Therefore, the fibre-optic bOBP biosensor developed at this stage has not yet been able to achieve continuous monitoring using a single membrane. Conclusions and future works including applications of the biosensor are discussed in the next chapter.

CHAPTER 9

CONCLUSIONS AND FUTURE WORK

9.1 Conclusions

A fibre-optic biosensor based on bOBP has been constructed. The instrument used a bifurcated bundle of silica optical fibres for both delivery of excitation light from the LLS-385 LED light source to the 1-AMA-bound bOBP immobilized onto the distal end of the fibres *via* entrapment onto nitrocellulose membrane disk, and emission from the immobilized bOBP to the 2048-element CCD array detector system of a HR2000 spectrometer. The method employed competitive binding of 1-AMA to quantify thymol concentration. Using 100µM bOBP/100µM 1-AMA immobilized on 0.5cm-diameter nitrocellulose membrane as a sensing material, this biosensor could measure thymol in the liquid phase at 14 ± 6 µM. In addition, it was capable of sensing thymol in the vapour phase.

In the first stage of the thesis, wild-type and five cysteine mutants of bOBP were expressed in *E. coli* BL21(DE3) in soluble form and purified by using Ni-NTA sepharose affinity chromatographic column with total yield comprised between 13 and 691 mg.

The purified wild type bOBP in solution phase was then characterized the binding interaction with thymol; a ligand for bOBP [34, 36] by means of CD spectroscopy. The near- and far-UV CD spectroscopy was performed at the temperature of 20^{o}C, and the structural information upon the binding was obtained that the secondary and tertiary structures of bOBP are largely maintained on binding to thymol, suggesting the presence of thymol in the interior cavity of bOBP did not perturb the protein structure. This finding was in good agreement with several previous studies that reported on bOBP and porcine odorant-binding protein (pOBP) [38, 85, 87, 88].

The role of the ligand binding interaction on the protein thermal stability was studied via thermal unfolding, which was carried out by monitoring the protein far-UV CD signal at 195nm. It was found that bOBPwt was highly thermostable with T_m of the unfolding transition of 74 ± 0.3°C in the absence of thymol, which is considerably lower than that observed in the presence of thymol at 82 ± 0.4°C, consistent with a stabilizing role played by bound thymol. The phenomenon found was similar to those already described for the mutant bOBP [64, 90], as well as natural pOBP [88]. Additionally, the T_m in this finding was in a similar range of temperature as two other reports of thermal denaturation of bOBPwt at 75 - 85^{o}C [63] and pOBP at 69°C [85]. Furthermore, the high thermal stability of bOBP found in this study has been similar to those reported in the mutant bOBP [64] and pOBP [88], demonstrating the suitability to use it for construction of biosensors as for monitoring samples, possibly where temperatures can be high.

Thermodynamic parameters of unfolding consisting of the enthalpy (ΔH), the free energy (ΔG), the entropy (ΔS) of unfolding and binding, and the dissociation constant (K_d) for the binding of bOBP to thymol were calculated. CD measurements indicated that the unfolding of bOBP in the absence and presence of thymol were entropically driven ($+\Delta S_U$) and energetically favourable ($-\Delta G_U$). The positive ΔH and ΔS in both cases were attributed to the release of ordered water molecules and the associated entropy gain (due to the hydrophobic effect). The data were consistent with the notion that exposing of the hydrophobic core of the β-barrel structure was the main driving force for bOBP thermal unfolding. The results implied systems that strongly distorted

the protein had net unfavourable ΔH as a result of molecular strain, primarily associated with the bonding destacking, so ΔS were net favourable.

While the binding interaction of bOBPwt with thymol was enthalpically driven ($-\Delta H_B$) with an unfavourable change of entropy ($-\Delta S_B$). Therefore, the mechanism of binding of thymol to bOBP is not dominated by a hydrophobic effect related to any change in the hydration state of protein and ligand groups but, most likely, is driven by van der Waals and polar interactions, and hydrogen bonding. This finding is in agreement with that of pOBP either binding to IBMP or DMO, which was characterized by isothermal titration calorimetry (ITC) [85].

The five recombinant bOBP mutants of WT, I22C, S24C, F54C, and F91C were characterized the binding interaction with eight different ligands at their labelling positions by calculation of SASA at their cysteine residue in order to obtain information for the likelihood of the labelling efficiency of mutant bOBPs. It was found that the order of the cysteine-mutated residues from the highest to the lowest SASA was 91C, 54C, 22C, and 24C.

The five recombinant bOBP mutants were characterized in quantifying free thiol groups based on the reaction with Ellman's reagent and also investigation of the reactivity of DTNB with the proteins. It was found that the DTNB solution could not access to the thiol groups on the proteins. Nevertheless, this compound could interact with the thiols in denatured-phase protein. The concentration of free thiol in each mutant bOBP was therefore determined, and indicated that each mutant bOBP had a comparable concentration of free thiol and this is consistent with the introduction of a single cysteine residue into each recombinant protein mutant. Additionally, the stoichiometric binding between bOBP and DTNB compound appeared to be 1:1.

In order to investigate whether IANBD amide could be a possible good reporting probe for engineering bOBP biosensor, the characterization of the ligand binding interaction between the recombinant bOBP and the fluorescent IANBD amide has been performed. It was found that a mixture of covalent and non-covalent bonding existed in the interaction between IANBD amide and bOBP, making it difficult to distinguish ligand dependent conformational changes from ligand dependent displacement. Therefore, no further work was carried out on IANBD/thiol mutants.

A simple fluorophore 1-aminoanthracene (1-AMA) that provided ligand displacement was then used in the characterization of binding interaction with the recombinant bOBPwt. The functionality of bOBPwt was analysed by binding assays with 1-AMA, and resulting in a 1:1 stoichiometry with good affinity with the K_d value of 0.16 ± 0.023 μM. This value is comparable with the one of Mazzini *et al.* 2007 (0.23 ± 0.01 μM) [87], and with which typical values that have been reported by others are between 0.66 - 1μM for either recombinant or natural bOBPwt [38, 46, 54, 62, 126, 127].

The K_d values for several known or possible ligands including thymol, bromocresol green, malachite green, and methyl salicylate were determined by competitive titrations with 1-AMA on bOBPwt. It was found that most of the ligands were good ligands with the K_d values in the micromolar range, at which 1-AMA was the best ligand. However, methyl salicylate was found not to bind to this protein. The significant differences of ligand binding affinity confirmed the broad binding specificity of OBPs.

In order to present the K_d value of the ligand with improved accuracy, dual ligand competitive titration with 1-AMA on bOBPwt that 1-AMA and ligand concentrations were varied was also executed, which was compared to typical competitive binding methods that only ligand concentration was varied. It was found that the K_d value of thymol for bOBPwt obtained by this method was 1.03 ± 0.153 μM, which is slightly different from that from the single ligand titration (0.58 ± 0.28 μM) and that determined by CD spectroscopy (0.75 μM).

A number of chromophores in the laboratory have been investigated for the ability to be used as a probe in the competitive binding to bOBP based on absorbance spectrophotometry, and it was found that none of them gave a signal in the displacement analysis. This is because the signal from absorption spectroscopy is low when compared to that of fluorescence. Thus, the fluorophore 1-AMA has been used to detect ligand binding events for bOBP biosensors in this study.

Ten different solid supports for the bOBP biosensors were examined for their biocompatibility with bOBP function using 1-AMA as a probe, and the result was that nitrocellulose was chosen as the best membrane for immobilization. This is probably due to the 3-D micro-porous matrix (sponge structure) of nitrocellulose membrane that provides a much larger surface area for protein binding compared with 2-D surfaces.
The optimum operating concentrations of bOBP and 1-AMA immobilized on nitrocellulose for the bOBP biosensor were illustrated by titrations of the concentrations of bOBP and 1-AMA on nitrocellulose. The result was the concentrations of 100µM bOBP and 100µM 1-AMA as the reagent phase were selected to use for subsequent studies on nitrocellulose membrane.

It was found that at 100µM (or 2.5nmol) of total protein applied yielded 1.4 ± 0.01 nmol of bOBP immobilized on 0.5-cm diameter nitrocellulose, which was calculated as 7 ± 0.1 nmol bOBP per cm^2 of membrane, and had 55 ± 1% of bOBP immobilized on nitrocellulose relative to total protein applied.

The two different methods of immobilizing bOBP and 1-AMA on nitrocellulose were evaluated, and the result was incubation of nitrocellulose with the complex of bOBP and 1-AMA solution was chosen as the immobilization method for bOBP biosensors. The extent of the functional bOBP on nitrocellulose immobilized by this method was found to be 1.4 ± 0.1 nmol on 0.5-cm diameter disk, or 7 ± 0.4 nmol per cm^2 of membrane, which was equivalent to 54 ± 3% of functional bOBP immobilized on nitrocellulose relative to total protein applied.

In the final chapter of this thesis, the fibre-optic biosensor based on bOBP was constructed. It has been an extrinsic sensor with bOBP immobilized on a nitrocellulose membrane disk and mounted to the front surface of the probe at the end of a bifurcated bundle of optical fibres that was in turn connected to the light source and the spectrometer. Light from the LLS-385 light-emitting diode (LED) light source (at 385nm) was directed through one leg of a bifurcated bundle of optical fibres to the probe tip where the bOBP is immobilized membrane disk. The light intensity emitted by the bOBP immobilized membrane was monitored by transmission through the second leg of silica fibre and reflecting onto the 2048-element CCD array detector system of the HR2000 high-resolution spectrometer. The HR2000 spectrometer was connected to a laptop with the supplied SpectraSuite software.

Three different biosensing formats– solution-phase bOBP in microplate reader format, immobilized bOBP in microplate reader format, and fibre-optic bundle format had their S/B ratios determined for based on three different backgrounds, on which the effect of 1-AMA background on the solution phase format was shown. In order to obtain quantitative information for the utility of the three biosensing systems, the systems were used to measure thymol in the liquid phase. The LODs were found to be 0.5 ± 0.2 µM, 5 ± 2 µM, and 14 ± 6 µM (calculated as S/N = 3), respectively, demonstrating the versatility of the system. The differences of LOD values resulted from the effect of higher background of membrane scattering as well as configurations of optical detection format. The fibre-optic bOBP biosensor with the LOD that is well within the working range that is below the guideline values considered toxic to humans of the U.S. Environmental Protection Agency [185]. Therefore, this bOBP biosensor has been able to be employed for detection of liquid-phase thymol in samples that will provide a first warning when levels exceed the allowed limits and indicate the necessity of performing more accurate analyses.

Besides, it was also found that the fibre-optic biosensor based on bOBP was capable of sensing thymol vapour. However, its LOD value could not yet be reported correctly from the preliminary non-equilibrium experimental set-up due to photobleaching problems arising from using this fibre-optic biosensor. Therefore, the fibre-optic bOBP biosensor developed at this stage has not yet been able to achieve continuous monitoring using a single membrane, which would establish a closed equilibrium system designed for the quantification of thymol vapour. Future improvement is necessary to address this problem and will result in the development of a more practical sensor system.

9.2 Future Work

9.2.1 Optimization of the fibre-optic biosensor based on bOBP

Based on the photobleaching problem found from using the fibre-optic bOBP biosensor, it is recommended that the very important further work will be either one or combined approaches to the following four different methods; firstly, reconfiguration of HR2000 spectrometer with a larger entrance slit, so a lower LED intensity will be required. Secondly, the use of a neutral density filter in order to reduce the intensity of the excitation light. Thirdly, the replacement of the HR2000 spectrometer with a simple photodiode and filter. Lastly, the use of a more robust photostable fluorophore e.g. Alexa, DyLight or Atto Fluors may be tried, although these would need to bind bOBP.

Further optimization of the fibre-optic bOBP biosensor will be by varying different experimental conditions, to increase its sensitivity, such as the use of a higher level of immobilized protein, protein immobilization materials (hydrogel).

9.2.2 Development of a more practical fibre-optic biosensor based on bOBP

After the fibre-optic bOBP biosensor has the photobleaching problem solved and the optimization with the sensitivity improved, further work will be in the development of a more practical fibre-optic biosensor that will make it more attractive. Therefore, a fibre-optic biosensor based on bOBP for continous monitoring of samples either in the liquid or particularly vapour phase will be created. Subsequently, an ultimate plan will be the invention of an electronic nose. The electronic nose is defined as a fibre-optic array biosensor based on bOBPs that employs a number of bOBP mutants as 'multichannel recognition elements' [127]. The instrument will comprise an array of optical fibres immobilized with bOBP mutants that have partial specificity and an appropriate pattern recognition system, capable of recognizing different types of sample vapours. Pattern recognition techniques include artificial neural network (ANN), principal components analysis (PCA), discriminant function analysis and fuzzy logic. The sensor array will sense the vapours from a sample and provide a series of measurements. The pattern recognition system will then compare the measurement pattern with known patterns (standards) [187].

9.2.3 Application of the fibre-optic biosensor based on bOBP

The bOBP-based fibre-optic biosensor will be useful for remote sensing in areas not easily accessible for testing. Moreover, as the small-sized and lightweight sensor with the LED light source (LLS-385) of 5 x 5 x 4.5 inches, 0.34 kg and the spectrometer (HR2000) of 5.8 x 4 x 1.8 inches, 0.57 kg (compared to the SPECTRAmax™ GEMINI XS microplate spectrofluorometer of 22.8 x 15 x 8.6 inches, 16 kg), and the fibre of 400 µM diameter that can also be miniaturized, this test system is easily portable for use at on-site testing of samples. Therefore, the application of the system for in-situ and remote sensing is a part of future studies. In addition, the fact that performance of biosensors is strictly dependent on the affinity and specificity of the

recognition element [127], and consequently the binding properties and specificity of bOBP are necessary to be investigated to provide the basis of the biosensor [188].

The capability of the bOBP biosensor system for detection of various samples is more likely to be applicable, which will therefore need to be investigated. For instance, the detection of explosive components [127, 189], pollutants [65], toxic compounds [190], foods, fragrances, narcotics, etc.

It has been reported that OBPs that present unique characteristics of thermal and chemical stability bind explosive molecules. The binding capacities of pOBP and bOBPs (that are wild type, two mutants of a truncated form, and a deswapped monomeric form of bOBP) have been shown for the detection of explosive components such as diphenylamine, dimethylphthalate, resorcinol and dinitrotoluene with affinity constants ranging between 80 nM and 10.6 mM [127, 189].

Polycyclic aromatic hydrocarbons are portion of the most threatening pollutants widespread in the environment, nevertheless, the pOBP appeared binding capability with good affinities to several aromatic polycyclic compounds, such as benzyl benzoate and diphenylketone [65], at which the orientations of such ligands in the binding pocket has been visualised in crystallographic studies [59].

Additionally, it was found the binding capacity and chemical resistance of bOBP and pOBP to 4-hydroxy-2-nonenal (HNE); a toxic compound that produced in nasal tissue in consequence of oxidative stress, with K_d values of 4.9 and 9.0 µM for pOBP and bOBP, respectively [190].

Several papers reported the property of bOBP in odor sensing. For example, development of a bOBP-based affinity matrix for odorants by bOBP that coupled to CNBr-sepharose resin and packed into columns shows high specificity and affinity for odorants, including 2-isobutyl-3-methoxy pyrazine (bell pepper odorant), geosmin (earthy odorant), (-)-carvone (minthy odorant), and thymol (disinfectant odorant) [191].

Furthermore, twenty floral smelling tetrahydropyranyl and tetrahydrofuranyl ethers, and twelve additional compounds with different odours were tested with bOBP and pOBP. It was found that most of them are good ligands for both proteins with K_d values in the μM range. The data confirm the broad binding specificity of OBPs and indicate the possibility of using these olfactory proteins in biosensors for discriminating odours and other volatile chemicals. Their proposed biosensors were designed by the incorporation of several types of OBPs with different and broad overlapping specificities for recognizing a great variety of odours [34].

Lastly, a study reported the binding capacity of bOBP and pOBP to nutty and green-smelling pyrazines and thiazoles. From testing thirty-two green and nutty-smelling compounds by ligand binding assays, it was shown that all the green odorants are good ligands for both proteins, while the nutty ones are not [192].

The evidence of the OBPs binding capacities indicated that the biosensors based on OBPs should be able to detect and identify substances that allow continuous monitoring and measurements taken in real time. Finally, the system described here can be generalized to use any forms of OBP that have remarkable differences in their binding spectrum. This would be virtually useful for detection of all types of molecules.

REFERENCES

1. Scheller, F.W., *Research and development in biosensors.* Current opinion in biotechnology, 2001. **12**(1): p. 35.
2. Villaverde, A., *Allosteric enzymes as biosensors for molecular diagnosis.* Febs Letters, 2003. **554**(1-2): p. 169-172.
3. Scheller, F.W., et al., *Analytical Aspects of Internal Signal Processing in Biosensors.* Annals of the New York Academy of Sciences, 1990. **613**: p. 68-78.
4. Madou, M., *Required technology breakthroughs to assume widely accepted biosensors.* Applied biochemistry and biotechnology, 1993. **41**(1): p. 109-128.
5. Brennan, J.D., *Preparation and entrapment of fluorescently labeled proteins for the development of reagentless optical biosensors.* Journal of Fluorescence, 1999. **9**(4): p. 295-312.
6. Hellinga, H.W. and J.S. Marvin, *Protein engineering and the development of generic biosensors.* Trends in Biotechnology, 1998. **16**(4): p. 183-189.
7. Lakowicz, J.R., *Principles of fluorescence spectroscopy.* Journal of biomedical optics, 2008. **13**(2): p. 029901.
8. Gispert, J.R., *Coordination Chemistry*2008: John Wiley & Sons.
9. Peter TC So, C.Y.D., *Fluorescence Spectrophotometry.* ENCYCLOPEDIA OF LIFE SCIENCES, 2002: p. 1-4.
10. Pope, A.J., U.M. Haupts, and K.J. Moore, *Homogeneous fluorescence readouts for miniaturized high-throughput screening: theory and practice.* Drug discovery today, 1999. **4**(8): p. 350-362.
11. Brian Herman, J.R.L., Douglas B. Murphy, Thomas J. Fellers, Michael W. Davidson *Fluorescence Excitation and Emission Fundamentals*. Available from: http://www.olympusmicro.com/primer/techniques/confocal/fluoroexciteemit.html

12. Diffey, B.L., *What is light?* Photodermatology, Photoimmunology & Photomedicine, 2002. **18**(2): p. 68-74.
13. *Fluorescence*. Available from: http://www.art.ca/en/preclinical/optical-molecular-imaging/fluorescence.php.
14. Guthrie, C. and G.R. Fink, *Guide to Yeast Genetics and Molecular and Cell Biology Part C*2002.
15. Thomas, S.W.I., *Chemical sensors based on amplifying fluorescent conjugated polymers.* Chemical reviews, 2007. **107**(4): p. 1339.
16. Tsien, R.Y., L. Ernst, and A. Waggoner, *Fluorophores for Confocal Microscopy: Photophysics and Photochemistry Handbook Of Biological Confocal Microscopy*, J.B. Pawley, Editor 2006, Springer US. p. 338-352.
17. Piston, D.W. and G.-J. Kremers, *Fluorescent protein FRET: the good, the bad and the ugly.* Trends in Biochemical Sciences, 2007. **32**(9): p. 407-414.
18. Gert-Jan Kremers, D.W.P., Michael W. Davidson *Fundamental Principles of Förster Resonance Energy Transfer (FRET)*. Available from: http://www.microscopyu.com/articles/fluorescence/fret/fretintro.html.
19. Iqbal, A., et al., *Orientation dependence in fluorescent energy transfer between Cy3 and Cy5 terminally attached to double-stranded nucleic acids.* Proceedings of the National Academy of Sciences, 2008. **105**(32): p. 11176-11181.
20. Brian Herman, V.E.C.F., Joseph R. Lakowicz, Thomas J. Fellersk, Michael W. Davidson *Fluorescence Resonance Energy Transfer (FRET) Microscopy*. Available from: http://www.olympusmicro.com/primer/techniques/fluorescence/fret/fretintro.html.
21. Stryer, L., *Energy transfer: a spectroscopic ruler.* Proceedings of the National Academy of Sciences of the United States of America, 1967. **58**(2): p. 719.
22. Gambin, Y., *Multicolor single-molecule FRET to explore protein folding and binding.* Molecular bioSystems, 2010. **6**(9): p. 1540.
23. Tadross, M.R., et al., *Robust approaches to quantitative ratiometric FRET imaging of CFP/YFP fluorophores under confocal microscopy.* Journal of Microscopy, 2009. **233**(1): p. 192-204.

24. Wang, H., E. Nakata, and I. Hamachi, *Recent Progress in Strategies for the Creation of Protein-Based Fluorescent Biosensors.* ChemBioChem, 2009. **10**(16): p. 2560-2577.
25. Nakata, M., et al., *Recent progress in the construction methodology of fluorescent biosensors based on biomolecules*. Biosensors - Emerging Materials and Applications2011.
26. Tainaka, K., *Design strategies of fluorescent biosensors based on biological macromolecular receptors.* Sensors, 2010. **10**(2): p. 1355.
27. Zhang, J., et al., *Creating new fluorescent probes for cell biology.* Nat Rev Mol Cell Biol, 2002. **3**(12): p. 906-918.
28. Mank, M. and O. Griesbeck, *Genetically Encoded Calcium Indicators.* Chemical reviews, 2008. **108**(5): p. 1550-1564.
29. Stiner, L., *Development and characterization of a green fluorescent protein-based bacterial biosensor for bioavailable toluene and related compounds.* Applied and environmental microbiology, 2002. **68**(4): p. 1962.
30. Goldman, E.R., et al., *A Hybrid Quantum Dot−Antibody Fragment Fluorescence Resonance Energy Transfer-Based TNT Sensor.* Journal of the American Chemical Society, 2005. **127**(18): p. 6744-6751.
31. Meadows, D. and J.S. Schultz, *Fiber-optic biosensors based on fluorescence energy transfer.* Talanta, 1988. **35**(2): p. 145-150.
32. Spinelli, S., et al., *The structure of the monomeric porcine odorant binding protein sheds light on the domain swapping mechanism.* Biochemistry, 1998. **37**(22): p. 7913-7918.
33. Lobel, D., *Odorants of different chemical classes interact with distinct odorant binding protein subtypes.* Chemical Senses, 2002. **27**(1): p. 39-44.
34. Dalmonte, M., et al., *Binding of selected odorants to bovine and porcine odorant-binding proteins.* Chemical Senses, 1993. **18**(6): p. 713-721.
35. Flower, D.R., *The lipocalin protein family: structure and function.* Biochemical journal, 1996. **318**(Pt 1): p. 1.
36. Pelosi, P., *Odorant-binding proteins.* Critical reviews in biochemistry and molecular biology, 1994. **29**(3): p. 199.

37. Flower, D.R., *The lipocalin protein family: structural and sequence overview.* Biochimica et biophysica acta. G, General subjects, 2000. **1482**(1-2): p. 9-24.
38. Vincent, F., *Crystal structures of bovine odorant-binding protein in complex with odorant molecules.* European journal of biochemistry, 2004. **271**(19): p. 3832-3842.
39. Pelosi, P., *The role of perireceptor events in vertebrate olfaction.* Cellular and molecular life sciences, 2001. **58**(4): p. 503-509.
40. Briand, L., et al., *Evidence of an odorant-binding protein in the human olfactory mucus: Location, structural characterization, and odorant-binding properties.* Biochemistry, 2002. **41**(23): p. 7241-7252.
41. Flower, D.R., *Beyond the superfamily: the lipocalin receptors.* Biochimica et Biophysica Acta (BBA) - Protein Structure and Molecular Enzymology, 2000. **1482**(1–2): p. 327-336.
42. Skerra, A., *Lipocalins as a scaffold.* Biochimica et biophysica acta. Protein structure and molecular enzymology, 2000. **1482**(1-2): p. 337.
43. Flower, D.R., *Experimentally determined lipocalin structures.* Biochimica et Biophysica Acta (BBA) - Protein Structure and Molecular Enzymology, 2000. **1482**(1–2): p. 46-56.
44. Åkerstrom, B., D.R. Flower, and J.-P. Salier, *Lipocalins: unity in diversity.* Biochimica et Biophysica Acta (BBA) - Protein Structure and Molecular Enzymology, 2000. **1482**(1–2): p. 1-8.
45. D'Auria, S., *The tryptophan phosphorescence of porcine and mutant bovine odorant-binding proteins: A probe for the local protein structure and dynamics.* Journal of proteome research, 2008. **7**(3): p. 1151-1158.
46. Ramoni, R., *Control of domain swapping in bovine odorant-binding protein.* The Biochemical journal, 2002. **365**: p. 739-748.
47. Pevsner, J., et al., *Odorant-binding protein. Characterization of ligand binding.* Journal of Biological Chemistry, 1990. **265**(11): p. 6118-6125.
48. Tegoni, M., *Mammalian odorant binding proteins.* Biochimica et Biophysica Acta (BBA) - Protein Structure and Molecular Enzymology, 2000. **1482**(1-2): p. 229-240.

49. Graziadei, P.P.C. and G.A. Montigraziadei, *Neurogenesis and neuron regeneration in the olfactory system of mammals. I. Morphological aspects of differentiation and structural organization of the olfactory sensory neurons.* Journal of Neurocytology, 1979. **8**(1): p. 1-18.
50. Buck, L. and R. Axel, *A novel multigene family may encode odorant receptors: a molecular basis for odor recognition.* Cell, 1991. **65**(1): p. 175-187.
51. Lancet, D., *Vertebrate olfactory reception.* Annual Review of Neuroscience, 1986. **9**: p. 329-355.
52. Blanchet, M., *The three-dimensional structure of bovine odorant binding protein and its mechanism of odor recognition.* Nature structural biology, 1996. **3**(11): p. 934-939.
53. Tegoni, M., *Domain swapping creates a third putative combining site in bovine odorant binding protein dimer.* Nature structural biology, 1996. **3**(10): p. 863-867.
54. Ramoni, R., *The insect attractant 1-octen-3-ol is the natural ligand of bovine odorant-binding protein.* The Journal of biological chemistry, 2001. **276**(10): p. 7150-7155.
55. Pevsner, J., et al., *Isolation and characterization of an olfactory receptor protein for odorant pyrazines.* Proceedings of the National Academy of Sciences of the United States of America, 1985. **82**(9): p. 3050-3054.
56. Ikematsu, M., *Chemical sensor and method of detecting chemicals*, 2002, Google Patents: US Patent Application 10/110,221.
57. Topazzini, A., et al., *Specificity of a pyrazine binding protein from cow olfactory mucosa.* Chemical Senses, 1985. **10**(1): p. 45-49.
58. Pelosi, P., *Structure/activity studies and characterization of an odorant-binding protein.* Chemical Senses, 1989. **1**: p. 207-226.
59. Vincent, F., et al., *Complexes of porcine odorant binding protein with odorant molecules belonging to different chemical classes.* Journal of Molecular Biology, 2000. **300**(1): p. 127-139.
60. Tcatchoff, L., *A single lysyl residue defines the binding specificity of a human odorant-binding protein for aldehydes.* FEBS letters, 2006. **580**(8): p. 2102.

61. Löbel, D., *Subtypes of odorant-binding proteins.* The FEBS journal, 1998. **254**(2): p. 318.
62. Ramoni, R., *Deswapping bovine odorant binding protein.* Biochimica et biophysica acta. Proteins and proteomics, 2008. **1784**(4): p. 651-657.
63. Marabotti, A., *Wild-Type and Mutant Bovine Odorant-Binding Proteins To Probe the Role of the Quaternary Structure Organization in the Protein Thermal Stability.* Journal of proteome research, 2008. **7**(12): p. 5221-5229.
64. Marabotti, A., *Mutant bovine odorant-binding protein: Temperature affects the protein stability and dynamics as revealed by infrared spectroscopy and molecular dynamics simulations.* Proteins, 2008. **72**(2): p. 769-778.
65. Wei, Y., *Binding of polycyclic aromatic hydrocarbons to mutants of odorant-binding protein: A first step towards biosensors for environmental monitoring.* Biochimica et biophysica acta. Proteins and proteomics, 2008. **1784**(4): p. 666.
66. Ikematsu, M., *Chemical sensor and method of detecting chemical*, 2003, EP Patent 1,310,795: Munich, Germany: European Patent Office.
67. Ramoni, R., *Carbon nanotube-based biosensors.* Journal of physics. Condensed matter, 2008. **20**(47): p. 474201.
68. Pietrantonio, F., et al., *Surface Acoustic Wave Biosensor Based on a Recombinant Bovine Odorant-Binding Protein*, in *Sensors and Microsystems*, P. Malcovati, et al., Editors. 2010, Springer Netherlands. p. 201-205.
69. Lide, D.R., *CRC handbook of chemistry and physics: a ready-reference book of chemical and physical data*2004.
70. Rojano, B., et al., *Experimental and theoretical determination of the antioxidant properties of isoespintanol (2-isopropyl-3,6-dimethoxy-5-methylphenol).* Journal of Molecular Structure, 2008. **877**(1–3): p. 1-6.
71. Kordali, S., *Antifungal, phytotoxic and insecticidal properties of essential oil isolated from Turkish Origanum acutidens and its three components, carvacrol, thymol and p-cymene.* Bioresource technology, 2008. **99**(18): p. 8788.
72. Filoche, S.K., K. Soma, and C.H. Sissons, *Antimicrobial effects of essential oils in combination with chlorhexidine digluconate.* Oral Microbiology and Immunology, 2005. **20**(4): p. 221-225.

73. Mazzanobile, S. and N. Ibrahim, *Antimicrobial Toothpaste*, 1992, Google Patents: US Patent 5,094,843.
74. Lindenbaum, J., *Hepatic necrosis associated with halothane anesthesia.* The New England journal of medicine, 1963. **268**(10): p. 525.
75. EE Aziz, S.H., AAE El-Din, EA Omer *Effect of soil type and irrigation intervals on plant growth, essential oil yield and constituents of Thymus vulgaris plant.* Am. Euras. J. Agric. & Environ. Sci, 2008. **4**(4): p. 443-450.
76. Edelhoch, H., *Spectroscopic Determination of Tryptophan and Tyrosine in Proteins*.* Biochemistry, 1967. **6**(7): p. 1948.
77. Bianchet, M.A., *The three-dimensional structure of bovine odorant binding protein and its mechanism of odor recognition.* Nature structural & molecular biology, 1996. **3**(11): p. 934.
78. Haugland, *Handbook of Fluorescent Probes and Research Products.* Molecular Probes Inc., 2002: p. Chapter 2, pp79-98.
79. Lew, M.J., *Analysis of competitive agonist-antagonist interactions by nonlinear regression.* Trends in pharmacological sciences, 1995. **16**(10): p. 328.
80. Ikematsu, M., *Odorant binding to bovine odorant binding protein detected by intrinsic fluorescence.* Chemistry Letters, 2005. **34**(9): p. 1256-1257.
81. Paula, P.A.a.J.d., *Elements of Physical Chemistry.* Oxford University Press, 2005 **4th ed.**
82. Woody, K.N.N.B.R., *Circular dichroism: principles and applications.* 1994: p. p. 473.
83. Johnson, W.C., *Protein Secondary Structure and Circular Dichroism: A Practical Guide.* Proteins, 1990. **7**(205).
84. Kelly, S.M., *How to study proteins by circular dichroism.* Biochimica et biophysica acta. Proteins and proteomics, 2005. **1751**(2): p. 119.
85. Burova, T.V., et al., *Conformational Stability and Binding Properties of Porcine Odorant Binding Protein.* Biochemistry, 1999. **38**(45): p. 15043-15051.
86. Philo, J. *Circular dichroism*. Available from: http://www.ap-lab.com/CD_services.htm.

87. Mazzini, A., *Dissociation and unfolding of bovine odorant binding protein at acidic pH.* Journal of structural biology, 2007. **159**(1): p. 82-91.
88. Paolini, S., *Porcine odorant-binding protein: structural stability and ligand affinities measured by Fourier-transform infrared spectroscopy and fluorescence spectroscopy.* Biochimica et biophysica acta. Protein structure and molecular enzymology, 1999. **1431**(1): p. 179.
89. Greenfield, N.J., *Using circular dichroism collected as a function of temperature to determine the thermodynamics of protein unfolding and binding interactions.* Nature protocols, 2006. **1**(6): p. 2527.
90. Polverini, E., et al., *Characterization of a Deswapped Triple Mutant Bovine Odorant Binding Protein.* International Journal of Molecular Sciences, 2011. **12**(4): p. 2294-2314.
91. Greenfield, N.J., *Applications of circular dichroism in protein and peptide analysis.* TrAC. Trends in analytical chemistry, 1999. **18**(4): p. 236.
92. Chun, P.W., *Thermodynamic molecular switch in biological systems.* International journal of quantum chemistry, 2000. **80**(6): p. 1181.
93. Chun, P., *A Thermodynamic Molecular Switch in Biological Systems: Ribonuclease S' Fragment Complementation Reactions.* Biophysical journal, 2000. **78**(1): p. 416-429.
94. Stepanenko, O.V., *Hydrophobic interactions and ionic networks play an important role in thermal stability and denaturation mechanism of the porcine odorant-binding protein.* Proteins, 2008. **71**(1): p. 35.
95. Harano, Y., *Large gain in translational entropy of water is a major driving force in protein folding.* Chemical Physics Letters, 2004. **399**(4): p. 342-348.
96. Kinoshita, M., *Roles of translational motion of water molecules in sustaining life.* Frontiers in bioscience, 2009. **14**: p. 3419-3454.
97. Kinoshita, M., *Importance of translational entropy of water in biological self-assembly processes like protein folding.* International journal of molecular sciences, 2009. **10**(3): p. 1064.
98. Kim, Y., *Efficient site-specific labeling of proteins via cysteines.* Bioconjugate chemistry, 2008. **19**(3): p. 786.
99. Hermanson, G., *Bioconjugate techniques.* Academic Press; San Diego, 1996.

100. Shrake, A. and J.A. Rupley, *Environment and exposure to solvent of protein atoms. Lysozyme and insulin.* Journal of Molecular Biology, 1973. **79**(2): p. 351-371.
101. Lee, B., *The interpretation of protein structures: estimation of static accessibility.* Journal of Molecular Biology, 1971. **55**(3): p. 379.
102. Ellman, G.L., *Tissue sulfhydryl groups.* Archives of Biochemistry and Biophysics, 1959. **82**(1): p. 70-77.
103. *Instuctions: Ellman's Reagent*. Available from: http://www.piercenet.com/instructions/2160311.pdf.
104. Read, B., *Why fluorescence detection is getting glowing reviews. American Biotechnology Laboratory*, 2000.
105. Enander, K., et al., *A peptide-based, ratiometric biosensor construct for direct fluorescence detection of a protein analyte.* Bioconjugate Chemistry, 2008. **19**(9): p. 1864-1870.
106. Miyawaki, A., Llopis, J., Heim, R., McCaffery, J. M., Adams, J. A., Ikura, M., and Tsien, R. Y., *Fluorescent indicators for Ca2+ based on green fluorescent proteins and calmodulin.* Nature, 1997. **388**: p. 882.
107. Karlstrm, A., and Nygren, P. Å., *Dual labeling of a binding protein allows for specific fluorescence detection of native protein.* Analytical biochemistry, 2001. **295**: p. 22.
108. Wei, A.P., Blumenthal, D. K., and Herron, J. N. , *Antibody-mediated fluorescence enhancement based on shifting the intramolecular dimer-monomer equilibrium of fluorescent dyes.* Analytical chemistry, 1994. **66**: p. 1500.
109. Jiskoot, W., Hoogerhout, P., Beuvery, E. C., Herron, J. N., and Crommelin, D. J. A. , *Preparation and application of a fluorescein-labeled peptide for determining the affinity constant of a monoclonal antibody hapten complex by fluorescence polarization.* Analytical biochemistry, 1991. **196**: p. 421.
110. Sun, Y.J., et al., *The structure of glutamine-binding protein complexed with glutamine at 1.94 angstrom resolution: Comparisons with other amino acid binding proteins.* Journal of Molecular Biology, 1998. **278**(1): p. 219-229.

111. Hur, S. and T.C. Bruice, *Molecular dynamic study of orotidine-5 '-monophosphate decarboxylase in ground state and in intermediate state: A role of the 203-218 loop dynamics.* Proceedings of the National Academy of Sciences of the United States of America, 2002. **99**(15): p. 9668-9673.

112. Tian, Y., *Structure-based design of robust glucose biosensors using a Thermotoga maritima periplasmic glucose-binding protein.* Protein science, 2007. **16**(10): p. 2240.

113. Vercillo, N.C., et al., *Analysis of ligand binding to a ribose biosensor using site-directed mutagenesis and fluorescence spectroscopy.* Protein science, 2007. **16**(3): p. 362-368.

114. Gilardi, G., *Engineering the maltose binding protein for reagentless fluorescence sensing.* Analytical chemistry, 1994. **66**(21): p. 3840.

115. Chung, D.G. and P.N. Lewis, *INTERNAL ARCHITECTURE OF THE CORE NUCLEOSOME - FLUORESCENCE ENERGY-TRANSFER STUDIES AT METHIONINE-84 OF HISTONE-H4.* Biochemistry, 1986. **25**(18): p. 5036-5042.

116. Jullien, M. and J.R. Garel, *FLUORESCENT-PROBE OF RIBONUCLEASE-A CONFORMATION.* Biochemistry, 1981. **20**(24): p. 7021-7026.

117. Patonay, G., et al., *Noncovalent Labeling of Biomolecules with Red and Near-Infrared Dyes.* Molecules, 2004. **9**(3): p. 40-49.

118. Colyer, C., *Noncovalent labeling of proteins in capillary electrophoresis with laser-induced fluorescence detection.* Cell biochemistry and biophysics, 2000. **33**(3): p. 323.

119. Stoyanov, A.V., *On the possibility of applying noncovalent dyes for protein labeling in isoelectric focusing.* Analytical biochemistry, 2006. **350**(2): p. 263.

120. Lobel, D., et al., *Identification of a third rat odorant-binding protein (OBP3).* Chemical Senses, 2001. **26**(6): p. 673-680.

121. Kmiecik, D. and J. Albani, *Effect of 1-Aminoanthracene (1-AMA) Binding on the Structure of Three Lipocalin Proteins, the Dimeric β Lactoglobulin, the Dimeric Odorant Binding Protein and the Monomeric α1-Acid Glycoprotein. Fluorescence Spectra and Lifetimes Studies.* Journal of Fluorescence, 2010. **20**(5): p. 973-983.

122. Nespoulous, C., et al., *Odorant Binding and Conformational Changes of a Rat Odorant-binding Protein.* Chemical Senses, 2004. **29**(3): p. 189-198.
123. Butts, C.A., *Identification of a fluorescent general anesthetic, 1-aminoanthracene.* Proceedings of the National Academy of Sciences of the United States of America, 2009. **106**(16): p. 6501.
124. Paolini, S., *Amino acid sequence, post-translational modifications, binding and labelling of porcine odorant-binding protein.* Chemical Senses, 1998. **23**(6): p. 689.
125. Parisi, M., *Role of the disulphide bridge in folding, stability and function of porcine odorant binding protein: Spectroscopic equilibrium studies on C63A/C155A double mutant.* Biochimica et biophysica acta. Proteins and proteomics, 2005. **1750**(1): p. 30.
126. Mazzini, A., *Reversible unfolding of bovine odorant binding protein induced by guanidinium hydrochloride at neutral pH.* Biochimica et biophysica acta. Proteins and proteomics, 2002. **1599**(1-2): p. 90-101.
127. Ramoni, R., *The protein scaffold of the lipocalin odorant-binding protein is suitable for the design of new biosensors for the detection of explosive components.* Journal of physics. Condensed matter, 2007. **19**(39): p. 395012.
128. Colyer, C., *Noncovalent labeling of proteins in capillary electrophoresis with laser-induced fluorescence detection.* Cell biochemistry and biophysics, 2000. **33**(3): p. 323-337.
129. Yin, Y., *Protein immobilization capacity and covalent binding coverage of pulsed plasma polymer surfaces.* Applied surface science, 2010. **256**(16): p. 4984.
130. Siegrist, J., *Continuous glucose sensor using novel genetically engineered binding polypeptides towards< i> in vivo</i> applications.* Sensors and actuators. B, Chemical, 2010. **149**(1): p. 51.
131. Premkumar, J.R., *Antibody-based immobilization of bioluminescent bacterial sensor cells.* Talanta, 2001. **55**(5): p. 1029.
132. Arenkov, P., *Protein microchips: use for immunoassay and enzymatic reactions.* Analytical Biochemistry, 2000. **278**(2): p. 123.

133. Lee, Y., *ProteoChip: A highly sensitive protein microarray prepared by a novel method of protein immobilization for application of protein-protein interaction studies.* Proteomics, 2003. **3**(12): p. 2289.
134. *Protein Arrays Resource Page*. 20 May 2009; Available from: http://www.functionalgenomics.org.uk/sections/resources/protein_arrays.htm.
135. Tanaka, Y., *Exploring enzymatic catalysis at a solid surface: a case study with transglutaminase-mediated protein immobilization.* Organic & biomolecular chemistry, 2007. **5**(11): p. 1764.
136. Chan, L., *Covalent attachment of proteins to solid supports and surfaces via sortase-mediated ligation.* PLoS ONE, 2007. **2**(11): p. e1164.
137. Reis, E.F., *Synthesis and characterization of poly (vinyl alcohol) hydrogels and hybrids for rMPB70 protein adsorption.* Materials research, 2006. **9**(2): p. 185.
138. Clark, M.F., *Characteristics of the microplate method of enzyme-linked immunosorbent assay for the detection of plant viruses.* Journal of general virology, 1977. **34**(3): p. 475.
139. Voller, A., *A microplate method of enzyme-linked immunosorbent assay and its application to malaria.* Bulletin of the World Health Organization, 1974. **51**(2): p. 209.
140. Kai, J., et al., *A novel microfluidic microplate as the next generation assay platform for enzyme linked immunoassays (ELISA).* Lab on a Chip, 2012.
141. Charles, P.T., et al., *Fabrication and characterization of 3D hydrogel microarrays to measure antigenicity and antibody functionality for biosensor applications.* Biosensors and Bioelectronics, 2004. **20**(4): p. 753-764.
142. Yoshimura, I., *Molecular recognition in a supramolecular hydrogel to afford a semi-wet sensor chip.* Journal of the American Chemical Society, 2004. **126**(39): p. 12204.
143. Rucker, V.C., *Functional antibody immobilization on 3-dimensional polymeric surfaces generated by reactive ion etching.* Langmuir, 2005. **21**(17): p. 7621.
144. MacBeath, G., *Printing proteins as microarrays for high-throughput function determination.* Science, 2000. **289**(5485): p. 1760.
145. Ziauddin, J., *Microarrays of cells expressing defined cDNAs.* Nature, 2001. **411**(6833): p. 107.

146. Blawas, A.S., *Protein patterning.* Biomaterials, 1998. **19**(7-9): p. 595.
147. *NEXTERION® Product Catalogue*. Available from: http://www.schott.com/nexterion/english/download/nexterion_product_catalogue_row_2010_1.pdf.
148. Nakanishi, K., *A novel method of immobilizing antibodies on a quartz crystal microbalance using plasma-polymerized films for immunosensors.* Analytical chemistry, 1996. **68**(10): p. 1695.
149. Mendoza, L.G., *High-throughput microarray-based enzyme-linked immunosorbent assay (ELISA).* BioTechniques, 1999. **27**: p. 778.
150. Høyer Hansen, G., *Loss of ELISA specificity due to biotinylation of monoclonal antibodies.* Journal of immunological methods, 2000. **235**(1): p. 91.
151. Zhang, J., *Electrochemical analysis of immobilised chemical and genetic biotinylated alkaline phosphatase.* Analytica Chimica Acta, 2000. **408**(1-2): p. 241.
152. Wang, C.Y., *Specific immobilization of firefly luciferase through a biotin carboxyl carrier protein domain.* Analytical Biochemistry, 1997. **246**(1): p. 133.
153. Wilchek, M. and E.A. Bayer, *[13] Biotin-containing reagents*, in *Methods in Enzymology*, W. Meir and A.B. Edward, Editors. 1990, Academic Press. p. 123-138.
154. Templin, M.F., *Protein microarray technology.* Drug discovery today, 2002. **7**(15): p. 815.
155. Charvolin, D., *The use of amphipols as universal molecular adapters to immobilize membrane proteins onto solid supports.* Proceedings of the National Academy of Sciences of the United States of America, 2009. **106**(2): p. 405.
156. Zhu, H., *Global analysis of protein activities using proteome chips.* Science, 2001. **293**(5537): p. 2101.
157. Cha, T.W., *Enzymatic activity on a chip: the critical role of protein orientation.* Proteomics, 2005. **5**(2): p. 416.

158. HollandNell, K., *Specifically immobilised aldo/keto reductase AKR1A1 shows a dramatic increase in activity relative to the randomly immobilised enzyme.* ChemBioChem, 2007. **8**(9): p. 1071.
159. Karyakin, A.A., *Oriented immobilization of antibodies onto the gold surfaces via their native thiol groups.* Analytical chemistry, 2000. **72**(16): p. 3805.
160. Neubert, H., *Enhanced affinity capture MALDI-TOF MS: orientation of an immunoglobulin G using recombinant protein G.* Analytical chemistry, 2002. **74**(15): p. 3677.
161. Kwon, Y., *Antibody arrays prepared by cutinase-mediated immobilization on self-assembled monolayers.* Analytical chemistry, 2004. **76**(19): p. 5713.
162. Shriver Lake, L.C., *Antibody immobilization using heterobifunctional crosslinkers.* Biosensors & bioelectronics, 1997. **12**(11): p. 1101.
163. Kusnezow, W., *Solid supports for microarray immunoassays.* Journal of molecular recognition, 2003. **16**(4): p. 165.
164. Vijayendran, R.A., *A quantitative assessment of heterogeneity for surface-immobilized proteins.* Analytical chemistry, 2001. **73**(3): p. 471.
165. Lueking, A., *Protein microarrays for gene expression and antibody screening.* Analytical Biochemistry, 1999. **270**(1): p. 103.
166. Nieba, L., *BIACORE analysis of histidine-tagged proteins using a chelating NTA sensor chip.* Analytical Biochemistry, 1997. **252**(2): p. 217.
167. *The Premier Protein Array Platform from Discovery to Diagnostics*. Available from: http://www.whatman.com/References/FAST%20Slides%20-%20The%20Premier%20Protein%20Array%20Platform.pdf.
168. Michael Walther, B.S., Andrea Friße and Jens Beator. *The FAST Guide to Protein Microarrays*. Available from: http://www.whatman.com/References/FAST%20Guide%20to%20Protein%20Microarrays.pdf.
169. *Blotting Membrane Sandwiches*. Available from: http://products.thomassci.com/blotting_membrane_sandwiches_104572043.php.
170. Powner, E.T., *Intelligent biosensors.* Sensor Review, 1997. **17**(2): p. 107.

171. *Optical Fiber*. Available from: http://www.fiber-optics.info/fiber_optic_glossary/optical_fiber.
172. Marazuela, M., *Fiber-optic biosensors-an overview*. Analytical and bioanalytical chemistry, 2002. **372**(5): p. 664.
173. Bosch, M.E., *Recent development in optical fiber biosensors*. Sensors, 2007. **7**(6): p. 797.
174. Eggins, B.R., *Chemical sensors and biosensors*2002: John Wiley.
175. Abrahamian, S., *Fiber Optic Training Guide*. Evertz Microsystems Ltd., 2006: p. 1-17.
176. BigRiz, *Fibre optic strands*, 2006, May 28
177. Agrawal, G.P. *Fiber-optic communication systems*. 2011; Available from: http://metalib.lib.ic.ac.uk:9003/sfx_local?sid=google&auinit=GP&aulast=Agrawal&title=Fiber-optic%20communication%20systems&genre=book&isbn=0470922826&date=2011.
178. Udd, E. *Fiber optic sensors*. 1991; Available from: http://metalib.lib.ic.ac.uk:9003/sfx_local?sid=google&auinit=E&aulast=Udd&title=Fiber%20optic%20sensors&genre=book&isbn=0471830070&date=1991.
179. Kersey, A.D., *A review of recent developments in fiber optic sensor technology*. Optical fiber technology, 1996. **2**(3): p. 291.
180. Nguyen, T.H., et al., *Intrinsic Fluorescence-Based Optical Fiber Sensor for Cocaine Using a Molecularly Imprinted Polymer as the Recognition Element*. IEEE Sensors Journal, 2012. **12**(1): p. 255-260.
181. Kudo, H., et al., *Biochemical gas sensor (bio-sniffer) for ultrahigh-sensitive gaseous formaldehyde monitoring*. Biosensors & bioelectronics, 2010. **26**(2): p. 854-858.
182. *MEDICAL APPLICATIONS OF FIBER-OPTICS: Optical fiber sees growth as medical sensors*. Available from: http://www.laserfocusworld.com/articles/2011/01/medical-applications-of-fiber-optics-optical-fiber-sees-growth-as-medical-sensors.html.
183. Coulet, P.R., *Polymeric membranes and coupled enzymes in the design of biosensors*. Journal of membrane science, 1992. **68**(3): p. 217.

184. Monk, D.J., *Optical fiber-based biosensors.* Analytical and bioanalytical chemistry, 2004. **379**(7): p. 931.
185. *THYMOL 5-methyl-2-isopropyl-1-phenol (PC Code 080402),* US Environmental Protection Agency, Office of Pesticide Programs, Biopesticides and Pollution Prevention Division. p. 1-23.
186. Dearfield, K.L., *Characteristics of the US EPA's Office of Pesticide Programs' toxicity information databases.* Environmental health perspectives, 1991. **96**: p. 53.
187. Deisingh, A., *Biosensors for microbial detection* Microbiologist, 2003: p. 30-33.
188. Cai, Q., *An AFM-based study of porcine OBP film for artifical olfaction*2001.
189. Staiano, M., *New trends in bio/nanotechnology: stable proteins as advanced molecular tools for health and environment.* Environmental technology, 2010. **31**(8-9): p. 935.
190. Grolli, S., *Odorant binding protein has the biochemical properties of a scavenger for 4-hydroxy-2-nonenal in mammalian nasal mucosa.* The FEBS journal, 2006. **273**(22): p. 5131.
191. Bussolati, L., *Preparation of an affinity resin for odorants by coupling odorant binding protein from bovine nasal mucosa to Sepharose 4B.* Journal of biotechnology, 1993. **30**(2): p. 225-230.
192. Hérent, M.F., *Affinities of nutty and green-smelling pyrazines and thiazoles to odorant-binding proteins, in relation with their lipophilicity.* Chemical Senses, 1995. **20**(6): p. 601.

APPENDIX A

DNA AND AMINO ACID SEQUENCE OF bOBP-WT

The verified sequence shows flanking regions of *Bam* HI and *Eco* RI cloning sites to be inserted into pET24a, T7 tag at N-terminus, and Histidine tag at C-terminus.

```
    EcoRI
  1 AATTCCTAAT GATGATGATG ATGATGATGA TGATGATGTT CAGGGTGGGG ATGGTTTTCA TTTTCCAAGA AATTCACAAC GTTTTTCTTG TCAATTCCTT
    TTAAGGATTA CTACTACTAC TACTACTACT ACTACTACAA GTCCCACCCC TACCAAAAGT AAAAGGTTCT TTAAGTGTTG CAAAAAGAAC AGTTAAGGAA
    3′ E  *  H    H  H  H    H  H  H  H    H  H  E    P  H  P    H  N  E  N    E  L  F    N  V  V    N  K  K  D    I  G  K ·
101 TGTCTTCCGT CAGCTTCCAG AATTTCTCCA AGTCTTCATC TTCAACATTC AGTTTAACAA ACAGTCCGGT GAGCTCTGTC TTCTGGCCGT GCTTATCCAC
    ACAGAAGGCA GTCGAAGGTC TTAAAGAGGT TCAGAAGTAG AAGTTGTAAG TCAAATTGTT TGTCAGGCCA CTCGAGACAG AAGACCGGCA CGAATAGGTG
    .  D  E  T    L  K  W  F    K  E  L    D  E  D    E  V  N  L    K  V  F    L  G  T    L  E  T  K    Q  G  H    K  D  V
201 GTTGATGTTA TGTGCTACCA GATGCGTCCT CGACAGAGAG ACAATTTTAA AAACGTTTTG ACCCTCATAG TCAGCAACAT AAGTACCATC GTCTTGCTTT
    CAACTACAAT ACACGATGGT CTACGCAGGA GCTGTCTCTC TGTTAAAATT TTTGCAAAAC TGGGAGTATC AGTCGTTGTA TTCATGGTAG CAGAACGAAA
     N  I  N  H    A  V  L    H  T  R    S  L  S  V    I  K  F    V  N  Q    G  E  Y  D    A  V  Y    T  G  D    D  Q  K  T ·
301 GTAGCCTTGA CATGTACATT CTTCCATTTT CCATCCCGCT TGACAGAAAA GTAAAAGTCC ACCGTGCCCT TTTCATCATC AAACACAAGT TCACGGAAGT
    CATCGGAACT GTACATGTAA GAAGGTAAAA GGTAGGGCGA ACTGTCTTTT CATTTTCAGG TGGCACGGGA AAAGTAGTAG TTTGTGTTCA AGTGCCTTCA
    ..  A  K  V    H  V  N    K  W  K  G    D  R  K    V  S  F    Y  F  D  V    T  G  K    E  D  D    F  V  L  E    R  F  Y ·
401 AAGTCCTGAA TGGTCCATTC TCCTGGATTT TCTCTGGGTT GGTCGACCCA ATGTACACTG TTCTCCATGG TCCTGAAAGC TCTGAGAGAT TTTGCTCAGC
    TTCAGGACTT ACCAGGTAAG AGGACCTAAA AGAGACCCAA CCAGCTGGGT TACATGTGAC AAGAGGTACC AGGACTTTCG AGACTCTCTA AAACGAGTCG
    .  T  R  F    P  G  N  E    Q  I  K    E  P  N    T  S  G  I    Y  V  T    R  W  P    G  S  L  E    S  L  N    Q  E  A
                      BamHI
501 TTCCTCCTCT TGCGCCCAGG ATCCGCGACC CATTTGCTGT CCACCAGTCA TGCTAGCCAT
    AAGGAGGAGA ACGCGGGTCC TAGGCGCTGG GTAAACGACA GGTGGTCAGT ACGATCGGTA
     E  E  E  Q    A  W  S    G  R  G    M  Q  Q  G    G  T  M    S  A  M    5′
                                      T7 tag
```

APPENDIX B

SUMMARY OF PERMISSION FOR THIRD PARTY COPYRIGHT WORKS

Page no.	Figure no.	Source work	Copyright holder	Permission granted	Note
Page 19	Figure 1.1	Brennan, J.D., *Preparation and entrapment of fluorescently labeled proteins for the development of reagentless optical biosensors.* Journal of Fluorescence, 1999. **9**(4): p. 295-312.	Springer	✓	Page 198
Page 21	Figure 1.2	Brian Herman, J.R.L., Douglas B. Murphy, Thomas J. Fellers, Michael W. Davidson *Fluorescence Excitation and Emission Fundamentals*. Available from: http://www.olympusmicro.com/primer/techniques/confocal/fluoroexciteemit.html	©2012 Olympus America Inc., Michael W. Davidson	✓	Page 199 and 200
Page 24	Figure 1.4	Gert-Jan Kremers, D.W.P., Michael W. Davidson *Fundamental Principles of Förster Resonance Energy Transfer (FRET)*. Available from: http://www.microscopyu.com/articles/fluorescence/fret/fretintro.html.	© 2000-2012, Michael W. Davidson	✓	Page 199 and 200

Page 25	Figure 1.5	Brian Herman, V.E.C.F., Joseph R. Lakowicz, Thomas J. Fellersk, Michael W. Davidson *Fluorescence Resonance Energy Transfer (FRET) Microscopy*. Available from: http://www.olympusmicro.com/primer/techniques/fluorescence/fret/fretintro.html.	© 2012 Olympus America Inc., Michael W. Davidson	✓	Page 199 and 200
Page 28	Figure 1.7	Wang, H., E. Nakata, and I. Hamachi, *Recent Progress in Strategies for the Creation of Protein-Based Fluorescent Biosensors.* ChemBioChem, 2009. **10**(16): p. 2560-2577.	John Wiley and Sons.	✓	Page 201
Page 29	Figure 1.8	Goldman, E.R., et al., *A Hybrid Quantum Dot−Antibody Fragment Fluorescence Resonance Energy Transfer-Based TNT Sensor.* Journal of the American Chemical Society, 2005. **127**(18): p. 6744-6751.	American Chemical Society	✓	Page 202
Page 32	Figure 1.10 and 1.11	Buck, L. and R. Axel, *A novel multigene family may encode odorant receptors: a molecular basis for odor recognition.* Cell, 1991. **65**(1): p. 175-187.	Elsevier	✓	Page 203
Page 34	Figure 1.12	Tegoni, M., *Mammalian odorant binding proteins.* Biochimica et Biophysica Acta (BBA) Protein Structure and Molecular Enzymology, 2000. **1482**(1-2): p. 229-240.	Elsevier	✓	Page 204
Page 79	Figure 4.3	Philo, J. *Circular dichroism*. Available from: http://www.ap-lab.com/CD_services.htm.	© 2000-2012 Alliance Protein Laboratories, Dr. John Philo	✓	Page 206

Page 106	Figure 5.5	Enander, K., et al., *A peptide-based, ratiometric biosensor construct for direct fluorescence detection of a protein analyte.* Bioconjugate Chemistry, 2008. **19**(9): p. 1864-1870.	American Chemical Society	✓	Page 207
Page 153	Figure 8.5A	Nguyen, T.H., et al., *Intrinsic Fluorescence-Based Optical Fiber Sensor for Cocaine Using a Molecularly Imprinted Polymer as the Recognition Element.* IEEE Sensors Journal, 2012. **12**(1): p. 255-260.	IEEE	✓	Page 208
Page 153	Figure 8.5B	Kudo, H., et al., *Biochemical gas sensor (bio-sniffer) for ultrahigh-sensitive gaseous formaldehyde monitoring.* Biosensors & bioelectronics, 2010. **26**(2): p. 854-858.	Elsevier	✓	Page 209

APPENDIX C

PERMISSION INFORMATION FOR THIRD PARTY COPYRIGHT WORKS

SPRINGER LICENSE
TERMS AND CONDITIONS

Jan 24, 2013

This is a License Agreement between Imperial College London ("You") and Springer ("Springer") provided by Copyright Clearance Center ("CCC"). The license consists of your order details, the terms and conditions provided by Springer, and the payment terms and conditions.

All payments must be made in full to CCC. For payment instructions, please see information listed at the bottom of this form.

License Number	3067740134309
License date	Jan 14, 2013
Licensed content publisher	Springer
Licensed content publication	Journal of Fluorescense
Licensed content title	Preparation and Entrapment of Fluorescently Labeled Proteins for the Development of Reagentless Optical Biosensors
Licensed content author	John D. Brennan
Licensed content date	Jan 1, 1999
Volume number	9
Issue number	4
Type of Use	Thesis/Dissertation
Portion	Figures
Author of this Springer article	No
Order reference number	
Title of your thesis / dissertation	BIOSENSORS BASED ON BOVINE ODORANT BINDING PROTEIN (bOBP)
Expected completion date	Feb 2013
Estimated size(pages)	202

Total	0.00 GBP

From: Michael Davidson [mailto:davidson@magnet.fsu.edu]
Sent: 24 January 2013 19:21
To: Bunyarataphan, Sasinee
Subject: RE: Image Request: Olympus Micrsocopy Reource Center

That will be fine.

Regards---Mike

Michael W. Davidson
National High Magnetic Field Laboratory
1800 E. Paul Dirac Dr.
The Florida State University
Tallahassee, Florida 32310
Phone: 850-644-0542
Fax: 850-644-8920
Email: davidson@magnet.fsu.edu
Web: http://micro.magnet.fsu.edu

From: Bunyarataphan, Sasinee [mailto:sasinee.bunyarataphan08@imperial.ac.uk]
Sent: Thursday, January 24, 2013 12:21 PM
To: 'davidson@magnet.fsu.edu'
Subject: FW: Image Request: Olympus Micrsocopy Reource Center

Dear Michael,
May I ask your permission to reproduce the 3 figures onto my thesis, please?

1. Figure 1 from http://www.olympusmicro.com/primer/techniques/confocal/fluoroexciteemit.html
2. Figure 1 from http://www.microscopyu.com/articles/fluorescence/fret/fretintro.html
3. Figure 4 from http://www.olympusmicro.com/primer/techniques/fluorescence/fret/fretintro.html.

Thank you very much
Best regards,
Sasinee
P.S. It's fine that you don't have to send me the images.

From: Jennifer.Reed@olympus.com [mailto:Jennifer.Reed@olympus.com]
Sent: 21 January 2013 15:55
To: Bunyarataphan, Sasinee
Cc: davidson@magnet.fsu.edu
Subject: Image Request: Olympus Micrsocopy Reource Center

Dear Sasinee: I am writing in response to your web inquiry below and have copied Mike Davidson from Florida State University, who manages this web site and can send and grant permission on the use of it.

Dear Mike - Would you kindly send the image referenced below.

Kind regards,

Jennifer

```
Send Date              : 2013/01/16(Wed) 07:21
Reference number       : E201301160078421
Category               : Corporate (Olympus Website)
Product name           :
Title                  : Ms.
First name             : SASINEE
Last name              : BUNYARATAPHAN
Address                : Imperial College London, South Kensington
Campus
State or province      : London
Postal code            : SW7 2AZ
Country                : UK
Company / Organization: Imperial College London
Department             : Chemistry
Phone number           : 07551059429
Fax number             :
E-mail address         : SB2408@IC.AC.UK
Message                : Regarding to this website
(http://www.olympusmicro.com/primer/techniques/confocal/fluoroexciteemit.html),
may I ask you for the permission of reproducing the Figure 1  onto my
thesis, please?
I look forward to hearing from you soon.
Thanks
Regards,
Sasinee
```

Jennifer Reed
Manager, Marketing Communications
Olympus America Inc.
Scientific Equipment Group
3500 Corporate Parkway
Center Valley, PA 18034
- -
Phone: 484-896-3188
Cell: 484-788-4466
E-mail: Jennifer.Reed@olympus.com

JOHN WILEY AND SONS LICENSE TERMS AND CONDITIONS

Jan 28, 2013

This is a License Agreement between Imperial College London ("You") and John Wiley and Sons ("John Wiley and Sons") provided by Copyright Clearance Center ("CCC"). The license consists of your order details, the terms and conditions provided by John Wiley and Sons, and the payment terms and conditions.

All payments must be made in full to CCC. For payment instructions, please see information listed at the bottom of this form.

License Number	3077771145499
License date	Jan 28, 2013
Licensed content publisher	John Wiley and Sons
Licensed content publication	ChemBioChem
Licensed content title	Recent Progress in Strategies for the Creation of Protein-Based Fluorescent Biosensors
Licensed copyright line	Copyright © 2009 WILEY-VCH Verlag GmbH & Co. KGaA, Weinheim
Licensed content author	Hangxiang Wang,Eiji Nakata,Itaru Hamachi
Licensed content date	Aug 19, 2009
Start page	2560
End page	2577
Type of use	Dissertation/Thesis
Requestor type	University/Academic
Format	Print and electronic
Portion	Figure/table
Number of figures/tables	1
Original Wiley figure/table number(s)	Figure 2
Will you be translating?	No
Total	0.00 USD

ELSEVIER LICENSE
TERMS AND CONDITIONS

Jan 28, 2013

This is a License Agreement between Imperial College London ("You") and Elsevier ("Elsevier") provided by Copyright Clearance Center ("CCC"). The license consists of your order details, the terms and conditions provided by Elsevier, and the payment terms and conditions.

All payments must be made in full to CCC. For payment instructions, please see information listed at the bottom of this form.

Supplier	Elsevier Limited The Boulevard,Langford Lane Kidlington,Oxford,OX5 1GB,UK
Registered Company Number	1982084
Customer name	Imperial College London
Customer address	Imperial College London, LONDON, SW7 2AZ
License number	3077780417738
License date	Jan 28, 2013
Licensed content publisher	Elsevier
Licensed content publication	Cell
Licensed content title	A novel multigene family may encode odorant receptors: A molecular basis for odor recognition
Licensed content author	Linda Buck,Richard Axel
Licensed content date	5 April 1991
Licensed content volume number	65
Licensed content issue number	1
Number of pages	13
Start Page	175
End Page	187
Type of Use	reuse in a thesis/dissertation
Intended publisher of new work	other
Portion	figures/tables/illustrations
Number of figures/tables/illustrations	1

Format	both print and electronic
Are you the author of this Elsevier article?	No
Will you be translating?	No
Order reference number	
Title of your thesis/dissertation	BIOSENSORS BASED ON BOVINE ODORANT BINDING PROTEIN (bOBP)
Expected completion date	Feb 2013
Estimated size (number of pages)	202
Elsevier VAT number	GB 494 6272 12
Permissions price	0.00 GBP
VAT/Local Sales Tax	0.0 USD / 0.0 GBP
Total	0.00 GBP

ELSEVIER LICENSE
TERMS AND CONDITIONS

Jan 24, 2013

This is a License Agreement between Imperial College London ("You") and Elsevier ("Elsevier") provided by Copyright Clearance Center ("CCC"). The license consists of your order details, the terms and conditions provided by Elsevier, and the payment terms and conditions.

All payments must be made in full to CCC. For payment instructions, please see information listed at the bottom of this form.

Supplier	Elsevier Limited The Boulevard,Langford Lane Kidlington,Oxford,OX5 1GB,UK
Registered Company Number	1982084
Customer name	Imperial College London
Customer address	Imperial College London, LONDON, SW7 2AZ
License number	3067791476357
License date	Jan 14, 2013
Licensed content	Elsevier

publisher	
Licensed content publication	Biochimica et Biophysica Acta (BBA) - Protein Structure and Molecular Enzymology
Licensed content title	Mammalian odorant binding proteins
Licensed content author	Mariella Tegoni,Paolo Pelosi,Florence Vincent,Silvia Spinelli,Valérie Campanacci,Stefano Grolli,Roberto Ramoni,Christian Cambillau
Licensed content date	18 October 2000
Licensed content volume number	1482
Licensed content issue number	1–2
Number of pages	12
Start Page	229
End Page	240
Type of Use	reuse in a thesis/dissertation
Intended publisher of new work	other
Portion	figures/tables/illustrations
Number of figures/tables/illustrations	1
Format	both print and electronic
Are you the author of this Elsevier article?	No
Will you be translating?	No
Order reference number	
Title of your thesis/dissertation	BIOSENSORS BASED ON BOVINE ODORANT BINDING PROTEIN (bOBP)
Expected completion date	Feb 2013
Estimated size (number of pages)	202
Elsevier VAT number	GB 494 6272 12
Permissions price	0.00 USD
VAT/Local Sales Tax	0.0 USD / 0.0 GBP
Total	0.00 USD

-----Original Message-----
From: John Philo [mailto:jphilo@ap-lab.com]
Sent: 16 January 2013 16:08
To: Bunyaratapha n, Sasinee
Subject: RE: Your message to Alliance Protein Laboratories

Sasinee, yes you may use the figure (it has appeared in more than 20 theses already). Here are two high-resolution scalable versions (Windows metafiles).

John

John Philo, Ph.D.
VP & Director of Biophysical Chemistry
Alliance Protein Laboratories, Inc.
1-858-550-9401, fax 1-858-550-9403
6042 Cornerstone Ct West, Suite A1
San Diego, CA 92121 U.S.A.

-----Original Message-----
From: SASINEE [mailto:SB2408@IC.AC.UK]
Sent: Tuesday, January 15, 2013 3:41 PM
To: jphilo@ap-lab.com
Subject: Your message to Alliance Protein Laboratories

To: jphilo@ap-lab.com
From: SB2408@IC.AC.UK (SASINEE)
X-Originating-IP: [155.198.14.110]
Subject: Your message to Alliance Protein Laboratories

Below is the result of your feedback form. It was submitted by SASINEE (SB2408@IC.AC.UK) on Tuesday, January 15, 2013 at 18:41:02
---
phone: 07551059429

company: Imperial College London, South Kensington Campus, London SW7 2AZ, UK

MessageFor: Anyone

comments: Regarding to this website (http://www.ap-lab.com/CD_services.htm),
may I ask you for the permission of reproducing the Figure onto my thesis, please?

I look forward to hearing from you soon.
Thanks
Regards,
Sasinee

Engage: Submit

ELSEVIER LICENSE
TERMS AND CONDITIONS

Jan 26, 2013

This is a License Agreement between Imperial College London ("You") and Elsevier ("Elsevier") provided by Copyright Clearance Center ("CCC"). The license consists of your order details, the terms and conditions provided by Elsevier, and the payment terms and conditions.

All payments must be made in full to CCC. For payment instructions, please see information listed at the bottom of this form.

Supplier	Elsevier Limited The Boulevard,Langford Lane Kidlington,Oxford,OX5 1GB,UK
Registered Company Number	1982084
Customer name	Imperial College London
Customer address	Imperial College London, LONDON, SW7 2AZ
License number	3076670279893
License date	Jan 26, 2013
Licensed content publisher	Elsevier
Licensed content publication	Biosensors and Bioelectronics
Licensed content title	Biochemical gas sensor (bio-sniffer) for ultrahigh-sensitive gaseous formaldehyde monitoring
Licensed content author	Hiroyuki Kudo,Yuki Suzuki,Tomoko Gessei,Daishi Takahashi,Takahiro Arakawa,Kohji Mitsubayashi
Licensed content date	15 October 2010
Licensed content volume number	26
Licensed content issue number	2
Number of pages	5
Start Page	854
End Page	858
Type of Use	reuse in a thesis/dissertation
Intended publisher of new work	other
Portion	figures/tables/illustrations

Number of figures/tables/illustrations	1
Format	both print and electronic
Are you the author of this Elsevier article?	No
Will you be translating?	No
Order reference number	
Title of your thesis/dissertation	BIOSENSORS BASED ON BOVINE ODORANT BINDING PROTEIN (bOBP)
Expected completion date	Feb 2013
Estimated size (number of pages)	202
Elsevier VAT number	GB 494 6272 12
Permissions price	0.00 GBP
VAT/Local Sales Tax	0.0 USD / 0.0 GBP
Total	0.00 GBP